

**TABLE OF CONTENTS**

1. Introduction.....	2
2. Review of literature.....	4
2.1. Psychiatric disorders.....	4
2.2. Bipolar disorder.....	7
2.2.1. Genomics of bipolar disorder.....	7
2.2.2. Clinical management of bipolar disorder.....	8
2.2.3. Mechanisms of action of Lithium (Li <sup>+</sup> ) in bipolar disorder.....	8
2.3. Shared genetic risk and biology between bipolar disorder and schizophrenia.....	10
2.4. Cell-types implicated in bipolar disorder and schizophrenia.....	14
2.5. Astrocytes.....	16
2.5.1. Astrocyte metabolism.....	18
2.5.2. Astrocytes in bipolar disorder and schizophrenia.....	21
2.5.3. Astrocytes in neurodegeneration.....	21
2.6. Tools to study metabolism.....	22
2.6.1. Experimental methods.....	22
2.6.2. Computational modeling.....	22
2.6.3. Constraint-based reconstruction and analysis (COBRA).....	22
2.7. Preview of dissertation.....	23
3. Aims and objectives.....	24
4. Metabolic modeling of astrocytes in bipolar disorder and schizophrenia.....	25
4.1. Introduction.....	25
4.2. Materials and methods.....	28
4.3. Results and discussion.....	37
5. Identifying the metabolic impact of loss-of-function (LoF) mutations implicated in bipolar disorder, schizophrenia and neurodegeneration.....	45
5.1. Introduction.....	45
5.2. Materials and methods.....	46
5.3. Results and discussion.....	47
6. Abstract.....	48
7. Summary and future directions.....	49
8. Supplementary: figures, tables and methods.....	50
9. References.....	74

## 1. Introduction.

Psychiatric disorders, encompassing conditions like bipolar disorder (BD), schizophrenia (SCZ), major depressive disorder (MDD), obsessive-compulsive disorder (OCD), substance abuse disorder (SUD), etc., contribute significantly to morbidity<sup>1</sup> and mortality<sup>2</sup> globally, and has a profound impact on an individual's daily life. While twin studies have shown high heritability<sup>3</sup>, most psychiatric disorders don't align with the Mendelian monogenic model; rather, they arise from multifactorial causes influenced by multiple genes<sup>4</sup>. Psychiatric symptoms transcend contemporary diagnostic boundaries. In the case of BD and SCZ, there's a significant overlap in terms of clinical symptoms<sup>5</sup>, genetics<sup>6-8</sup>, brain structure anomalies<sup>9,10</sup>, cellular/molecular factors<sup>11,12</sup>. Despite available treatments, there's variability in responses and potential side effects. Predicting the course of the illness and treatment response upon patients' arrival at the clinic remains challenging<sup>13,14</sup>. Genome-wide association studies (GWAS) and sequencing studies have been successful in identifying thousands of genetic variants associated with various psychiatric disorders<sup>15,16</sup>. However, translating the genetic insights into clinical risk assessment and treatment prediction remains elusive. The main reason for this is our limited foundational understanding of the biological pathways, networks, cell-types and neuronal/glial circuits that these genes operate on. Genomic discoveries on psychiatric disorders, particularly BD and SCZ, tend to converge on altered synaptic pathways in specific excitatory and inhibitory neurons<sup>17-19</sup>. However, there's growing recognition that glial cells, especially astrocytes, through non-cell autonomous functions, mediate neuronal function and contribute to the etiology of BD and SCZ<sup>12,20-22</sup>.

Astrocytes constitute around 20-40% of CNS cell count<sup>23</sup> and play a vital role in maintaining CNS homeostasis. They provide trophic support to neurons<sup>24</sup>, facilitate synapse formation and pruning during development<sup>25</sup>, and form physical contacts with the vasculature enabling metabolite and ion exchange<sup>26</sup>. Historically, astrocyte subtypes have been known to occupy specific brain areas<sup>27,28</sup>, however more recently, it is shown that astrocytes exhibit transcriptomic and functional diversity across brain regions and even within cortical layers<sup>28,29</sup>. These cells are crucial for brain energy metabolism, which is substantial, accounting for 20-25% of the body's energy consumption<sup>30</sup>. Astrocytes primarily generate ATP through glycolysis, releasing lactate into the extracellular space<sup>31-35</sup>. They regulate the balance in the extracellular environment, sensing messenger molecules like glutamate<sup>36</sup>, potassium<sup>37</sup>, nitric oxide<sup>38-40</sup>, hydrogen peroxide<sup>41,42</sup>, and ammonia<sup>43</sup>. Although glucose metabolism is key, research emphasizes the significance of lipid metabolism in maintaining brain equilibrium, especially through astrocytic fatty acid oxidation (FAO)<sup>44</sup>. Astrocytic networks contribute to brain activity, plasticity, and behavior<sup>45</sup>. Astrocytes operate within defined territories<sup>46</sup>, and it is essential for them to form functional networks that are essential for complex behaviors. And finally, these cells exhibit diverse responses to various

pathological conditions, including acute infection<sup>47-49</sup>, injury<sup>50-52</sup>, and diseases like Huntington's<sup>53,54</sup>, Alzheimer's<sup>55,56</sup>, Parkinson's<sup>57</sup>, glioblastoma<sup>58</sup>, but also in the context of psychiatric disorders like BD<sup>59</sup> and SCZ<sup>60</sup>.

## 2. Review of literature.

### 2.1. Psychiatric disorders.

Psychiatric disorders are a group of mental health conditions characterized by persistent changes in behavior, thoughts, moods, and emotions that can have a profound impact on an individual's daily life. They significantly contribute to morbidity<sup>1</sup> and mortality<sup>2</sup> globally, imposing a considerable burden on individuals and society. Onset usually occurs during adolescence or young adulthood, leading to prolonged periods of illness. Those with severe mental illness often face lower socioeconomic status<sup>61,62</sup>, experience stigma<sup>63</sup>, and are more prone to substance use<sup>64</sup> and somatic disease<sup>65</sup>, all of which negatively impact their well-being and quality of life. Individuals with severe mental illness have an average life expectancy about 10 years shorter than the general population<sup>2,66</sup>, with excess mortality attributed to physical health issues, especially cardiovascular disease<sup>67,68</sup>, and mental health-related causes like suicide<sup>69</sup>. Psychiatric disorders could be classified into different categories, including mood disorders (e.g., depression, bipolar disorder), anxiety disorders (e.g., generalized anxiety disorder, panic disorder), impulse control disorders (e.g., attention-deficit/hyperactivity disorder), substance use disorders (alcohol and drug abuse with or without dependence), and psychotic disorders (e.g., schizophrenia). The median lifetime prevalence estimates for mood disorders are 3.3-21.4%, for anxiety disorders are 4.8-31.0%, for impulse control disorders are 0.3-25.0%, for substance use disorders are 1.3-15.0%, and for psychotic disorders are 3.06-3.48%, as estimated by epidemiology studies<sup>70,71</sup>. The prevalence of these conditions can vary depending on the population, but overall, psychiatric disorders account for a significant amount of lived years with disability. The urgent need to improve mental health care has been emphasized by the World Health Organization<sup>72</sup>.

In terms of treatment, psychiatric disorders are managed through a combination of medication and therapy. Antidepressant medications<sup>73</sup>, such as selective serotonin reuptake inhibitors (SSRIs), can be effective in treating depression, while mood stabilizers<sup>74</sup> and antipsychotics<sup>13</sup> are commonly used to manage BD and SCZ, respectively. Psychotherapy, such as cognitive behavioral therapy (CBT)<sup>75</sup>, can also help individuals manage their symptoms, learn coping strategies, and improve their overall quality of life. Electroconvulsive therapy (ECT)<sup>76</sup> is a treatment that involves applying electrical stimulation to the brain through electrodes placed on the scalp, and is typically considered a last resort for patients who have not responded to other treatments such as medications, psychotherapy or other forms of brain stimulation. While existing treatments may have clinically meaningful effects in psychiatric disorders<sup>76,77</sup>, they are rarely curative, leading to relapses and adverse effects experienced by many patients, and therapeutic non-response is common<sup>13,14</sup>. Inadequate therapeutic options can largely be attributed to the limited

understanding of the causes of mental illness, despite intensive research efforts over decades. Psychiatric nosology still relies on traditional diagnostic distinctions based on clinical observations. The current leading diagnostic classification systems, the International Classification of Diseases<sup>78</sup> and the Diagnostic and Statistical Manual of Mental Disorders<sup>79</sup>, primarily diagnose psychiatric disorders based on signs and symptoms, lacking objective biomarkers, which makes clinical psychiatry more susceptible to unwanted variability in both diagnostic and therapeutic decision-making<sup>80</sup>. Although the present diagnostic categories are clinically useful, there is little evidence to suggest that they represent truly discrete entities with natural boundaries<sup>81,82</sup>, as indicated by high comorbidity and shared symptomatology across different mental disorders<sup>83,84</sup> and high heterogeneity within diagnostic categories<sup>85</sup>.

Genetics play a significant role in the development of psychiatric disorders<sup>86</sup>. The history of psychiatry is intimately connected to heredity. Mental illnesses' tendency to run in families was observed by early physicians and later systematically evaluated through twin<sup>87</sup>, family<sup>88-90</sup>, and adoption<sup>91</sup> genetic epidemiological studies in the 20th century. This exceptional body of evidence revealed that common psychiatric disorders are moderately to strongly heritable, providing a significant etiological clue for the field<sup>3</sup>. However, it is now understood that these genetic effects are relatively small and non-deterministic<sup>4</sup>: most individuals with a strong family history are not affected, similar to observations in many complex biomedical diseases. Additionally, most psychiatric disorders do not necessarily show a consistent pattern within families. For instance, relatives of individuals with SCZ have increased risks not only for SCZ but also for various other conditions like BD, MDD and autism<sup>92,93</sup>. The wide range of clinical presentations and varying courses seen in many common psychiatric disorders align with the notion of complex and relatively small genetic effects. In particular, adult-onset common psychiatric disorders often exhibit development within normal limits, although higher cognitive functions may be impaired to some extent<sup>94</sup>. It is also important to note that genetics alone do not determine the development of a psychiatric disorder. Environmental factors, such as trauma<sup>95</sup>, stress<sup>96</sup>, and substance abuse<sup>97</sup>, can also contribute to the onset of these conditions.

A better understanding of the underlying biological mechanisms is needed to improve the care and prevention of mental illness. However, challenges in studying the living human brain and uncertain validity of animal models of mental illness have limited progress in biological research in psychiatry<sup>98</sup>. As a result, there have been no major therapeutic advances in psychiatry in the past decades<sup>99</sup>, and current attention is focused on potential new treatment options, such as repurposing existing drugs like ketamine<sup>100</sup> or psychedelics<sup>101</sup>. Nevertheless, the substantial heritability of psychiatric disorders<sup>3,102</sup> indicates that genetic research could provide valuable pathobiological insights and help in understanding gene-environment interplay and environmental effects.

Despite the high expectations for psychiatric genetics with the increasing availability of DNA sequencing technologies in the second half of the 20th century, a false start occurred in the 1990s and early 2000s. Findings from the candidate gene approach lacked reproducibility, leading to decreased confidence in discovering mental illness genes<sup>103,104</sup>. However, major breakthroughs occurred with the sequencing of the human genome in 2003<sup>105</sup>, and the establishment of reference datasets documenting human genetic variation across different populations<sup>106,107</sup>. These advancements allowed for a systematic exploration of DNA sequence variants associated with human traits and diseases. Since then, a steady and accelerating progress in human genetics<sup>108</sup> has been observed, driven by a combination of technological innovations, more advanced statistical analytical tools, reduced costs for genotyping and sequencing DNA, enhanced knowledge about the genome, and increased international collaboration. Psychiatric genetics has been at the forefront of these efforts, recognizing the importance of assembling large-scale case-control cohorts of psychiatric disorders to reliably identify genetic variants, most of which have very weak effects. These efforts have gradually led to the discovery of multiple genetic risk variants for mental illness<sup>15,16</sup> ([Fig.S1](#)). Despite major advances in our understanding of the genetic architecture of mental illness over the last decade, these discoveries have not yet translated into improved care for individuals with mental illness, which remains the key challenge for the field.

Gaining insights into the underlying etiology of illness is one of the key aims of human genetics, informing the development of new therapeutic interventions and aiding biomarker identification. However, translating genetic findings into biological mechanisms is not straightforward. A complete mechanistic understanding of a disorder's genetic risk architecture necessitates identifying the specific causal variant underlying a genetic signal, determining the functional impact of the genetic variant, and understanding how all the genetic risk variants collectively influence biological pathways in specific cell types, tissues, and organs, throughout developmental stages, and in conjunction with environmental factors<sup>109,110</sup>. This presents a considerable challenge, requiring comprehensive animal studies, cell-biology experiments, and advanced computational approaches. The current mechanistic interpretation is also limited by the incomplete understanding of the physiological role of most genes and proteins, including their interactions within signaling networks and pathways<sup>111</sup>.

## 2.2. Bipolar disorder.

Bipolar disorder (BD) is a severe psychiatric illness characterized by manic/depressive episodes and persistent neurocognitive impairments<sup>112</sup>, affecting 0.5% of the population (ca. 7 million in India)<sup>113</sup>. It is a significant cause of disability, morbidity, and mortality (15% die by suicide)<sup>114</sup>. The concept of BD was originally included in the idea of manic-depressive illness put forth by Kraepelin in 1899<sup>115</sup>. This included both single and recurring forms of MDD and BD. In 1957, Leonard proposed that BD-I and MDD were separate syndromes<sup>116</sup>, which was confirmed by family studies showing that relatives of BD-I patients had a 10-fold increased risk of BD and an increased risk of MDD, while relatives of MDD patients had elevated rates of MDD but only slightly higher rates of BD than those of control relatives<sup>117</sup>. Both twin and adoption studies indicate that genetics play an important role in BD, with heritability estimates ranging from 0.59 to 0.87 in twin studies<sup>118-120</sup>. Family/genetic strategies have also been used in efforts to validate potential subtypes of BD. The results of most such studies have been mixed, but supporting evidence is available for early versus late age at onset<sup>121</sup>, lithium responsivity<sup>122</sup>, psychotic BD<sup>123</sup>, puerperal mania<sup>124</sup>, comorbidity with panic disorder<sup>125</sup>, a preponderantly depressed vs. preponderantly manic course<sup>126</sup> and unipolar mania versus typical BD<sup>127</sup>. A large literature has examined the relationship between BD-I and BD-II disorder, requiring, respectively, full manic versus hypomanic episodes. Recent genetic studies have shown that BD-I has a higher single-nucleotide polymorphism (SNP) heritability and a higher genetic correlation with SCZ, while BD-II has a much higher genetic correlation with MDD<sup>128</sup>.

### 2.2.1. Genomics of bipolar disorder.

Advances in genotyping technology have made it possible to assay common variants in large-scale case-control studies, known as genome-wide association studies (GWAS). To date, there have been numerous GWAS studies performed on BD<sup>129-132</sup>, with the largest and most recent conducted by the Psychiatric Genomics Consortium (PGC) reporting 64 genetic loci linked to BD through analysis of 41,917 BD patients and 371,549 controls<sup>17</sup>. The genes identified include those involved in ion channels, neurotransmitter transporters, and synaptic components. On the other hand, the Bipolar Sequencing Consortium (BSC), despite having a sample of 13,933 cases and 14,422 controls, had not found significant associations with any specific gene but showed promising aggregate results: novel singleton protein truncating variants in genes intolerant to loss-of-function mutations are enriched in BP patients<sup>133</sup>. However, the BD genetic studies have several limitations. Firstly, the studies have limited power and have only identified a small portion (3.3% SNP heritability) of the genetic risk factors for BD. Secondly, most samples used in the studies have minimal phenotypic information, which can lead to less specific findings and lower heritability estimates. Thirdly, the studies have been mainly conducted using European populations, leading to uncertainty in how the findings can be applied to other populations and

potentially exacerbating healthcare disparities. Finally, the distribution of clinical features in BD patients may differ between human populations, highlighting the need for greater genetic diversity in research. To further the discovery of common and rare variants, more samples are required, and greater ancestral diversity should be prioritized.

#### 2.2.2. Clinical management of bipolar disorder.

Clinically, BD is characterized by mood swings with the patient alternating between mania and depression<sup>112</sup>. Managing BD effectively requires controlling these mood episodes and preventing relapse. Mood stabilizing agents are used for this purpose, with lithium (Li+) being the first-line mood stabilizer. Li+ has been used since 1949<sup>134</sup>, and is the only effective drug for preventing suicides<sup>74,135</sup> and improving cognition<sup>136</sup> in BD patients. While Li+ can be highly effective, not all patients respond to it: approximately 30% of patients have an excellent response, 30% show a partial response, and 40% are resistant to treatment and are considered non-responders, making their clinical management difficult<sup>137</sup>. When treating a chronic illness, being able to predict a patient's response to treatment is crucial for effective management. Without this capability, treatment often involves trial and error, leading to uncontrolled disease and a negative impact on long-term prognosis. The selection of mood stabilizers for BD is similarly challenging. Several studies have tried to link clinical parameters to response to Li+ treatment, but the predictive power of these remains limited<sup>138</sup>. To be able to predict a patient's response to Li+ would greatly benefit clinical management.

#### 2.2.3. Mechanisms of action of Lithium (Li+) in bipolar disorder.

The reason for the inability to predict responses to Li+ is due to a lack of understanding of its mechanisms of action. It is believed that Li+ affects brain cells by altering ongoing molecular processes, leading to changes in cellular function. The mechanism of action of Li+ in the brain is thought to be highly complex, inducing a multitude of effects on the protein expression, neurotransmission, circadian biology, ion transport, etc<sup>139</sup>. Two main proteins, inositol monophosphatase (IMPA1)<sup>140</sup> and glycogen synthase kinase-3 (GSK3)<sup>141</sup>, have been proposed as candidate targets, with others also being considered. Both of these proteins are inhibited at Li+ concentrations that approximate therapeutic blood levels, which are 0.5-1 mEq/L<sup>142</sup>. The 'inositol depletion' hypothesis, proposed by Berridge *et al.*<sup>143</sup>, suggests that Li+'s effectiveness in treating BD depends on inhibiting IMPA1, reducing inositol supply for phosphatidylinositol (PI) synthesis. Li+'s inhibition of IMPA1 shows unusual uncompetitive kinetics, and is seen only when the IMPA1 substrate inositol 1-phosphate (IP1) accumulates in cells. This mechanism implies selective inhibition in cells like neurons with high PI turnover. While a knockout of IMPA1 in mice suggested altered inositol signaling<sup>144</sup>, a suitable mouse model for BD remains elusive. GSK3 inhibition, instead of IMPA1, has been emphasized by researchers over the years<sup>145</sup>, but GSK3 inhibitors haven't progressed to BD clinical trials. Notably, amphibian studies indicated that Li+'s effects could

be blocked by inositol supplementation<sup>146</sup>. Observations in yeast<sup>147</sup> and mammalian neurons<sup>148</sup> demonstrated that GSK3 positively regulates myo-inositol 1-phosphate synthase, a key enzyme in inositol's de novo synthesis, further suggesting inositol homeostasis plays a vital role in Li+ 's action. Inositol and GSK3 have been the main focus in understanding Li+ 's mechanisms of action, emphasizing the pressing need for systematic and unbiased investigations to explore additional pathways involved.

### 2.3. Shared genetic risk and biology between bipolar disorder and schizophrenia.

Substantial overlap between BD and SCZ has been demonstrated by genetic and epidemiological studies, with a genetic correlation of around 0.6–0.7 for common variation<sup>6</sup>, along with high relative risks (RR) among relatives of both BD and SCZ patients (RRs for parent/offspring: BD/BD: 6.4, BD/SCZ: 2.4; SCZ/BD: 5.2, SCZ/SCZ: 9.9)<sup>149</sup>. Despite shared genetics and symptomatology, the current diagnostic systems<sup>79,81</sup> maintain historical distinctions from the late 19th century, presenting BD and SCZ as separate entities based on clinical presentation. BD is marked by predominant mood symptoms, mood-congruent delusions, and episodic course, while SCZ is seen as a prototypical psychotic disorder. These distinctions were initially suggested in the late 1950s and gained acceptance<sup>5</sup>. Syndromes like SCZ, BD, and MDD were separated based on symptom patterns and illness trajectory. However, features such as psychosis, mood dysregulation, and cognitive impairments were recognized to transcend diagnostic boundaries. Yet, uncertainties remain about whether these syndromes represent distinct entities, share foundations, or are different variations of an underlying disease due to the unknown biological understanding. For e.g., over time, the diagnosis for an individual patient has the potential to shift from BD to SCZ, or the other way around. These characteristics imply that the two disorders could potentially occupy distinct segments within a spectrum of psychosis. Research until the last decade indicated varying degrees of familial and genetic overlap for pairs of these disorders, and supports diagnostic boundaries between SCZ and BD, and BD and MDD<sup>118,150</sup>, but also implicate correlated familial and genetic liabilities<sup>118,149</sup>. Several genetic variants conferring risk for both SCZ and BD were also identified<sup>129,151,152</sup>.

However, the breakthrough came in 2013 when a study integrated SNP data from five neuropsychiatric disorders - autism spectrum disorder (ASD), attention deficit-hyperactivity disorder (ADHD), BD, MDD, and SCZ—in 33,332 cases and 27,888 controls<sup>7</sup>. This marked the first time all five conditions were simultaneously studied in a single GWAS. The study identified significant SNPs at four loci: regions on chromosomes 3p21 and 10q24, along with genes *CACNA1C* and *CACNB2*, related to L-type voltage-gated calcium channels. This suggests that genetic variation in fundamental systems like calcium channel signaling elevates the risk of general susceptibility to neuropsychiatric disorders, and a combination of other genetic and non-genetic risk factors guides this susceptibility towards specific disorder development.

In 2018, a more extensive and detailed genetic analysis of BD and SCZ, including 53,555 cases (20,129 BD, 33,426 SCZ) and 54,065 controls, along with 28 subphenotypes of BD (n=24) and SCZ (n=4), identified 114 shared genome-wide significant loci across these disorders<sup>8</sup>. While the study did indicate a substantial shared genetic risk, it also showcased that specific locations contribute to the observed differences in characteristics within these

disorders. The subphenotype examination indicated a significant positive correlation between i) BD PRS and manic symptoms in SCZ cases, and ii) BD PRS and psychotic attributes in BD patients. Additionally, the study noticed a significant increase in SCZ PRS in i) BD cases with psychotic traits, and ii) SCZ cases with increased negative symptoms. This was the first study that discovered distinct genomic locations distinguishing BD and SCZ, uncovering polygenic elements underlying numerous symptom dimensions. These findings emphasize the utility of genetics and deep clinical phenotyping to guide symptomology and potentially treatment in such complex traits.

While the shared genetic aspect is significant, studies also point to genetic architecture differences between these two disorders<sup>153,154</sup>. A polygenic risk score (PRS) derived from a case-only SCZ versus BD GWAS correlated significantly with SCZ or BD diagnosis in an independent sample<sup>154</sup>, indicating that differences between disorders have a genetic basis. SCZ patients show an enrichment of rare, moderate to highly penetrant copy-number variants (CNVs), de novo CNVs and somatic CNVs<sup>155-161</sup>, while CNV involvement in BD is less clear<sup>162</sup> and perhaps limited to schizoaffective cases<sup>163</sup>. Although the role of de novo single nucleotide variants (SNVs) in BD and SCZ has been explored in a limited number of studies, enrichment in pathways linked to the postsynaptic density has been reported for SCZ but not BD<sup>164,165</sup>. Identifying disorder-specific variants and quantifying the contribution of genetic variation to specific symptom dimensions remain important questions that will help comprehend dimensions of the disorders beyond dichotomous diagnosis. For example, it is known that SCZ patients with more manic symptoms have higher polygenic risk for BD<sup>154</sup>. These findings highlight shared genetic foundations for symptoms across disorders and might help stratify patients by genetic liability to symptom dimensions, thus informing disease course and treatment.

The genetic liability shared by SCZ and BD also manifests in terms of structural brain abnormalities, encompassing smaller total brain and hippocampal sizes on average, along with larger ventricular sizes, reduced white matter volumes, and common regions of thinner cortex, across both SCZ and BD<sup>10,166-172</sup>. Nonetheless, disorder-specific irregularities were also noted, where the genetic liability for SCZ correlated with thicker right parietal cortex, while the genetic liability for BD linked to larger intracranial volume (ICV)<sup>173</sup>. Whether it's genetic, brain imaging, or cellular/molecular studies, first-degree relatives (FDRs) of patients can represent individuals with a familial susceptibility to the disorder, devoid of confounding factors such as medication or duration of illness. Thus, they offer distinct insight into how familial risk for the disorder influences the brain. Nonetheless, only a few studies have directly compared brain structure between FDRs-BD and FDRs-SCZ, usually in cohorts of moderate sizes<sup>170,173-177</sup>. These studies revealed both distinct and overlapping brain irregularities for FDRs-SCZ and FDRs-BD, with findings being more accentuated in FDRs-SCZ than FDRs-BD.

However, it wasn't until 2019 when a comprehensive multicenter meta-analysis of magnetic resonance imaging (MRI) datasets, encompassing harmonized global and subcortical brain measurements, was undertaken, including data from a substantial number of participants, totaling 6,008 individuals (1,228 FDRs-SCZ, 852 FDRs-BD, 2,246 control subjects, 1,016 patients with SCZ, 666 patients with BD), hailing from 34 family cohorts associated with SCZ and/or BD<sup>9</sup>. This endeavor employed standardized methods to assess the patterns and extent of brain deviations in FDRs-BD and FDRs-SCZ, thus achieving increased power and generalizability. The outcomes revealed that FDRs-BD exhibited significantly larger intracranial volume (ICV), while FDRs-SCZ displayed reduced thalamic volumes when compared with control subjects. The findings suggested that despite their shared genetic liability, FDRs-SCZ and FDRs-BD manifest distinct structural brain irregularities, particularly in ICV. This divergence might suggest that the neurodevelopmental paths leading to brain abnormalities in SCZ or BD could be distinct.

The common variants reported by GWAS<sup>17,178,179</sup>, along with rare variants from exome sequencing<sup>164,180,181</sup> and transcriptomic analyses of post-mortem brains<sup>182,183</sup>, have consistently pinpointed synaptic function as a significant risk pathway in both BD and SCZ. With the potential for this to be manifested in molecular alterations within synapses of patients affected by these disorders, and considering advancements in biochemical fractionation for purifying synapses and mass spectrometry-based proteomics<sup>184-186</sup>, a comprehensive, in-depth, and unbiased proteomic profiling of synaptic fractions derived from the dorsolateral prefrontal cortex (DLPFC) of individuals with BD and SCZ was undertaken in 2023<sup>11</sup>, as a follow-up to uncover the molecular basis of the past decade's genomic findings. The research unveiled highly comparable alterations in several proteins and molecular pathways within human BD and SCZ synapses. These pathways notably encompassed synaptic function, revealing a decline in glutamate receptors (including AMPA, NMDA, and Kainate receptors), molecules within the glutamatergic signaling pathway (such as PLCB1 and APP), and postsynaptic scaffolding proteins (like HOMER1 and SHANK3). Surprisingly, the study also identified proteins associated with mitophagy, ribophagy, and aggrephagy, alongside other processes like enhanced vesicle tethering and proteins linked to forward and retrograde secretory trafficking, mitochondrial respiration, and mRNA translation, all disrupted within synapses of SCZ and BD patients.

These findings were in line with an earlier study from 2018<sup>12</sup>, which had the goal of examining the cortical molecular pathology across five major neuropsychiatric disorders (ASD, SCZ, BD, MDD, and alcoholism) through the meta-analysis of gene expression microarray datasets. The results unveiled a significant overlap in gene expression patterns among ASD, SCZ, and BD, as well as SCZ, BD, and MDD. Moreover, the study suggested a gradient of down-regulated synaptic genes, with ASD having the highest down-regulation, followed by SZ and BD. While BD and SCZ appeared notably similar in terms of synaptic

malfunction, MDD exhibited no synaptic pathology. However, MDD did show dysregulation in HPA-axis and hormonal signaling, which was absent in the other disorders. The data suggests that the degree of sharing of dysregulation in gene expression is related to polygenic overlap across disorders, suggesting a significant causal genetic component. Both the synapse proteomics<sup>11</sup> and the transcriptome meta-analysis<sup>12</sup> studies provides a comprehensive view of the neurobiological architecture of major neuropsychiatric illnesses, and demonstrates convergence but also specificity at the level of molecules and biological pathways.

## 2.4. Cell-types implicated in bipolar disorder and schizophrenia.

The genetic architectures of complex brain disorders are closely linked to the genes whose expression defines specific brain cell-types<sup>187</sup>, and connecting the genomic results to cellular studies is crucial for prioritizing cells underlying the genesis of such complex phenotypes<sup>188,189</sup>. The largest and most recent BD GWAS hits were enriched in both inhibitory (medium spiny neurons/MSNs, striatal interneurons) and excitatory (pyramidal neurons SS, pyramidal neurons CA1) neurons over other cell types within cortical and subcortical brain regions in mice<sup>17</sup>. Using human brain samples, the signal enrichment was observed in hippocampal pyramidal neurons and prefrontal cortex and hippocampal interneurons<sup>17</sup>.

In the case of SCZ GWAS, akin to BD, using mice scRNA-seq data<sup>19</sup>, the hits were enriched in both excitatory (glutamatergic pyramidal neurons from the cortex and hippocampus) and inhibitory (cortical interneurons and MSNs) cells, and notably less consistent with embryonic, progenitor, or glial cells<sup>179</sup>. Using human scRNA-seq data<sup>190</sup>, the enrichment was observed in excitatory (glutamatergic neurons from the cerebral cortex, hippocampus-pyramidal CA1 and CA3 cells, and granule cells of dentate gyrus) and inhibitory (cortical interneurons) cells<sup>179</sup>. In MDD GWAS, unlike SCZ or BD, the enrichment was limited to cortical interneurons and embryonic midbrain neurons<sup>19</sup>, but also to neuroblasts<sup>18</sup>. The molecular targets of antipsychotic medications, as defined by pharmacology, were also linked to the same cell types as those associated with the schizophrenia GWAS findings, including the neocortical S1 pyramidal cells, MSNs, hippocampal CA1 pyramidal cells, and cortical interneurons<sup>19</sup>.

Striatal MSNs have been of interest to SCZ due to several factors: i) their involvement in expressing dopamine type 2 and type 1 receptors (Drd2, Drd1), with Drd2 being a common target for effective antipsychotic medications<sup>191</sup>; ii) enrichment of MSNs through SCZ GWAS findings<sup>19</sup>; and iii) the significant overlap between antipsychotic-induced differentially expressed genes (DEGs) in mice striatum and the genes implicated in SCZ GWAS<sup>192</sup>. Drawing from these rationales, a recent investigation conducted single-cell RNA-seq analysis to scrutinize DEGs within distinct striatal cell types in C57BL/6 mice subjected to chronic exposure to a typical antipsychotic (haloperidol), an atypical antipsychotic (olanzapine), or a placebo<sup>193</sup>. The study determined that, for olanzapine, genes specifically upregulated in MSNs exhibited significantly greater overlap with the most recent SCZ GWAS discoveries. Nevertheless, when considering rare genetic variations, there was no convergence of any DEG (whether related to MSNs or other cell types) with genes identified in a meta-analysis of SCZ whole-exome sequencing<sup>180</sup>. These findings underscore a fundamental link between SCZ GWAS findings and genes upregulated in MSNs following exposure to olanzapine.

Glial cells (astrocytes, oligodendrocytes, and microglia) did not show enrichment for the most recent GWAS findings in BD or SCZ. However, a study in 2014<sup>20</sup>, utilizing the PGC1 SCZ GWAS data<sup>151</sup>, did reveal notable associations between expert-curated astrocyte and oligodendrocyte gene sets and the risk to SCZ. Similarly, analyses of transcriptome data from psychiatrically ill postmortem brains did reveal up-regulation of astroglial gene sets, potentially representing astrocytosis or activation, in SCZ, BD and ASD<sup>12,21</sup>. More recently, by integrating the latest SCZ GWAS findings with the transcriptome data of induced neurons from healthy human donors, co-cultured with murine glial cells, the study found significant correlations between variants adjacent to astrocyte-related genes and SCZ, which suggests that astrocytes might induce transcriptional programs related to SCZ in neurons<sup>22</sup>.

## 2.5. Astrocytes.

Astrocytes, constituting a significant cellular proportion in the central nervous system (CNS), account for 20-40% of the total CNS cell count<sup>23</sup>, depending on the species under investigation. Together with other brain and spinal cord glial cells (oligodendrocytes and microglia), the CNS's homeostasis is maintained by astrocytes throughout development<sup>27,194</sup>, normal physiology, and aging<sup>195</sup>. Astrocytes also play their roles in higher order functions like learning and memory<sup>196</sup>, control of emotional states<sup>197</sup>, sensory-motor responses<sup>198</sup> and decision making<sup>199</sup>. Despite profound changes occurring in response to disease<sup>200-208</sup>, astrocytes remain a fundamental element of the brain's usual environment. Notably, they offer essential trophic support to neurons<sup>24</sup>, facilitate synapse formation, function and pruning during development<sup>25</sup>, and form extensive networks with vasculature for metabolite uptake and distribution within the CNS<sup>26</sup>.

Core homeostatic functions in the brain are performed by astrocytes, making them an integral part of the blood-brain barrier (BBB)<sup>209</sup>. They sense and respond to peripheral insults like inflammation<sup>210</sup> while taking up metabolites to fuel the brain<sup>211</sup>. Specifically, glucose is taken up from the bloodstream, stored as glycogen, or converted into lactate to support active neurons through the astrocyte-neuron lactate shuttle<sup>212</sup>. This metabolite shuttle is closely tied to an antioxidant exchange system involving glutathione, ensuring homeostatic control of neuronal redox stress through astrocyte-mediated shuttling of glutathione precursors to neurons<sup>213</sup>. Moreover, astrocytes can uptake and metabolize synaptically released neurotransmitters<sup>214</sup>, partially contribute to the glymphatic system via aquaporin 4 (AQP4) channels<sup>215</sup>, and phagocytose synapses<sup>216,217</sup>. With each astrocyte connecting to thousands of synapses in rodents and millions in humans<sup>46,218</sup>, they have a far-reaching capacity to interact with numerous cells in the CNS, hinting at the possibility of integrating neuronal signaling and circuit functions<sup>194,219</sup>.

Astrocytes are derived from radial glial cells at the ventricular zone around embryonic day 18 in mice (approximately 16-18 weeks in human gestation), coinciding with the end of neurogenesis, until approximately post-natal day 7<sup>220,221</sup>. Following maturation, they spread throughout the entire brain, forming distinct domains due to contact inhibition between their processes. This maturation gives rise to various astrocyte subtypes occupying specific brain areas<sup>27,28</sup>. Conventionally, they were categorized as either grey matter, protoplasmic astrocytes, or white matter, fibrous astrocytes based on location and morphology<sup>222</sup>, but this oversimplified classification underestimates their true heterogeneity. In reality, astrocytes exhibit transcriptomic and functional diversity across brain regions and even within cortical layers<sup>28,29</sup>. While the exact mechanisms behind this maturational diversity remain unclear, it is believed to arise, in part, from their derivation from different precursors and the cues they receive from neurons and neuronal activity<sup>223-225</sup>.

In the CNS, various markers are utilized at the gene and protein level to characterize astrocytes, such as GFAP, vimentin, ALDH1L1, GLAST, AQP4 and S100 $\beta$ <sup>226,227</sup>. However, finding a perfect and specific cellular marker for all astrocytes is challenging as it depends on the context, CNS region, and methods employed. GFAP, for example, exhibits heterogeneity at the protein level<sup>226</sup>, and ALDH1L1 provides a homogeneous driver for genetically controlled reporters but has limited detection through immunofluorescence. Moreover, using Aldh1l1 as a driver in knockout/knockdown experiments raises concerns due to its high expression in the liver<sup>228</sup>. Continued exploration into astrocyte functions will be facilitated by the discovery of new markers for regionally constrained, developmentally regulated, or heterogeneous reactive populations of astrocytes. Moreover, these more specific markers will reveal potential novel druggable targets, aiding in the treatment of CNS diseases without a current cure.

Astrocytes, like other non-neuronal cells in the CNS, showcase rapid and diverse responses to various pathological insults, whether triggered by acute infection<sup>47-49</sup> or injury<sup>50-52</sup>, or linked to diseases like Huntington's<sup>53,54</sup>, Alzheimer's<sup>55,56</sup>, Parkinson's<sup>57</sup> and glioblastoma<sup>58</sup>. Traditionally, researchers examined astrocyte reactivity by observing morphological changes and GFAP upregulation<sup>229</sup>. However, recent attention revolves around uncovering the precise external molecular mediators driving these reactions and the internal pathways orchestrating changes at the transcriptomic, proteomic, morphological, and functional levels<sup>230-233</sup>. While some studies have defined specific changes, many have reported profound alterations in a few parameters. The field has flourished, embracing insights ranging from morphological shifts and cytoskeletal element upregulation to alterations in specific cell functions<sup>234</sup>. Astrocyte subtypes' various responses seem to fit within a triangle of 'normal physiological,' 'pathological trophic,' and 'pathological toxic,' with infinite possibilities in between<sup>235</sup>. Interestingly, what may seem toxic in one context might offer trophic support in another, revealing further intricacies. For comprehensive understanding, a collaborative endeavor is needed to unite modern discoveries with historical literature, spanning disease, sex<sup>236</sup>, CNS region<sup>23</sup>, circadian rhythm<sup>237,238</sup>, and species<sup>239</sup>. Embracing this contextual heterogeneity is pivotal to grasp the mechanisms behind how and why astrocyte subsets respond to diseases.

Recent discoveries have provided valuable insights into the specific functions, markers, spatial localization, and distinct subtypes of astrocytes that respond to various conditions in both permanent and transient ways. For example, during inflammation, reactive astrocytes swiftly alter gene expression, which returns to baseline levels within days<sup>230,240</sup>. In contrast, acute axonal injuries lead to astrocyte proliferation, forming enduring 'scar' or 'border' structures that can persist for decades in human patients<sup>241</sup>. While we comprehend much about astrocytes' vital role in normal health, there are still crucial gaps in understanding their function during disease, infection, and injury. Questions remain about

the number, duration, and consistency of reactive astrocyte populations across species, sex, brain regions, and different disease states<sup>235</sup>. While we have some knowledge of astrocyte-specific pathways and non-cell-autonomous molecules driving certain reactive states, a comprehensive unification of functional changes with transcriptomic and proteomic analyses is needed to further our understanding.

### 2.5.1. Astrocyte metabolism.

Astrocytes assume pivotal roles in governing brain energy metabolism, significantly influencing brain functions, encompassing memory<sup>242-244</sup>, neuroprotection<sup>245</sup>, resistance to oxidative stress<sup>246-248</sup>, and maintenance of homeostatic equilibrium<sup>211</sup>. The brain's energy requisites are substantial, constituting a continuous allocation of 20–25% of the entire body's energy consumption<sup>30</sup>. The brain's energy provision closely intertwines with neuronal activity<sup>249</sup>, underpinning the origins of signals detected by widely used functional brain imaging methods, including functional magnetic resonance imaging and positron emission tomography<sup>250-253</sup>. Notably, the orchestration of neuroenergetic coupling falls within the purview of astrocytes, accomplished through glutamate uptake, triggering astrocytic aerobic glycolysis, and culminating in glucose uptake and the release of lactate<sup>254,255</sup>, an operation christened the "Astrocyte Neuron Lactate Shuttle"<sup>256</sup>. This mechanism is complemented by neurotransmitters such as noradrenaline and Vasoactive Intestinal Peptide, invoking glycogen mobilization—exclusively ensconced within astrocytes—ultimately resulting in lactate release<sup>257-259</sup>. The consequential transfer of lactate to neurons is then used as a rapid energy source, following conversion to pyruvate<sup>260</sup>. Furthermore, lactate doubles as a signaling agent<sup>261,262</sup>, modulating neuronal excitability<sup>263-265</sup>, homeostasis<sup>266</sup>, and the expression of vital survival and plasticity genes<sup>196,267,268</sup>, suppresses interferon<sup>269</sup>, modifies histone<sup>270</sup>, activates GPCRs<sup>271</sup>, upregulates kinases<sup>272</sup>, controls Mg<sup>273</sup> and Fe<sup>274</sup>, links cannabis to social behavior<sup>275</sup>, inhibits proteases<sup>276</sup>, stabilizes HIF<sup>277</sup>, and activates electron transport chain (ETC)<sup>278</sup>. An important observation underscores the gradual decline of glycolysis in astrocytes and more broadly, cerebral glucose metabolism, particularly in the context of aging<sup>279-281</sup> and age-associated neurodegenerative disorders, exemplified by AD<sup>282-285</sup>.

In the normal functioning of the brain, astrocytes and neurons forge a complex and interdependent relationship. This serves a dual purpose: the upkeep of neuronal functionality, as well as providing vital sustenance to brain metabolism<sup>286-290</sup>. Predominantly, the central nervous system's aerobic metabolism is steered by neurons due to their considerable ATP prerequisites, notably during neuronal activation<sup>291</sup>. In contrast, astrocytes carve a more modest metabolic niche, essential for mitigating the fluctuations in neurons' interactions with the bloodstream<sup>292</sup>. In conjunction, astrocytes contribute significantly to maintaining the blood-brain barrier, an intricate structure that facilitates glucose conveyance to the extracellular arena, emerging as the primary initial metabolite

for the brain<sup>293-295</sup>. Additionally, astrocytes stockpile glycogen, offering a buffer against hypoglycemia<sup>296,297</sup>. The crux of astrocyte metabolism centers on deriving ATP via complete glycolysis, culminating in the expulsion of lactate into the extracellular domain<sup>31-35</sup>. Remarkably, extracellular lactate levels within the human brain outpace systemic levels<sup>298,299</sup>, imparting substantial support to neuronal aerobic metabolism, complementing the direct usage of glucose by neurons. The interaction between astrocytic lactate expulsion and neuronal uptake orchestrates an intricate equilibrium in response to neuronal activation timelines<sup>33,300</sup>.

Astrocytes adeptly oversee the equilibrium within the extracellular space. Their sensitivity to heightened neuronal metabolic requirements is accomplished through an array of intercellular messenger molecules, including glutamate<sup>36</sup>, potassium<sup>37</sup>, nitric oxide (NO)<sup>38-40</sup>, hydrogen peroxide (H<sub>2</sub>O<sub>2</sub>)<sup>41,42</sup>, and ammonia<sup>43</sup>. The functionality of mitochondria and the citric acid cycle (also known as the tricarboxylic acid cycle [TCA]) within astrocytes substantially diverges from that observed in neurons. Astrocytic metabolism prioritizes synthetic or cataplerotic pathways, crucial for generating glutamine, for neuronal use<sup>288,294,295,301</sup>. A notable facet of astrocytic activity revolves around the absorption of glutamate, arising from neuronal synaptic spillover<sup>302</sup>. Swift glutamate absorption, facilitated by transporters within astrocytes, moderates the synaptic activity of glutamate<sup>302</sup>, akin to the role of acetylcholinesterase at neuromuscular junctions<sup>303</sup>. This dynamic cycle reaches its zenith with the expulsion of glutamine by astrocytes, indispensable for the subsequent regeneration of neuronal glutamate. Much of this glutamine originates from the astrocytic TCA cycle through α-ketoglutarate (α-KG) synthesis. Consequently, astrocytes predominantly generate ATP through anaerobic glycolysis and lactate expulsion (while concurrently generating ATP through the TCA cycle). In contrast, neurons primarily thrive on a foundation of aerobic mitochondrial metabolism. This inherent resilience against oxygen deprivation is exemplified by the well-acknowledged ability to culture astrocytes (or astrocytoma cells) for up to 24 hours using adult brain tissue, and even cadaveric sources. This striking contrast is highlighted by neurons' inability to endure more than 3 to 5 minutes in an oxygen-depleted environment<sup>304</sup>.

While glucose catabolism is the primary energy source in the CNS, ongoing research underscores the significance of lipid metabolism in maintaining brain equilibrium. Around 20% of brain oxidative energy in rat brains is attributed to fatty acid oxidation (FAO)<sup>44</sup>. As the brain ages, there's an observed rise in the utilization of free fatty acids and ketone bodies<sup>305</sup>, possibly due to decreased glucose efficiency linked to aging and neurodegenerative diseases<sup>306</sup>. Interestingly, an essential component of the mitochondrial trifunctional protein complex in the FAO cycle<sup>307</sup>, hydroxyacyl-CoA dehydrogenase/3-ketoacyl-CoA thiolase/enoyl-CoA hydratase α (HADHA), is mainly

colocalized with GFAP+ astrocytes<sup>308</sup>, implying astrocytes as the primary site of brain FAO<sup>44</sup>. This suggests that astrocytic lipid metabolism might contribute to neurological diseases such as neurodegenerative disorders and brain injury. In essence, lipid droplets (LDs) are primarily generated to serve as fuel for  $\beta$ -oxidation<sup>309,310</sup>. Hyperactive neurons seem to channel excess/toxic fatty acids to astrocytic LDs for energy production via mitochondrial  $\beta$ -oxidation<sup>248</sup>, possibly due to higher expression of FAO genes in astrocytes compared to neurons<sup>311</sup>. Furthermore, upregulated astrocyte-specific energy production through FAO protects against ischemic stroke-induced damage<sup>308</sup>. Thus, astrocytic mitochondrial  $\beta$ -oxidation of LDs appears to both shield neurons from FA toxicity and provide energy. Although post-ischemic reactive astrocytes' upregulation of lipid metabolism might be beneficial<sup>230</sup>, there's a duality in their role, as seen in an HD mouse model where astrocytic shifts from glycolysis to FAO led to increased ROS-induced damage<sup>312</sup>. This suggests that the role of astrocyte LDs could either drive neuroprotection or contribute to neurodegenerative disorders, necessitating further investigation into the factors behind these varying effects on reactive astrocyte phenotypes.

Astrocytic networks play a significant role in being a key contributor to brain activity, plasticity, and behavior<sup>45</sup>. Because astrocytes claim their own tight and isolated territories<sup>46</sup>, it's essential for them to operate cohesively as functional networks to maintain complex behaviors. The spotting of astrocyte networks, intimately linked with neuronal circuits<sup>313</sup>, has pushed us to rethink how metabolic interactions between neurons and astrocytes might operate in the brain. In a groundbreaking 2008 paper, Nathalie Rouach and Christian Giaume uncovered that energetic metabolites are supplied through groups of connected astrocytes, more efficiently reaching distantly located sites with high neuronal demand<sup>294</sup>. They noted that two gap-junction subunit proteins (connexin 43, Cx43; connexins 30, Cx30) offer an activity-dependent pathway for transporting energetic metabolites from blood vessels to far-off neurons. Intriguingly, this trafficking of metabolites is regulated by glutamatergic synaptic activity, and directly delivering glucose or lactate to an astrocyte can uphold glutamatergic synaptic transmission even without external glucose. Subsequent studies have consistently supported these early findings and validated that astroglial metabolic networks have a crucial role in supporting complex behaviors and are disrupted in various brain diseases. Among these complex behaviors, sleep is universal across vertebrate and invertebrate animals. Adenosine acts as a transmitter that drives the need for sleep following extended wakefulness<sup>314</sup>. In 2009, experiments hinted that astrocytes might be the source of adenosine, which then influences neuronal A1 receptors to induce sleep<sup>315</sup>. This marked one of the earliest experimental instances of active glial participation in mammalian behavior<sup>249</sup>. Nearly a decade later, the same group offered evidence that an astrocyte network functioning in the lateral hypothalamus and mediated by Cx43 played a critical role in transporting lactate needed for the proper functioning of orexin neurons, a subset of neurons involved in the circadian

sleep/wake cycle and arousal<sup>316</sup>. Efficiently delivering energy substrates via gap junction-mediated astrocytic networks stands as a leading contender to effectively fulfill neuronal energy needs during activity.

### 2.5.2. Astrocytes in bipolar disorder and schizophrenia.

-----to be written-----

Increasingly, it's being known that Li+ might have an influence on glial cells, especially astrocytes<sup>317,318</sup>. Astrocyte dysfunction has been implicated in BD<sup>59,319</sup> and also in the mechanism of action of Li+<sup>317,320</sup>. Stable isotope-resolved metabolomics (SIRM) approach showed that Li+ enhanced glycolytic and Krebs cycle activity in both astrocytes and neurons, especially the anaplerotic pyruvate carboxylation (PC). The study also showed that Li+ stimulated the extracellular release of 13C labeled -lactate, -alanine (Ala), -citrate, and -glutamine (Gln), specifically by astrocytes<sup>317</sup>. It has also been shown that concentration of myo-inositol is higher in astrocytes than in neurons, and has been widely considered an astroglial metabolic marker<sup>321</sup>. In addition, cortical neuron cultures do not express the enzyme myo-inositol phosphate synthase (MIP-synthase), but rather depend on extracellular supply of myo-inositol<sup>322</sup>. In-vitro studies have shown that astrocytes are metabolically involved in the maintenance of the ionic and osmotic environment of the CNS. Increase in activity of oxidative enzymes (succinic dehydrogenase, DPN-diaphorase, etc.) in astrocytes has been associated with salt concentrations (NaCl, MgCl2 and LiCl) of the environment, and this was considered a specific metabolic response which was seen only in astrocytes<sup>318</sup>. Overall, these observations make astrocytes more attractive and a probable candidate for Li+'s action leading to myo-inositol homeostasis in the brain, compared to neurons.

### 2.5.3. Astrocytes in neurodegeneration.

-----to be written-----

2.6. Tools to study metabolism.

---

---

2.6.1. Experimental methods.

---

---

2.6.2. Computational modeling.

---

---

2.6.3. Constraint-based reconstruction and analysis (COBRA).

---

---

2.7. Preview of dissertation.

---

---

2.7.1. Rationale for the study.

---

---

### **3. Aims and objectives.**

To generate genome-scale metabolic models of human astrocytes using publicly available 'omic data obtained from psychiatrically ill patients (BD, SCZ) and healthy controls, and explore the metabolic changes associated with treatment responsiveness to Li<sup>+</sup> in BD, but also to understand the shared metabolic biology of BD with SCZ ([Figure 1](#)).

The objectives were as follows:

#### **3.1. Deriving the human astrocyte metabolic models.**

- a. Pre-processing and quality control of public data.
- b. Integrating phenotype-specific transcriptomes and glial proteome data with Recon3D.
- c. Expanding draft metabolic models through manual curation of literature.
- d. Imposing experimental nutrient uptake constraints.

#### **3.2. Using the models to identify disrupted metabolic fluxes in BD (Li<sup>+</sup> Responders and Non-Responders) and SCZ patients' astrocytes.**

- a. Setting up the analytical methods to solve metabolic models.
- b. Filtering reactions relevant to phenotype-of-interest.
- c. Metabolic-subSystem enrichment analysis (MSEA).
- d. Identifying disruptions that are significant across modules.

#### **3.3. Using the models to identify the impact of loss-of-function (LoF) mutations implicated in neuropsychiatric disorders.**

- a. Curating the genes with LoF mutations implicated in severe mental illness (SMI), Alzheimer's disease (AD) and Parkinson's disease (PD).
- b. Setting up the analytical method to simulate the effects of LoF mutations on the metabolic models.
- c. Identifying the fluxes disrupted by LoF mutations.

Objectives 3.1 and 3.2 will be executed in [Section 4](#), while objectives 3.3 will be executed in [Section 5](#).

## 4. Metabolic modeling of astrocytes in bipolar disorder and schizophrenia.

### 4.1. Introduction.

Bipolar disorder (BD) is a severe psychiatric illness characterized by manic/depressive episodes and persistent neurocognitive impairments<sup>3</sup>, affecting 0.5% of the population (ca. 7 million in India)<sup>4</sup>. It is a significant cause of disability, morbidity, and mortality (15% die by suicide)<sup>5</sup>. Lithium (Li+), a WHO “essential medicine”, is the only effective drug for preventing suicides<sup>27,28</sup> and improving cognition<sup>29</sup> in BD patients. There are many biochemical pathways which have been implicated in the pathobiology of BD and the mechanisms of Li+, including the inositol metabolism, cyclic nucleotide metabolism, glycogen synthase kinase 3β signaling, glutamate pathways, and circadian clock systems<sup>139</sup>. However, the exact mechanisms are enigmatic leading to absence of predictive markers.

Astrocyte dysfunction has been implicated in BD<sup>59,319</sup> and also in the mechanism of action of Li+<sup>317,320</sup>. Stable isotope-resolved metabolomics (SIRM) approach showed that Li+ enhanced glycolytic and Krebs cycle activity in both astrocytes and neurons, especially the anaplerotic pyruvate carboxylation (PC). The study also showed that Li+ stimulated the extracellular release of 13C labeled -lactate, -alanine (Ala), -citrate, and -glutamine (Gln), specifically by astrocytes<sup>317</sup>. It has also been shown that concentration of myo-inositol is higher in astrocytes than in neurons, and has been widely considered an astroglial metabolic marker<sup>321</sup>. In addition, cortical neuron cultures do not express the enzyme myo-inositol phosphate synthase (MIP-synthase), but rather depend on extracellular supply of myo-inositol<sup>322</sup>. In-vitro studies have shown that astrocytes are metabolically involved in the maintenance of the ionic and osmotic environment of the CNS. Increase in activity of oxidative enzymes (succinic dehydrogenase, DPN-diaphorase, etc.) in astrocytes has been associated with salt concentrations (NaCl, MgCl2 and LiCl) of the environment, and this was considered a specific metabolic response which was seen only in astrocytes<sup>318</sup>. Overall, these observations make astrocytes more attractive and a probable candidate for Li+'s action leading to myo-inositol homeostasis in the brain, compared to neurons.

Because screening for these metabolic pathways in astrocytes, in-vivo or in-vitro, is a substantial task, we adopted an alternative, computational approach to narrow down towards putative candidates that could be experimentally validated ([Fig.1](#)). First, by integrating publicly-available transcriptomics and proteomics data with the constraint-based reconstruction and analysis (COBRA) framework<sup>323</sup>, we have derived genome-scale metabolic models (GSMM) of astrocytes derived from BD, SCZ patients and healthy controls. We improved upon prior brain metabolic models by extensive manual curation of literature to identify the metabolic functions and extracellular nutrient uptake constraints relevant to astrocytes. In BD, we derived separate metabolic models for Li+

responders and non-responders to analyze metabolic fluxes related to treatment responsiveness. Despite the shared clinical symptomatology, genetics and biology between BD and SCZ, there is limited evidence supporting the effectiveness of Li<sup>+</sup> as a standalone treatment for SCZ patients<sup>324</sup>. To explore the specificity of Li<sup>+</sup>'s efficacy in BD compared to SCZ, we hypothesized that it might be reflected at the molecular/metabolic level, and thus we derived metabolic models of astrocytes from SCZ patients, particularly monozygotic twin pairs (SCZ twins and Healthy twins), along with matched controls. And subsequently, by using diverse analytical methods we have identified metabolic fluxes that are specifically disrupted in the astrocytes of BD, BD-Responders, BD-NonResponders and SCZ Twins, as compared to healthy/control models, thereby gaining insights into the differences between these conditions.

One of the advantages of GSMM is that it can describe the metabolic state of cells at a steady state without the need for detailed knowledge of enzymatic kinetics<sup>323</sup>, which is difficult to estimate at a network level. Modeling studies like this have been extensively used in the past decade to explain not only human metabolism in general<sup>325</sup> but also the effects of human disease phenotypes<sup>326-329</sup>.

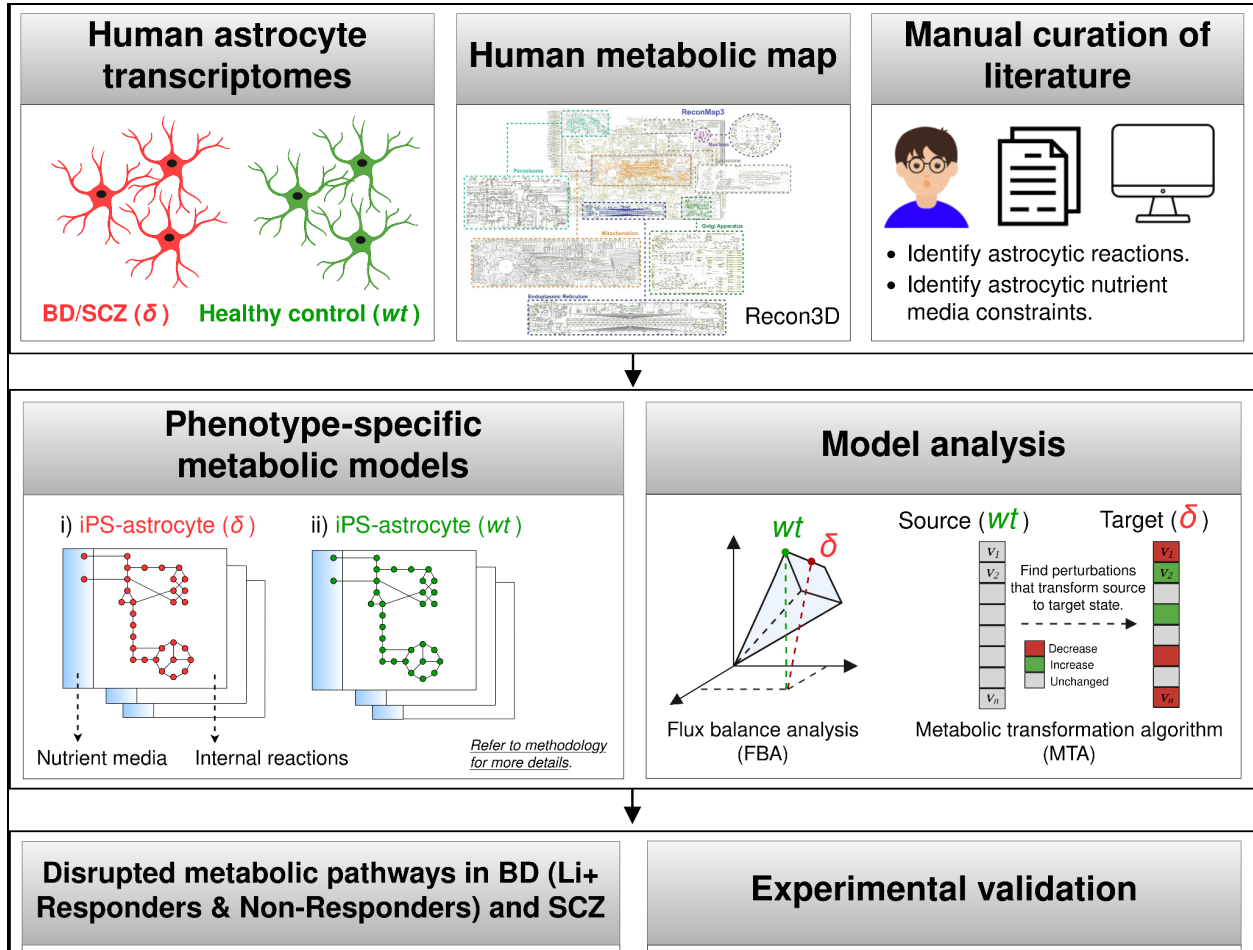


**Figure 1. Graphical abstract. Metabolic modeling of astrocytes in BD and SCZ.**

Firstly, genome-scale metabolic models (GSMM) of astrocytes from BD, SCZ patients, and healthy controls were constructed by integrating publicly-available transcriptomics data, proteomics data with the constraint-based reconstruction and analysis (COBRA) framework. Separate metabolic models for Li<sup>+</sup> responders and non-responders were derived to analyze metabolic fluxes related to treatment responsiveness. Metabolic models of astrocytes from SCZ patients were derived to explore the shared metabolic phenotypes with BD. Enhancements to previous brain metabolic models were achieved through comprehensive manual curation of literature, identifying relevant metabolic functions and extracellular nutrient uptake constraints relevant to astrocytes. Subsequently, diverse analytical methods were employed to identify disrupted metabolic fluxes in astrocytes from BD, BD-Responders, BD-NonResponders and SCZ Twins.

## 4.2. Materials and methods.

### 4.2.1. Key resources table

REAGENT or RESOURCE	REFERENCE	IDENTIFIER or LINK
<b>Data</b>		
Zhang, Human Primary Astrocyte, RNA-Seq	<sup>330</sup>	GSE73721
Vadodaria, Human iPSC Astrocyte, BD/Ctrl, RNA-Seq	<sup>59</sup>	GSE157509
Koskuvi, Human iPSC Astrocyte, SCZ/Ctrl, RNA-Seq	<sup>60</sup>	GSE191248
Human glia, Proteomics (semi-quantitative immunohistochemistry abundance)	<sup>331</sup>	<a href="https://www.proteinatlas.org/download/normal_tissue.tsv.zip">https://www.proteinatlas.org/download/normal_tissue.tsv.zip</a>
Recon3D	<sup>325</sup>	<a href="https://www.vmh.life/#downloadview">https://www.vmh.life/#downloadview</a>
<b>Software and Algorithms</b>		
FastQC	-	<a href="https://www.bioinformatics.babraham.ac.uk/projects/fastqc/">https://www.bioinformatics.babraham.ac.uk/projects/fastqc/</a>
Cutadapt	-	<a href="https://cutadapt.readthedocs.io/en/stable/">https://cutadapt.readthedocs.io/en/stable/</a>
HISAT2	<sup>332</sup>	<a href="http://daehwankimlab.github.io/hisat2/">http://daehwankimlab.github.io/hisat2/</a>
Samtools	<sup>333</sup>	<a href="http://samtools.sourceforge.net/">http://samtools.sourceforge.net/</a>
Cufflinks	<sup>334</sup>	<a href="http://cole-trapnell-lab.github.io/cufflinks/">http://cole-trapnell-lab.github.io/cufflinks/</a>

org.Hs.eg.db	-	<a href="https://bioconductor.org/packages/release/data/annotation/html/org.Hs.eg.db.html">https://bioconductor.org/packages/release/data/annotation/html/org.Hs.eg.db.html</a>
COBRA Toolbox v3.0	323	<a href="https://opencobra.github.io/cobratoolbox/stable/">https://opencobra.github.io/cobratoolbox/stable/</a>
iMAT	335	-
GIMME	336	-
MBA	337	-
FastCore	338	-
Metabolic Transformation Algorithm (MTA)	326,339,340	<a href="https://github.com/ImNotaGit/MTA">https://github.com/ImNotaGit/MTA</a>
Gurobi optimizer	-	<a href="https://www.gurobi.com/">https://www.gurobi.com/</a>
MATLAB R2015b	-	<a href="https://in.mathworks.com/products/matlab.html">https://in.mathworks.com/products/matlab.html</a>
R version 3.6.3	-	<a href="https://www.r-project.org/">https://www.r-project.org/</a>
Custom scripts for model generation and analysis	This study	<a href="https://github.com/anin90/AstroModel">https://github.com/anin90/AstroModel</a>

#### 4.2.2. Dataset overview.

Three previously published transcriptome datasets: "Zhang"<sup>330</sup>, "Vadodaria"<sup>59</sup>, "Koskuvi"<sup>60</sup>, were utilized. In Zhang, the astrocytes were purified from mice, human fetal, and adult brain tissues using immunopanning. The mice data were excluded from our analysis leaving us with 41 human subjects including six fetal astrocyte samples, 12 adult astrocyte samples, eight glioblastoma multiforme (GBM) or sclerotic hippocampal samples, four whole human cortex samples, and 11 human samples of other purified CNS cell types. Healthy astrocytes, except for the GBM and sclerotic samples, were obtained from fetal brain tissue from elective pregnancy terminations at 17–20 gestational weeks or healthy temporal lobe cortices from patients undergoing neurological surgeries. In Vadodaria, the astrocytes were derived from induced pluripotent stem (iPS) cells generated from fibroblasts of BD patients (n=5), which includes both Li+ responders (n=3) and non-responders (n=2), as well as healthy controls (n=4). The astrocytes were differentiated

for five weeks, and subsequently stimulated with 10 ng/mL IL-1b or phosphate buffered saline (PBS) for 5h, followed by RNA-Seq. Similarly, in Koskuvi, the astrocytes were derived from iPS cells generated from fibroblasts of monozygotic twin pairs discordant for SCZ (n=4), which includes both healthy twins (HT, n=4) and SCZ twins (ST, n=4), as well as age- and sex- matched healthy controls (n=6). RNA was extracted from the monolayer culture of iPS-derived astrocytes (150 DIV i.e., days in vitro), followed by RNA-Seq. All three datasets were uniformly processed using a consensus set of tools. After processing and quality control, "Zhang" was used to derive metabolic models of primary astrocytes, while "Vadodaria" and "Koskuvi" were used to derive metabolic models of iPS-astrocytes.

#### 4.2.3. Pre-processing and quality control of public data.

##### 4.2.3.1. RNA-sequencing.

Transcriptome data (FastQ) were obtained by downloading from public repositories (Zhang/Vadodaria/Koskuvi). The non-human samples, if any, were removed from Zhang, Vadodaria and Koskuvi. FastQC (<http://www.bioinformatics.babraham.ac.uk/projects/fastqc>) was used to assess the quality of the reads and Cutadapt (<https://cutadapt.readthedocs.io/en/stable/>) was used to remove adapter contamination. HISAT2<sup>332</sup> was used to align the filtered reads to the human reference genome (GRCh37). Samtools<sup>333</sup> was used for SAM to BAM conversion and sorting. Cufflinks<sup>334</sup> was used to estimate gene-level expression (FPKM), and gene symbols were annotated for NCBI Entrez IDs using org.Hs.eg.db. The non-specific genes i.e., same gene symbol mapping to multiple Entrez IDs or multiple symbols mapping to the same ID were excluded. For Zhang, Vadodaria and Koskuvi, the genes with FPKM  $\geq 0.1$  in at least 50% of all samples were considered, resulting in 13,423, 14,543 and 16,724 genes respectively.

##### 4.2.3.2. Proteomics.

The human cortical glial proteomics data from the human protein atlas (HPA)<sup>331</sup> were utilized to provide further evidence of expression in Zhang, Vadodaria and Koskuvi. The reliability scores ('Enhanced', 'Supported', 'Approved', or 'Uncertain') and the semi-quantitative nature of the immunohistochemistry protein abundance ('High', 'Medium', 'Low') were retained<sup>341</sup>.

#### 4.2.4. Metabolic modeling of astrocytes.

##### 4.2.4.1. Integration of phenotype-specific astrocyte transcriptomes with Recon3D.

Recon3D<sup>325</sup>, the latest human metabolic reaction library, was used to extract draft metabolic models. While all the samples in the Zhang, Vadodaria, and Koskuvi datasets were processed (FASTQ to FPKM), only a subset of samples was chosen from each dataset for

metabolic modeling. In Zhang, only cortical astrocytes from adult samples (n=12) were included. In the Vadodaria dataset, only PBS treated iPS-astrocytes from BD patients (n=5) and healthy controls (n=4) were considered. However, in the Koskuvi dataset, the entire dataset, including iPS-astrocytes from SCZ twin pairs (n=4) and healthy controls (n=6), was utilized for modeling. In Vadodaria, the BD patient data was further divided into Li+ responders (n=3) and non-responders (n=2) for modeling treatment responsiveness. In Koskuvi, the monozygotic twin pairs were further divided into SCZ twins (n=4) and healthy twins (n=4) for modeling the effects of familial/genetic risk. Genes that were detected in the transcriptome (n=13,423, Zhang; n=14,543, Vadodaria; n=16,724, Koskuvi) but had 'uncertain' reliability in the HPA glial proteome were excluded, resulting in a subset of genes that were "transcriptome & proteome" evident (n=4,105, Zhang; n=4,040, Vadodaria; n=4,203, Koskuvi). Metabolic models for eight distinct phenotypes were obtained by constraining Recon3D with the transcriptome data of:

1. Zhang: Primary astrocytes (Primary-Ctrl),
2. Vadodaria: iPS-astrocytes from Healthy controls (iPS-Ctrl-a),
3. Vadodaria: iPS-astrocytes from BD patients (iPS-BD),
4. Vadodaria: iPS-astrocytes from BD patients - responders (iPS-BD-R),
5. Vadodaria: iPS-astrocytes from BD patients - non-responders (iPS-BD-NR),
6. Koskuvi: iPS-astrocytes from Healthy controls (iPS-Ctrl-b),
7. Koskuvi: iPS-astrocytes from monozygotic twin pairs - SCZ twins (iPS-ST),
8. Koskuvi: iPS-astrocytes from monozygotic twin pairs - Healthy twins (iPS-HT).

The genes were mapped to reactions using the function *mapExpressionToReactions* in COBRA Toolbox. The reactions were associated with a core reaction set (n=1843, Zhang; n=1765, Vadodaria; n=1836, Koskuvi). Different variants of the model extraction methods (MEMs) such as iMAT<sup>335</sup>, GIMME<sup>336</sup>, MBA<sup>337</sup> and FastCore<sup>338</sup> were considered. Both absolute (abs) and normalized (norm) FPKM values were used to generate the metabolic models. Three gene expression thresholds ( $FPKM_{abs}$ ,  $FPKM_{norm.t1}$ ,  $FPKM_{norm.t2}$ ) were used, and for each of them, the high-confidence (HC), medium-confidence (MC) and inactive (IA) reactions were defined as follows,

a.)  $FPKM_{abs}$ :

$$\begin{aligned}
 G_i &= \text{rowMax}_i(\text{abs}(FPKM)) \\
 HC &\leftarrow \text{if } G_i > 2 \\
 MC &\leftarrow \text{if } 2 \leq G_i \leq 0.1 \\
 IA &\leftarrow \text{if } G_i < 0.1
 \end{aligned}$$

b.)  $FPKM_{norm.t1}$ :

$$\begin{aligned} G_i &= \text{rowMax}_i(\text{quantilenorm}(\log_{10}(FPKM + 1))) \\ HC &\leftarrow \text{if } G_i > 50\text{th percentile}(\bar{G}) \\ MC &\leftarrow \text{if } 50\text{th percentile}(\bar{G}) \leq G_i \geq 25\text{th percentile}(\bar{G}) \\ IA &\leftarrow \text{if } G_i < 25\text{th percentile}(\bar{G}) \end{aligned}$$

c.)  $FPKM_{norm.t2}$ :

$$\begin{aligned} G_i &= \text{rowMax}_i(\text{quantilenorm}(\log_{10}(FPKM + 1))) \\ HC &\leftarrow \text{if } G_i > 25\text{th percentile}(\bar{G}) \\ MC &\leftarrow \text{if } 25\text{th percentile}(\bar{G}) \leq G_i \geq 10\text{th percentile}(\bar{G}) \\ IA &\leftarrow \text{if } G_i < 10\text{th percentile}(\bar{G}) \end{aligned}$$

Where  $G_i$  is the maximum expression value of the  $i^{th}$  gene across all samples. The above thresholds were also used to define inactive reactions (IA), unless manual curation of literature dictated otherwise.

Draft metabolic models of astrocytes were generated from the transcriptomes of eight phenotypes (Primary-Ctrl, iPS-Ctrl-a, iPS-BD, iPS-BD-R, iPS-BD-NR, iPS-Ctrl-b, iPS-ST and iPS-HT) using four MEMs (iMAT, GIMME, MBA, and FastCore) across three gene expression thresholds ( $FPKM_{abs}$ ,  $FPKM_{norm.t1}$ ,  $FPKM_{norm.t2}$ ). iMAT and MBA require a 'medium-confidence' threshold to be defined by users, while GIMME and FastCore do not. The MEMs maximize the number of high-confidence and minimize the number of medium-confidence reactions in their output models. The 24 models that captured the least fluxInconsistent reactions, the highest number of core reactions, and the highest overlap with astrocytic reactions ( $n=649$ ) from Lewis et al. 2010, for each of the eight phenotypes, were chosen for further expansion.

#### 4.2.4.2. Manual curation of astrocytic reactions for the expansion of draft metabolic models and defining model function tests.

Extensive manual curation of the literature was conducted to identify biochemical reactions ( $n=159$ ) in astrocytes, which exhibited behavioral, cellular, or molecular phenotypes upon disruption. Their rationale for inclusion, along with PMIDs supporting and refuting their activity in astrocytes, was also provided. Most of the literature evidence was derived from studies on rodent models. While these curated reactions were mostly part of Recon3D, a significant number of them were not detected by the automated model extraction methods

(MEMs) across all 24 models. Consequently, it became necessary to identify the missing metabolites and reactions, conduct gap-filling, and incorporate these reactions into the models. As part of this effort, an additional extracellular compartment 'synapse' [s], along with exchange ( $n=15$ ) and transport reactions ( $n=14$ ), were included in the 'Primary-Ctrl' models to capture astrocyte-synapse metabolic crosstalk ([Fig.S3](#)). However, the synaptic compartment and corresponding reactions were not included in the iPS-astrocyte models. Additionally, the curated reactions were also used as model function tests (MFTs), ensuring that all 24 models carried non-zero flux through the curated reactions, subject to nutrient media constraints.

#### 4.2.4.3. Imposing astrocytic nutrient uptake constraints.

A crucial assumption was made that culture media components exist in systemic circulation<sup>342</sup>, traverse the blood-brain barrier (BBB), and are accessible for astrocyte uptake. Hence, the 'Primary-Ctrl' models' extracellular compartment [e] was constrained by all metabolites and ions that i) constitute the astrocyte sustenance medium (ASM)<sup>343</sup>, and ii) cross the blood brain barrier (BBB)<sup>344</sup>. The remaining iPS-astrocyte models' extracellular [e] compartments were constrained by ASM alone, representing culture media conditions ([Fig.S3](#)). The metabolic components of the ASM, which consists of Neurobasal medium, Minimum Essential Medium - Non-Essential Amino Acids Solution, GlutaMAX Supplement, and N-2 Supplement, were obtained from the Thermo Fisher Scientific™ website. The metabolic components of the BBB were obtained from Thiele et al.<sup>344</sup>. There are 22 components that overlap between the ASM ( $n=44$ ) and BBB ( $n=45$ ). To simulate nutrient uptake, all nutrient uptakes in the model except for the 67 exchanges added to the extracellular compartment [e], for which uptake rates were set to -10mmol/gDw/h, were set to 0.

#### 4.2.5. Identifying disrupted reactions & subSystems in BD and SCZ astrocyte metabolic models.

##### 4.2.5.1. Flux balance analysis (FBA)

A metabolic network consisting of  $m$  metabolites and  $n$  reactions is represented by a stoichiometric matrix  $S$  where  $S_{ij}$  represents the stoichiometric coefficient of metabolite  $i$  in reaction  $j$ . The flux vector for each reaction in the network is represented by  $v$ . Flux balance analysis (FBA) assumes a steady-state mass balance wherein the sum of the input flux equals the sum of the output flux. This follows as,  $dx_i / dt = 0$  i.e. the change in concentration of the  $i^{th}$  metabolite over time is zero<sup>345</sup>. Flux variability analysis (FVA) was used to calculate the minimum and maximum flux through each reaction in all five metabolic models subject to constraints,

$$\min/\max c^t x, \text{ s.t. } s.v = dx/dt = 0, \quad (1)$$

$$v_{\min} \leq v_j \leq v_{\max}, \quad (2)$$

where the equation (1) corresponds to the steady-state mass-balance constraints, whereas equation (2) corresponds to the reaction directionality and capacity constraints. The ratio of flux span ( $FSr$ )<sup>346</sup> for each reaction was calculated as follows,

$$FSr (\text{healthy vs disease}) = \frac{\text{abs}(FVAm_{j,\text{healthy}} - FVAmin_{j,\text{healthy}})}{\text{abs}(FVAm_{j,\text{disease}} - FVAmin_{j,\text{disease}})}, \quad (3)$$

where  $FVAm$  and  $FVAmin$  are the maximum and minimal flux through the  $j^{th}$  reaction in the model.  $FSr$  can be calculated only for those reactions that are captured by both the models under comparison. The reactions with  $FSr > 1.5$  and  $< 0.8$  were identified for each phenotype-of-interest (n=4 i.e., BD; BD\_Responder; BD\_NonResponder; SCZ-Twin), and subsequently considered for downstream analysis.

#### 4.2.5.2. Metabolic transformation algorithm (MTA)

The metabolic transformation algorithm (MTA)<sup>326,339,340</sup> identifies reactions in a metabolic network whose inhibition facilitates a transformation between two metabolic states (e.g., from diseased to healthy states, or vice-versa). The inputs to MTA are i) the transcriptomic measurements of the source and target states, and ii) the reference metabolic model. For each transformation analysis, MTA follows a two-step process: i) determining the flux distribution of the source metabolic state ( $v^{ref}$ ) using iMAT followed by ACHR sampling of the solution space. ii) determining the set of genes whose expression has significantly elevated or reduced between the source and target states. Using i) and ii), MTA computes a transformation score for each of the metabolic reactions in the cell, and usually, the 10-20% reactions with the highest MTA score contain promising candidate targets. For each phenotype-of-interest, we ran MTA twice, by swapping the source and the target states. E.g., in order to identify the reactions relevant to BD, we identified the reactions that transformed i) “iPS-Ctrl” to “iPS-BD”, and ii) “iPS-BD” to “iPS-Ctrl”. For either runs, the top 20% predictions were first identified, and subsequently their union sets were considered for downstream analysis.

#### 4.2.5.3. Filtering reactions relevant to phenotype-of-interest.

From the reactions as identified by FVA ( $FSr > 1.5$ ;  $FSr < 0.8$ ) or MTA (top 20%), filters were applied to select for reactions that were relevant to the phenotype-of-interest ([Table.1](#)). While defining the filters, it was important to consider the fact that the treatment

responders and the non-responders together comprise the BD cohort. Hence the fluxes relevant to “BD\_R” and “BD\_NR” can share overlaps with “BD”. A detailed protocol is provided in [supplementary section 8.1](#).

Phenotype-of-interest	Filtering criteria
BD <sup>a</sup>	Specifically disrupted in “iPS-Ctrl vs iPS-BD” & unchanged between control models.
BD-Responder <sup>b</sup>	Specifically disrupted in “iPS-Ctrl vs iPS-BD-Responder” & unchanged between control models.
BD-NonResponder <sup>c</sup>	Specifically disrupted in “iPS-Ctrl vs iPS-BD-NonResponder” & unchanged between control models.
SCZ-Twin <sup>d</sup>	Specifically disrupted in “iPS-Ctrl vs iPS-SCZ-Twin” & unchanged between control models.

<sup>a</sup>Can share overlaps with BD-Responder, BD-NonResponder and SCZ-Twin.  
<sup>b</sup>Can share overlaps with BD and SCZ-Twin but not with BD-NonResponder.  
<sup>c</sup>Can share overlaps with BD and SCZ-Twin but not with BD-Responder.  
<sup>d</sup>Can share overlaps with BD, BD-Responder and BD-NonResponder.

Table 1. Reaction filtering criteria. “Unchanged between control models” means the reactions that were not found to be disrupted in “iPS-Ctrl vs Primary-Ctrl”.

#### 4.2.5.4. Metabolic subSystem enrichment analysis (MSEA).

To test for enrichment of disrupted metabolic subSystems, a hypergeometric test was applied to each subSystem, and the P-value was calculated for each subSystem using the *phyper* function in R as below,

$$\text{phyper}(x - 1, m, n - m, k, \text{lower.tail} = \text{FALSE}) \quad (4)$$

Where  $n$  is the number of all reactions in the model,  $k$  is the number of the disrupted reactions within each tested subSystem,  $m$  is the total number of reactions within each disrupted subSystem, and  $x$  is the overlap size between  $k$  and  $m$ . This was followed by multiple-testing corrections using the Benjamini-Hochberg false discovery rate<sup>347</sup>, and subSystems with  $P_{FDR} < 0.05$  were considered as significant.

#### 4.2.5.5. Identifying disruptions that are significant across modules.

Here, a ‘module’ was defined as the list of subSystems that were predicted to be significant by MSEA, using either of the analytical approaches i.e., FBA/MTA. E.g. ‘FVA\_BD\_NR\_norm\_t1’ is a module - where ‘FVA’ is the analytical method, ‘BD\_NR’ is the phenotype-of-interest and ‘norm\_t1’ is the gene expression thresholding of the metabolic model. For each phenotype-of-interest (BD, BD-Responder, BD-NonResponder and SCZ-Twin), we generated

six modules (i.e., derived using three expression thresholds and two analytical methods), and identified the subSystems that were disrupted in at least two or more modules.

#### 4.2.6. Data, figures and code availability.

This study did not generate experimental data. Raw transcriptome data used in this study were publicly available. Figure panels were generated programmatically in R with the exception of Fig.1, Fig.3.b-c, and Fig.4 which was created using [BioRender.com](#) (full license) and [Diagrams.net](#) (open source). All original code has been deposited at GitHub (<https://github.com/anin90/AstroModel>) and will be made publicly available. References and identifiers are provided in the [key resources table](#).

#### 4.3. Results and discussion.

##### 4.3.1. Deriving and testing the human astrocyte metabolic models. ([Figure.2](#))

Draft metabolic models of astrocytes (n=56) were extracted for eight distinct phenotypes, including BD patients (iPS-BD, iPS-BD-R, iPS-BD-NR), SCZ twin (iPS-ST), healthy twin (iPS-HT) and healthy controls (Primary-Ctrl, iPS-Ctrl-a, iPS-Ctrl-b), by using transcriptome data and glial proteomics data as a constraint on the Recon3D human metabolic knowledgebase. The gene expression threshold determines the model contents, and there's no one model that's poised to explain the underlying biology<sup>348</sup>. Hence, three metabolic models were derived for each of the eight phenotypes by using different FPKM thresholds. Of the 56 models, only the iMAT-derived models (n=24) satisfied our selection criteria and only those were further expanded (refer Methodology section 3.3. for more details). First, the properties of the 24 models, before (preExpansion) and after expansion (postExpansion), were evaluated ([Fig.2.a-e](#)). The final models (i.e., postExpansion) consisted of 5,342–6,305 reactions and 3,679–4,273 metabolites. The flux inconsistency, which refers to the blocked reactions, ranged between ~22-29% in the final models, which is primarily driven by the nutrient media constraints, as opposed to zero blocked reactions in the draft models due to the unconstrained nutrient media. This constraint was necessary to ensure that the final models operated solely on physiologically relevant nutrient media conditions. The core reactions captured by all models ranged between ~70-98%, and the Lewis et al. astrocytic reactions captured by all models ranged between ~40-53%. The literature curated reactions (n=159) were also used as “metabolic tasks”, and all 24 models passed ~90-93% of the tasks. A comparison was performed between our models (This Study, n=24) and previously published mass-action models of brain metabolism (Predecessor, n=11) ([Fig.2.f-g](#)). The growth in the size of the models over time is mainly due to the ongoing development of larger metabolic knowledge bases like Recon3D. Overall, the statistics indicated that our models do recapitulate astrocyte physiology; were in-par with its equivalents<sup>327</sup> and were ready to be deployed for downstream analysis. We have provided the comprehensive details of all 24 models on Github for open access for the scientific community.

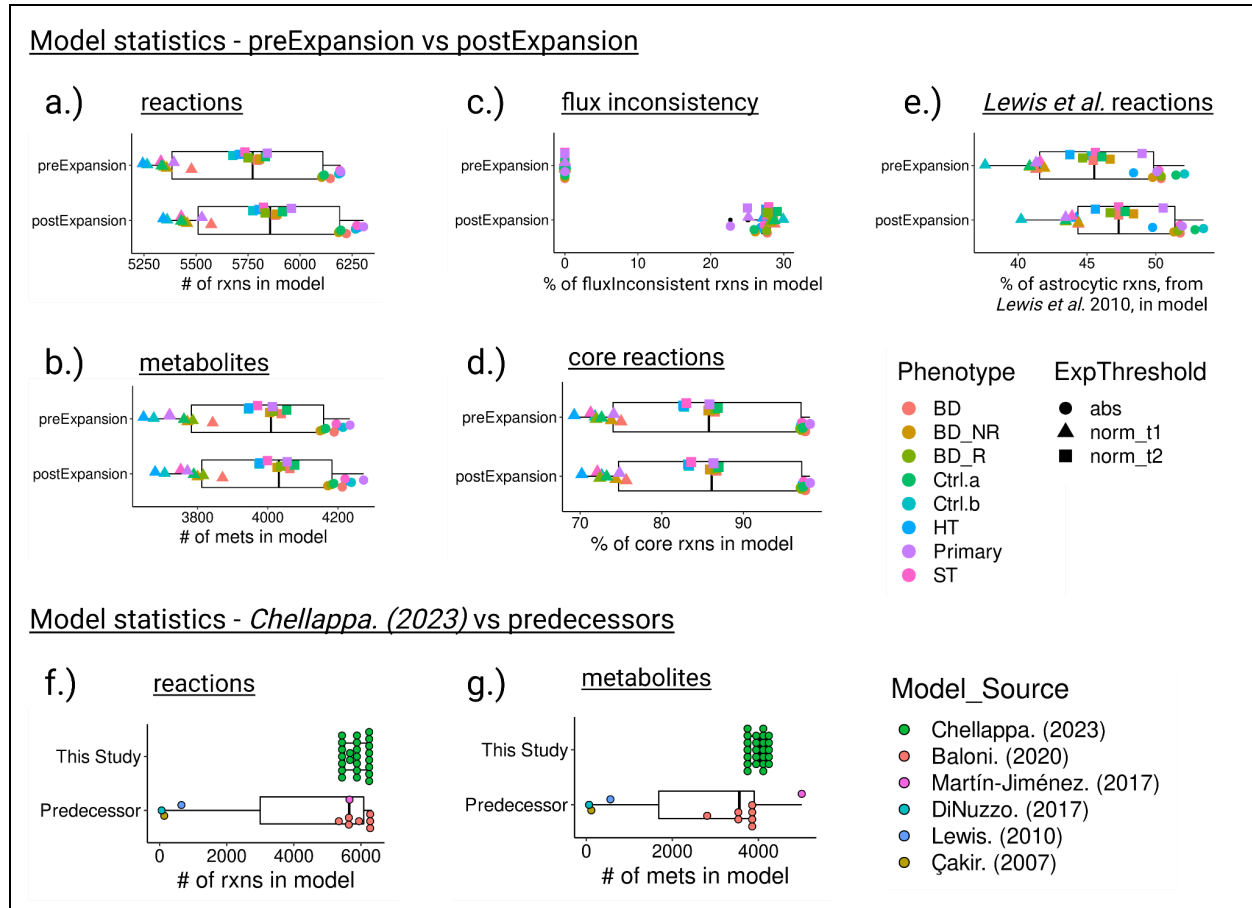


**Figure 2: Model statistics.** (a-e) Differences in model statistics observed between the iMAT-derived draft models (preExpansion, n=24) and the final models (postExpansion, n=24) of astrocyte metabolism, that were generated for five phenotypes across three gene expression thresholds. The model statistics include the # of reactions, # of metabolites, % of flux inconsistent reactions, % of core reactions and % of astrocytic reactions (Lewis et al. 2010), captured in the respective models. (f-g) Differences in model statistics observed between the models that were derived as a part of this study (This Study, n=24) and those captured by previous studies (Predecessor, n=11). Because the reconstructions of most predecessors were not publicly accessible, except for Lewis et al. (2010) and Baloni et al. (2020), the comparison was conducted solely based on the number of reactions and metabolites.

#### 4.3.2. Metabolic subsystems disrupted in BD/SCZ patients' astrocytes ([Figure 3](#))

To identify fluxes that are disrupted in our phenotypes-of-interest (BD, BD-Responder, BD-NonResponder and SCZ-Twin), the models ( $n=24$ ) were first divided into groups based on their FPKM thresholds ( $n=3$ ). This resulted in five models within each group. The flux distributions of the models within each group were analyzed using two methods - FVA and MTA. Filters were applied to select for reactions that were relevant to each phenotype-of-interest, followed by Metabolic-subSystem enrichment analysis (MSEA). The metabolic subsystems that were disrupted ( $P_{FDR} < 0.05$ ) in at least two or more modules were identified (Refer to the Methodology section 3.4. for more details). Thirteen subsystems were predicted to be disrupted by at least two or more modules across either of the four phenotypes-of-interest ([Fig.3.a](#)). However, none of these disruptions were found to be significant across all six modules while considering the  $\text{mean}(P_{FDR}) < 0.05$ .

##### 4.3.2.1. Slower PI-cycle in Li<sup>+</sup> Non-Responder astrocytes. ([Figure 3](#))

Eight subsystems were predicted to be specifically disrupted in the Li<sup>+</sup> non-responders models, while three subsystems were specifically disrupted in the Li<sup>+</sup> responders models. There were no subsystems disrupted across both Li<sup>+</sup> responders and non-responders ([Fig.3.b](#)). Among the eight disrupted subsystems in non-responders, inositol phosphate (IP) metabolism was captured by two modules ([Fig.3.a](#)). The flux through the reactions in this pathway ( $n=4$ ) was reduced, indicating slower synthesis rates compared to the Li<sup>+</sup> responder and the control models ([Fig.3.c-d](#)). The myo-inositol 1-phosphate phosphatase (MI1PP/IMAPase, catalyzing IP<sub>1</sub>→Inositol), one of the four disrupted reactions in the IP metabolism, has a long-standing association with Li<sup>+</sup>'s mechanisms of action<sup>143</sup>. The "inositol depletion" hypothesis posits that the depletion of inositol by Li<sup>+</sup> reduces the brain excitability in BD<sup>143</sup>. And this may happen through the ability of Li<sup>+</sup> to,

1. Inhibit MI1PP activity<sup>143</sup>,
2. Inhibit plasma membrane inositol transporters<sup>349</sup>,
3. Regulate the rate of inositol synthesis<sup>350</sup>.

Our models also predict slower syntheses of phosphoinositide (PI5P4K, catalyzing PIP→PIP<sub>2</sub>) and phosphoinositols (MI145PP, catalyzing IP<sub>3</sub>→IP<sub>2</sub>; and MI14P4P, catalyzing IP<sub>2</sub>→IP<sub>1</sub>), specifically in Li<sup>+</sup> non-responder astrocytes ([Fig.3.c](#)). This seems to be consistent with Sade *et al.*<sup>144</sup>, which suggests that Li<sup>+</sup> affects the entire phosphatidylinositol (PI) signaling system in two ways: first, by depleting inositol, thereby reducing phosphoinositide levels; and second, by elevating inositol monophosphate levels, leading to phosphoinositols accumulation.

Regardless of the molecular mechanism of Li<sup>+</sup> action, in BD patients inositol concentrations can change, and may be further altered by Li<sup>+</sup> treatment<sup>351</sup>. In contrast to the majority of metabolism studies that focus on metabolite concentrations, our model predictions are exclusively on fluxes, which represent the rates of reactions, and alterations in flux levels do not always indicate changes in metabolite concentrations<sup>352</sup>. Metabolite concentrations in a cell can increase due to fast synthesis or slower degradation processes. As a result, two interpretations can be derived from our model prediction of slower rates of synthesis of inositol, PIP<sub>2</sub>, IP<sub>2</sub> and IP<sub>1</sub>, specifically in Li<sup>+</sup> non-responders:

1. Our models challenge the depletion hypothesis, expecting a faster PI cycle (specifically a higher flux through MI1PP and PI5P4K) for its metabolites (inositol and PIP<sub>2</sub>) to accumulate in BD patients. This implies that there may be other factors contributing to the slower PI cycle observed in Li<sup>+</sup> non-responders.
2. Alternatively, the slower PI cycle could be indicative of lower enzyme concentrations that hinder the actions of Li<sup>+</sup> and subsequently impact the responsiveness in BD patients. It is important to note that the slower PI cycle is only observed in the models of Li<sup>+</sup> non-responders, while in Li<sup>+</sup> responders, the inositol fluxes remain unaffected. This might suggest that the levels of inositol monophosphatase (IMPAse), and/or the other enzymes in the PI cycle, may be maintained at a higher level in Li<sup>+</sup> responders, facilitating the desired response.

While the latter explanation appears to be the most plausible and parsimonious based on our predictions, experimental validation is necessary to confirm these hypotheses. Our models successfully capture the disruption of the phosphatidylinositol (PI) signaling system, a well-known aspect of Li<sup>+</sup> biology<sup>144,351</sup>. This validation enhances trust in the model predictions, and justifies further investigation of the novel predictions, such as the involvement of remaining seven disrupted subsystems in Li<sup>+</sup> non-responders that may not have been previously reported in the literature regarding BD/Li<sup>+</sup> biology.

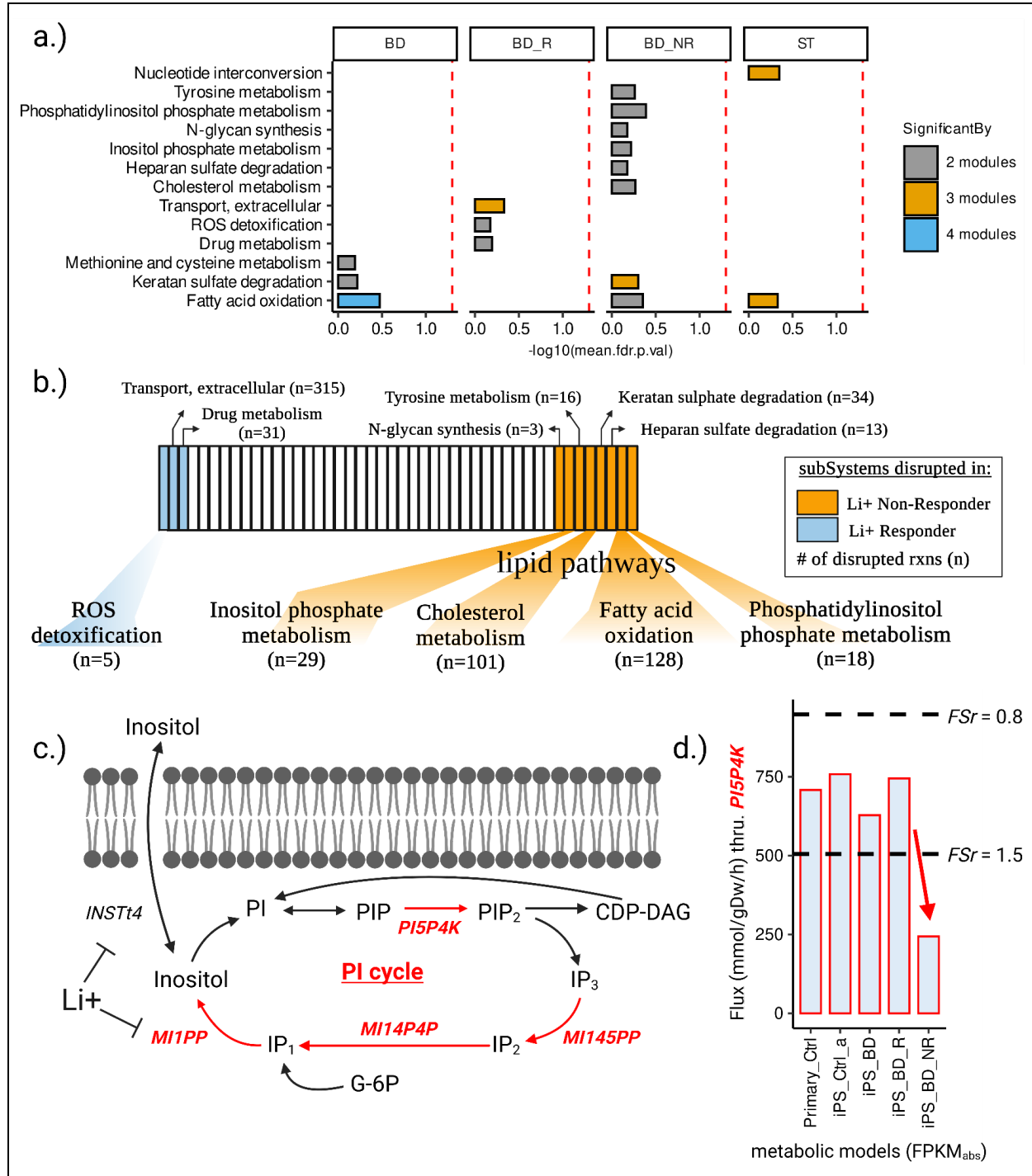


**Figure 3: Disrupted metabolic subsystems in BD and SCZ patients' astrocytes.**

**(a)** Metabolic subsystems ( $n=13$ ) predicted to be disrupted by at least two or more modules in any of the four target phenotypes (BD, BD-Responder, BD-NonResponder, and SCZ-Twin). **(b)** Metabolic subsystems predicted to be disrupted by at least two or more modules in Li<sup>+</sup> responders ( $n=3$ ) and non-responders ( $n=8$ ). The value 'n' represents the total number of disrupted reactions within each subsystem, captured by any of the six

modules. **(c)** Metabolic fluxes ( $n=4$ ) through the inositol phosphate metabolism (PI cycle) were found to be reduced (red) specifically in Li<sup>+</sup> non-responder metabolic models. **(d)** Bar plot highlighting the reduced flux through Phosphatidylinositol-5-Phosphate 4-Kinase (PIP4K), specifically within the Li<sup>+</sup> non-responder metabolic model.

#### 4.3.2.2. Other pathways disrupted in Li<sup>+</sup> Non-Responder astrocytes ([Figure.3](#))

Apart from inositol phosphate metabolism, the disrupted subsystems in BD-NR comprised fatty acid oxidation (FAO), cholesterol metabolism, phosphatidylinositol phosphate metabolism, tyrosine metabolism, N-glycan synthesis, keratan sulfate degradation and heparan sulfate degradation ([Fig.3.b](#)). However, the association of these biochemical pathways to mood/psychotic disorders remains patchy. The disruption of FAO was particularly intriguing, as it was the only one found to be perturbed across the other two phenotypes-of-interest, BD (four modules) and SCZ (three modules) ([Fig.3.a](#)). In all three contexts (BD, BD-NR and SCZ), disruptions in FAO were observed in both mitochondria and peroxisomes, indicating alterations in medium chain, long chain, and very-long chain fatty acids. The involvement of fatty acid oxidation (FAO) in psychotic disorders' etiology or treatment response is supported by sparse and inconsistent evidence<sup>353</sup>. The inconsistencies observed in these studies can be attributed to confounding factors such as medication usage, lifestyle, etc. Moreover, many of these studies investigated fatty acid alterations in peripheral samples like erythrocyte membranes, which may not necessarily corroborate findings from post-mortem brains or iPS-cells obtained from psychiatrically ill patients. However, a recent study revealed that the brain critically depends on the astrocytic oxidative phosphorylation (OxPhos) to break down fatty acids and maintain lipid balance. Disrupted astrocytic OxPhos leads to the accumulation of lipid droplets (LD) and subsequent neurodegeneration, resembling key aspects of Alzheimer's disease (AD)<sup>354</sup>, which shares clinical symptoms and biological processes with BD and SCZ. However, the disruptions in OxPhos fluxes were not predicted by our models, likely due to degeneracy in metabolic networks<sup>355</sup>, where a phenotype may not be apparent due to compensatory fluxes mediated through other genes/reactions.

#### 4.3.2.3. Identifying links between PI-cycle and other disrupted lipid pathways in Li<sup>+</sup> Non-Responder astrocytes. ([Figure.4](#))

To investigate the potential coupling of PI-cycle disruptions with other seven disrupted pathways in the Li<sup>+</sup> non-responders, the wiring diagram of pathways/fluxes feeding into and out of inositol metabolism was reconstructed ([Fig.4](#)). Subsequently, the disrupted fluxes were mapped onto the wiring diagram - limited to inositol metabolism, cholesterol metabolism, and FAO, considering tractability and the close links between these three pathways. The wiring diagram revealed that fatty acids (FAs) feed into the inositol cycle through diacylglycerol (DAG), however, our models did not predict disruptions in DAG synthesis or utilization reactions. This could be attributed either to the degeneracy in

metabolic networks, or limitations of metabolic models (or mass-action models in general) to encompass other biological mechanisms that may lead to the observed metabolic phenotype. The output of FAO is acetyl-CoA, which feeds into cholesterol biosynthesis through HMG-CoA and Mevalonate in the endoplasmic reticulum (ER). As anticipated, our models predicted disruption in the final steps of cholesterol metabolism, particularly slower fluxes through the conversion of lanosterol to cholesterol, and subsequent interconversions of cholesterol and cholesteryl esters, in the ER. The disruption of brain lipid metabolism in psychoses has been inconsistent in the literature, akin to FAO, and necessitates systematic re-investigations<sup>356</sup>. However, the slower turnover of fatty acyl-coAs and cholesteryl esters suggests the possibility of disruptions in the biogenesis of lipid droplets (LDs), which are critical for lipid and energy homeostasis<sup>309,357</sup>. Accumulation of LDs has been observed in astrocytes under stress<sup>358</sup>, and in the context of AD, astrocytes expressing the risk variant APOE4 form large LDs with impaired turnover and increased peroxidation sensitivity<sup>359</sup>. However, there is no literature evidence for alterations in LDs in the context of psychotic or mood disorders.

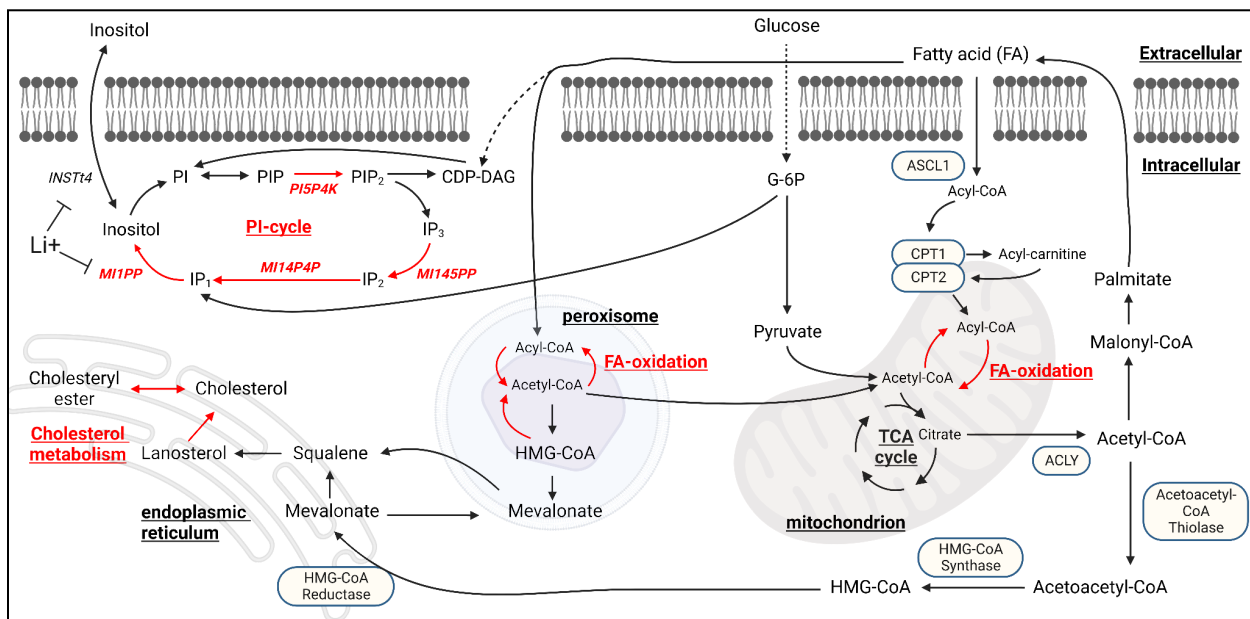


**Figure 4: Wiring diagram illustrating the metabolic coupling of inositol metabolism with FAO and cholesterol metabolism.**

Disruptions (highlighted in red) are distributed across various compartments, including the ER, peroxisome, mitochondrion and cytosol. In order to accommodate multiple subsystems, the presented diagram does not encompass all intermediate reactions, reflecting the adage that the map is not the territory.

Metabolic models of astrocytes from individuals with BD, SCZ and healthy controls were derived and analyzed using diverse analytical tools. Four “high-level” hypotheses were formulated, all of which require subsequent experimental validation.

1. Slower rates of FAO were observed in BD, BD-NonResponders, and SCZ-Twin astrocytes. To verify this, the levels of acylcarnitine or carnitine palmitoyltransferase I (CPT1), a key step in fatty acid oxidation, can be assessed in astrocytes from both BD and SCZ patients, as this pathway exhibited disruption in both phenotypes.
2. Slower cholesterol synthesis and PI cycle were observed in BD-NonResponders' astrocytes. This can be investigated using untargeted lipidomics in astrocytes from BD patients.
3. Slower turnover of fatty acyl-coAs and cholesteryl esters in BD-NonResponders' astrocytes suggests potential disruptions in the biogenesis or expansion of lipid droplets (LDs). This can be explored by analyzing or profiling LDs<sup>310</sup> in astrocytes from BD patients.
4. Maintaining a faster astrocytic inositol synthesis rate (i.e., an accelerated PI cycle) might be a necessary condition for Li+ responsiveness in BD. This can only be tested through stable-isotope tracing experiments, probing inositol metabolism using 13C-labeled myo-inositol<sup>360</sup>, in BD patients' astrocytes.

**5. Identifying the metabolic impact of loss-of-function (LoF) mutations implicated in bipolar disorder, schizophrenia and neurodegeneration.**

5.1. Introduction.

---

---

## 5.2. Materials and methods.

---

---

### 5.3. Results and discussion.

---

---

**6. Abstract.**

**7. Summary and future directions.**

## 8. Supplementary: figures, tables and methods.

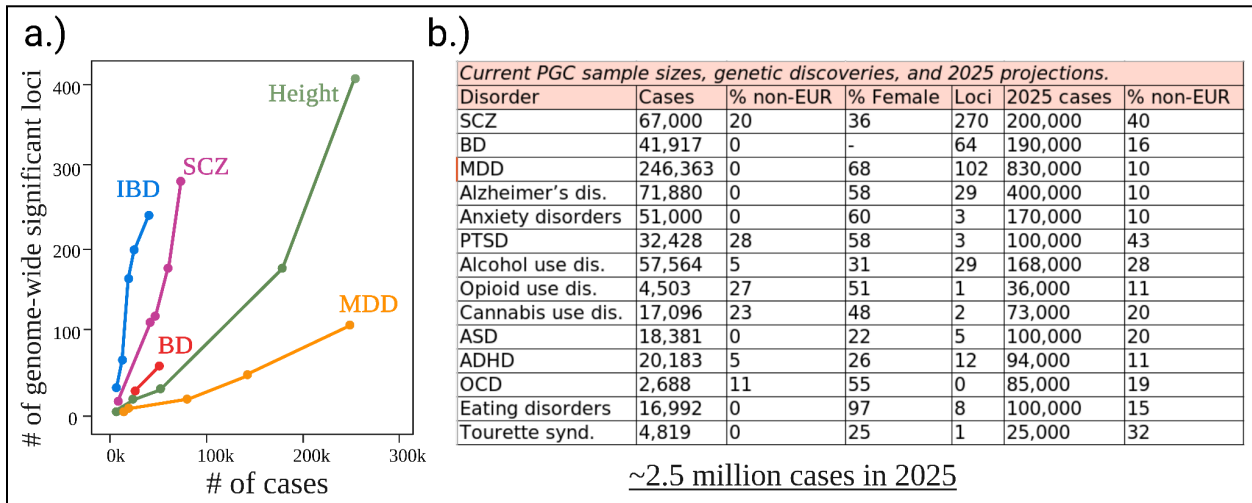


**Figure S1: Psychiatric Genomics Consortium (PGC) - GWAS Discoveries until 2023.**

**a)** Each data point corresponds to a PGC GWAS on conditions including SCZ, BD and MDD, compared to non-psychiatric GWAS such as Inflammatory bowel disease (IBD) and Height. The x-axis displays the number of cases included in the study, while the y-axis indicates the number of GWAS loci identified in that study. **b.)** The table presents current PGC sample sizes, discovered loci, the proportion of non-European samples, proportion of female samples, and projections for 2025 for 14 psychiatric phenotypes. The projections anticipate an increase in the number of cases up to 2.5 million samples.

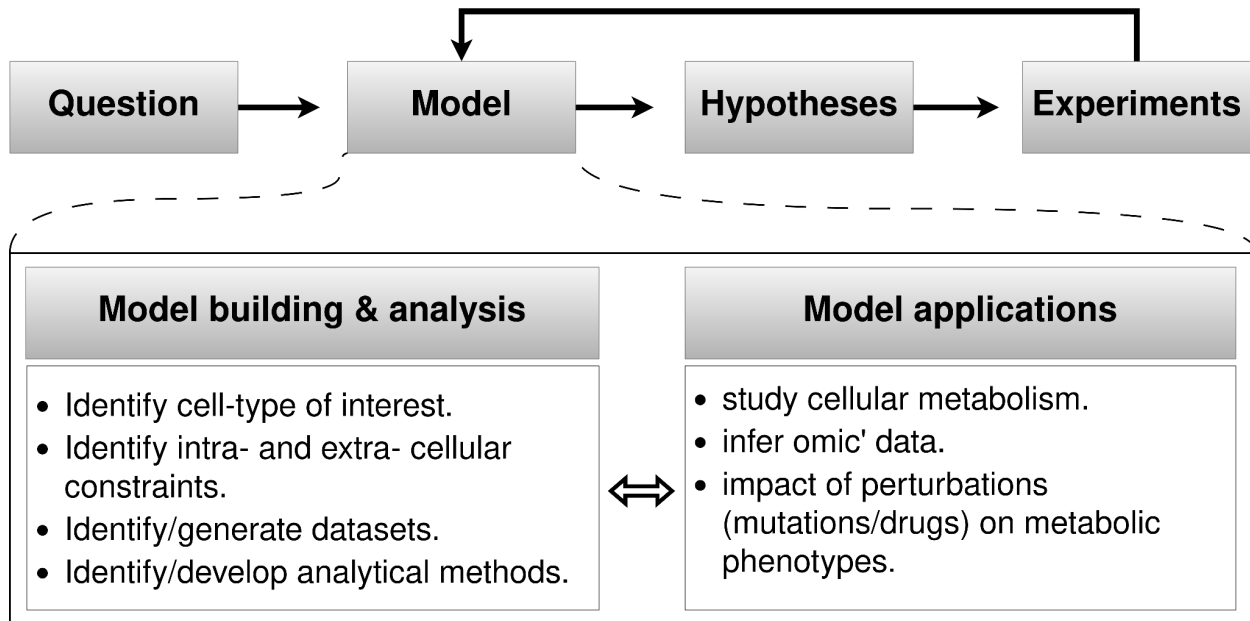


**Figure.S2: Computational modeling to understand cellular metabolism.**

Computational modeling, employed as a tool in scientific research, enables complex systems to be simulated and understood, resulting in the generation of hypotheses that can be tested through real-world experiments. Experimental data validate or refute the predictions generated by these models. This cyclical process of computational modeling and experimental validation fosters an ongoing refinement of hypotheses and models based on observed outcomes. Similar to other scientific inquiries, computational modeling initiates with the formulation of questions or specific applications in mind. The subsequent model building/analysis aligns with the chosen focus. Within the context of my PhD research, questions ranged from investigating the metabolic dependency of Li<sup>+</sup> response in BD, to exploring whether metabolic phenotypes cross-cut related clinical phenotypes like BD and SCZ. Considering the challenges of directly addressing these questions through experiments and capitalizing on public data, my approach involved repurposing publicly accessible 'omic data related to astrocytes, curating biochemical literature to determine the astrocytic constraints, and employing suitable analytical methods, which facilitated the building of computational models of astrocyte metabolism to address these questions comprehensively.

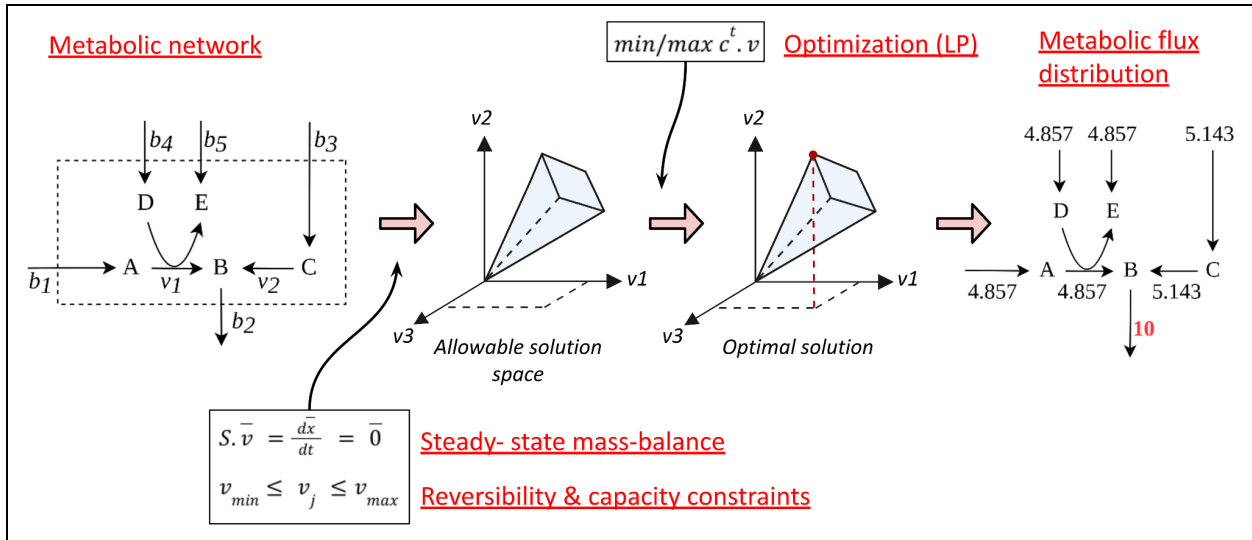


**Figure.SX: Flux balance analysis (FBA).**

Metabolite flow in a metabolic network is examined using flux balance analysis (FBA), involving the stoichiometric matrix containing metabolite coefficients reflecting production and consumption. Assuming steady-state, incoming flux equals outgoing flux, preventing metabolite accumulation. This balance is represented as a dot product between the stoichiometric matrix [S] and the flux vector [v], yielding linear equations. Solving these underdetermined linear equations, where variables exceed equations, results in infinite solutions. Optimization solves this problem by maximizing for an objective function, say metabolite 'B' production or its flux 'b2', subject to constraints including the steady-state mass-balance ( $S.v=0$ ) and further reaction inequalities. The outcome is a theoretically feasible flux distribution, revealing the rates of each reaction within the metabolic network. Notably, the flux distribution in FBA is often not unique, yet the objective value remains consistent. In other words, multiple alternative optimal solutions with the same objective value can coexist within the system. This concept can be likened to a system or cell adopting various functional states while optimizing toward a specific objective. Figure adapted from Raman/Chandra (2009)<sup>361</sup> and Orth/Thiele/Palsson (2010)<sup>345</sup>.

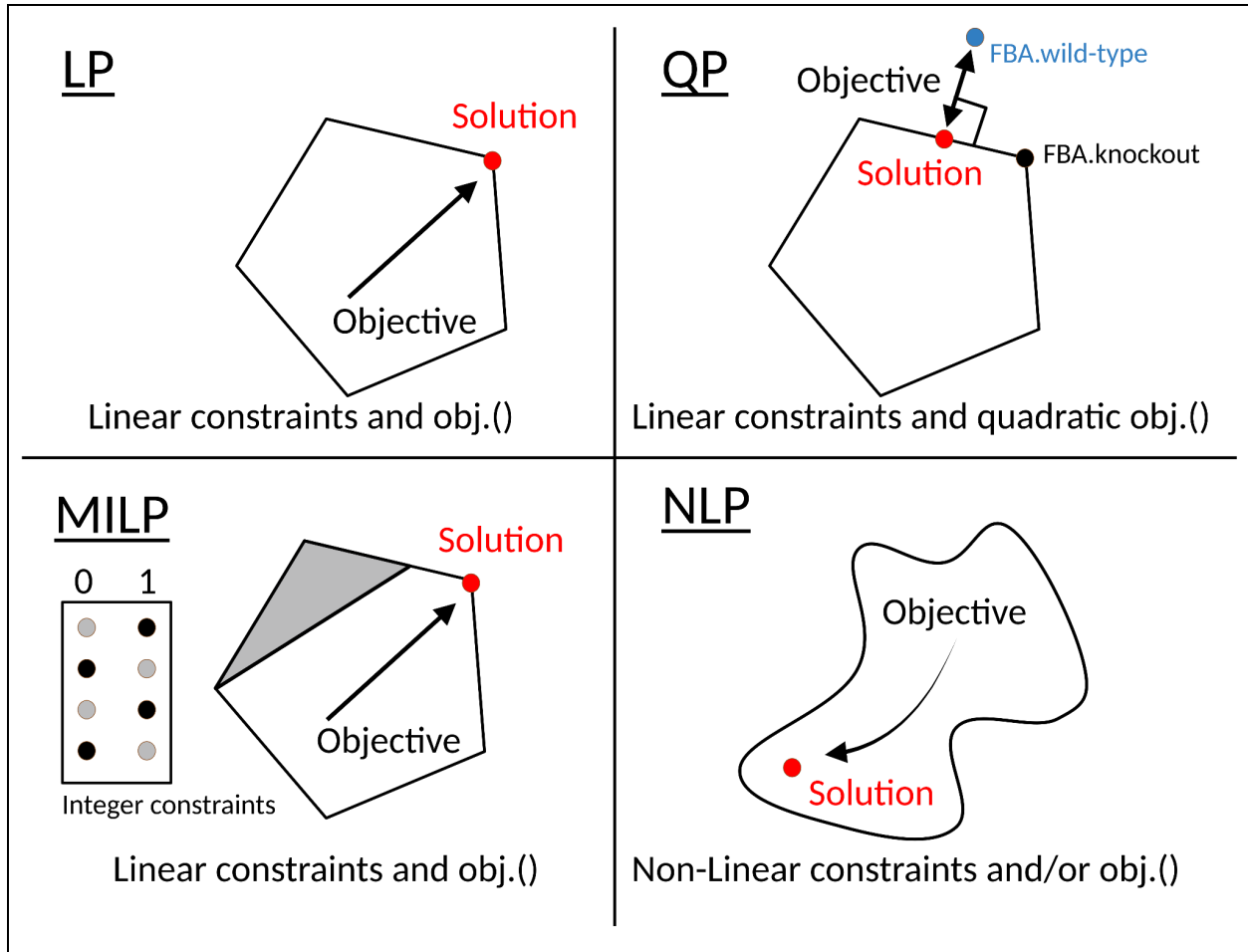


**Figure.SX: Major classes of optimization methods.**

The selection of optimization algorithms hinges on the defined objective and constraints. FBA optimizes a linear combination of fluxes using linear programming (LP) algorithms, useful in predicting minimum and maximum flux through reactions. However, FBA predictions may not always align with experimental growth rates or flux values, particularly for knockout phenotypes. To address this, the quadratic programming (QP)-based minimization of metabolic adjustment (MOMA) algorithm minimizes the Euclidean distance between knockout and wild-type FBA solutions. QP is chosen due to the quadratic objective. Regulatory on/off minimization (ROOM) shares the concept of MOMA but uses mixed-integer linear programming (MILP). Non-linear programming (NLP) algorithms with nonlinear constraints and objectives also exist. Notably, optimal solutions for LP, QP, and MILP methods lie within the solution space's corners or periphery, whereas NLP may encounter local minima. The convex solution space ensures optimal solutions for LP, QP, and MILP, while NLP might not guarantee solutions due to local minima challenges. Figure adapted from B.O. Palsson's COBRA textbook (2015), Chapter-18<sup>362</sup>.

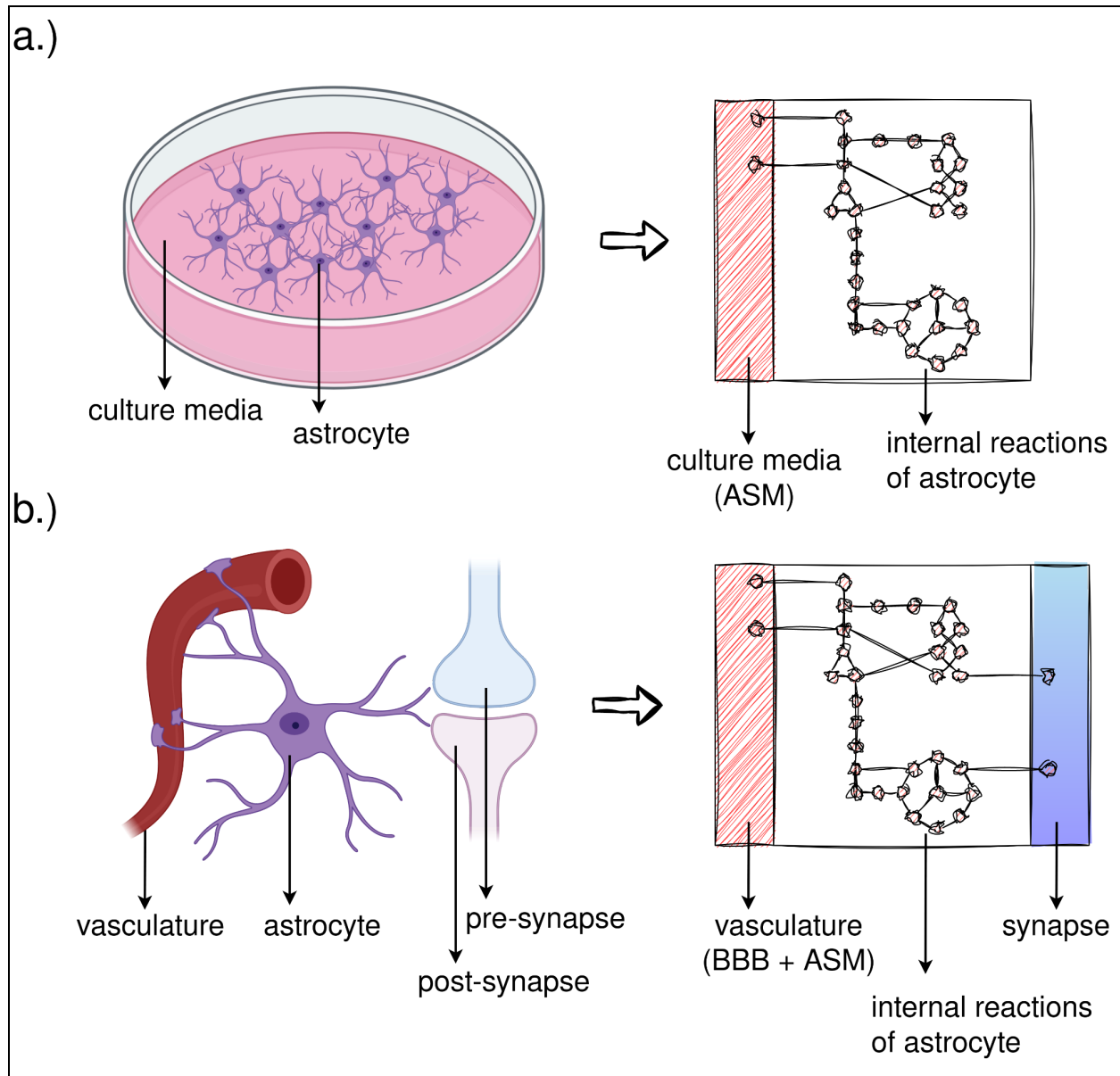


**Figure.S3: Conceptualization of astrocyte metabolic models.**

**a.)** In the context of a metabolic model, astrocytes in culture can be envisioned as having an internal reaction space fueled by nutrients from the culture media. The nutrient medium for all iPS-astrocyte models comprises the metabolites and ions constituting the astrocyte sustenance medium (ASM). **b.)** In the context of *in vivo* astrocytes, a crucial assumption was made that culture media components also exist in systemic circulation, traverse the blood-brain barrier (BBB), and are accessible for astrocyte uptake. Consequently, the extracellular compartments of Primary-astrocyte models were constrained by metabolites and ions from both ASM and BBB. An additional synapse compartment is introduced to capture astrocyte-synapse metabolic interactions. This logic informs all Primary-astrocyte models. Further details are available in methodology sections [4.2.4.2](#) and [4.2.4.3](#).

**8.1. Protocol: Filtering reactions relevant to phenotype-of-interest (BD, BD-Responder, BD-NonResponder, SCZ-Twin): expansion of [methodology section 4.2.5.3.](#)**

8.1.1. Prerequisites: generate FVA and MTA results.

- i. FVA results - ratio of flux span (FSr) between,
  - iPS-Ctrl-a and iPS-BD/iPS-BD-R/iPS-BD-NR models. Retain reactions with FSr>1.5 and FSr<0.8. [Script in github](#).
  - iPS-Ctrl-b and iPS-ST models. Retain reactions with FSr>1.5 and FSr<0.8. [Script in github](#).
  - iPS-Ctrl-a and Primary-Ctrl models. Retain reactions with FSr values between 1.5 and 0.8. [Script in github](#).
  - iPS-Ctrl-b and iPS-HT models. Retain reactions with FSr values between 1.5 and 0.8. [Script in github](#).
  - iPS-Ctrl-b and Primary-Ctrl models. Retain reactions with FSr values between 1.5 and 0.8. [Script in github](#).
- ii. MTA results - transformation scores between,
  - iPS-Ctrl-a  $\rightleftharpoons$  iPS-BD/iPS-BD-R/iPS-BD-NR/Primary-Ctrl models. [Script in github](#).
  - iPS-Ctrl-b  $\rightleftharpoons$  iPS-ST/iPS-HT/Primary-Ctrl models. [Script in github](#).

Prepare the above (i, ii) for models generated using 'abs', 'norm\_t1', and 'norm\_t2' expression thresholds, separately.

### 8.1.2. Filtering reactions: Using FVA Results:

8.1.2.1. **BD, BD-Responder and BD-NonResponder**: This protocol is prepared for replicating [Fig.S4](#), exemplified by analyzing the FVA results from 'abs' models. Similar logic must be extended for 'norm\_t1' ([Fig.S5](#)) and 'norm\_t2' models ([Fig.S6](#)).

- i. Start with four sets:
  - Reactions with altered rates: iPS-Ctrl-a vs iPS-BD (mentioned as "Ctrl\_vs\_BD" in [Fig.S4](#)).
  - Reactions with altered rates: iPS-Ctrl-a vs iPS-BD-R (mentioned as "Ctrl\_vs\_BD\_R" in [Fig.S4](#)).
  - Reactions with altered rates: iPS-Ctrl-a vs iPS-BD-NR (mentioned as "Ctrl\_vs\_BD\_NR" in [Fig.S4](#)).
  - Reactions with consistent rates: iPS-Ctrl-a vs Primary-Ctrl (mentioned as "Ctrl\_vs\_Primary\_Unchanged" in [Fig.S4](#)).
- ii. Visualize overlap between four sets using R's upset() function.
- iii. Apply filtering criteria from [Table.1](#):
  - Slice relevant subsets (reactions).
  - In [Fig.S4](#), BD relevant subsets are mentioned in blue, BD-R subsets in green, and BD-NR subsets in red. The union set was considered if multiple subsets per phenotype were found.
- iv. Obtain one reaction set for each phenotype (BD/BD-R/BD-NR). Sets may overlap; refer to [Table.1](#) for overlap criteria.
- v. Perform [Metabolic subSystem Enrichment Analysis \(MSEA\)](#) on the filtered subset of reactions for each of the three phenotypes (BD/BD-R/BD-NR).

Perform step i-iv using this [script in github](#) which also generates [Fig.S4](#), and step v using this [script in github](#). These processes should be iterated for FVA outcomes obtained from 'norm\_t1' and 'norm\_t2' models as well. Modify the script's filename suffix from '\_abs' to '\_norm\_t1' and '\_norm\_t2' to generate results corresponding to the respective conditions.

8.1.2.2. **SCZ-Twin:** This protocol is prepared for replicating [Fig.S7](#), exemplified by analyzing the FVA results from 'abs' models. Similar logic must be extended for 'norm\_t1' ([Fig.S8](#)) and 'norm\_t2' models ([Fig.S9](#)).

- i. Start with three sets:
  - Reactions with altered rates: iPS-Ctrl-b vs iPS-ST (mentioned as "Ctrl\_vs\_ST" in [Fig.S7](#)).
  - Reactions with consistent rates: iPS-Ctrl-b vs iPS-HT (mentioned as "Ctrl\_vs\_HT\_Unchanged" in [Fig.S7](#)).
  - Reactions with consistent rates: iPS-Ctrl-b vs Primary-Ctrl (mentioned as "Ctrl\_vs\_Primary\_Unchanged" in [Fig.S7](#)).
- ii. Visualize overlap between three sets using R's upset() function.
- iii. Apply filtering criteria from [Table.1](#):
  - Slice relevant subsets (i.e., reactions).
  - In [Fig.S7](#), ST relevant subsets are mentioned in red. The union set was considered if multiple subsets per phenotype were found.
- iv. Obtain one reaction set for the phenotype (ST). Sets may overlap with BD/BD-R/BD-NR; refer to [Table.1](#) for overlap criteria.
- v. Perform [Metabolic subSystem Enrichment Analysis \(MSEA\)](#) on the filtered subset of reactions for the phenotypes (ST).

Perform step i-iv using this [script in github](#) which also generates [Fig.S7](#), and step v using this [script in github](#). These processes should be iterated for FVA outcomes obtained from 'norm\_t1' and 'norm\_t2' models as well. Modify the script's filename suffix from '\_abs' to '\_norm\_t1' and '\_norm\_t2' to generate results corresponding to the respective conditions.

### 8.1.3. Filtering reactions: Using MTA Results:

8.1.3.1. **BD, BD-Responder and BD-NonResponder**: This protocol is prepared for replicating [Fig.S10](#), exemplified by analyzing the MTA results from 'abs' models. Similar logic must be extended for 'norm\_t1' ([Fig.S11](#)) and 'norm\_t2' models ([Fig.S12](#)).

- i. Start with eight sets i.e., the MTA scores for,
  - $iPS\text{-}Ctrl\text{-}a \rightleftharpoons iPS\text{-}BD$ . (one set for either direction).
  - $iPS\text{-}Ctrl\text{-}a \rightleftharpoons iPS\text{-}BD\text{-}R$ . (one set for either direction).
  - $iPS\text{-}Ctrl\text{-}a \rightleftharpoons iPS\text{-}BD\text{-}NR$ . (one set for either direction).
  - $iPS\text{-}Ctrl\text{-}a \rightleftharpoons Primary\text{-}Ctrl$ . (one set for either direction).
- ii. Identify reactions with top 20% MTA scores i.e., reactions that facilitate metabolic state transformations for " $iPS\text{-}Ctrl\text{-}a \rightleftharpoons iPS\text{-}BD/iPS\text{-}BD\text{-}R/iPS\text{-}BD\text{-}NR$ ".  
 ○ For instance, to pinpoint the top 20% of MTA reactions relevant to BD phenotype, run MTA between the  $iPS\text{-}Ctrl\text{-}a$  and  $iPS\text{-}BD$  models. This entails identifying the top 20% of reactions whose knockout transforms  $Ctrl \rightarrow BD$ , as well as the top 20% that transforms  $BD \rightarrow Ctrl$ . Subsequently, take the **union set of the top 20% reactions** from both runs.
- iii. Identify reactions with bottom 80% MTA scores i.e., reactions that do not facilitate metabolic state transformations for  $iPS\text{-}Ctrl\text{-}a \rightleftharpoons Primary\text{-}Ctrl$  models.  
 ○ Similar to the procedure in (ii), except in this case, focus on the **intersection of the bottom 80% reactions** from both runs, namely  $Ctrl \rightarrow Primary$  and  $Primary \rightarrow Ctrl$ .

The above steps (ii, iii) generates four reaction sets for,

- BD (mentioned as "BD\_top" in [Fig.S10](#)).
- BD-R (mentioned as "BD\_R\_top" in [Fig.S10](#)).
- BD-NR (mentioned as "BD\_NR\_top" in [Fig.S10](#)).
- Ctrl (mentioned as "Ctrl\_unchanged" in [Fig.S10](#)).

- iv. Visualize overlap between the four sets using R's `upset()` function.
- v. Apply filtering criteria from [Table.1](#):
  - Slice relevant subsets (reactions).
  - In [Fig.S10](#), BD relevant subsets are mentioned in blue, BD-R subsets in green, and BD-NR subsets in red. The union set was considered if multiple subsets per phenotype were found.

- vi. Obtain one reaction set for each phenotype (BD/BD-R/BD-NR). Sets may overlap; refer to [Table.1](#) for overlap criteria.
- vii. Perform [Metabolic subSystem Enrichment Analysis \(MSEA\)](#) on the filtered subset of reactions for each of the three phenotypes (BD/BD-R/BD-NR).

Perform step i-vii using this [script in github](#) which also generates [Fig.S10](#). These processes should be iterated for MTA outcomes obtained from 'norm\_t1' and 'norm\_t2' models as well. Modify the script's filename suffix from '\_abs' to '\_norm\_t1' and '\_norm\_t2' to generate results corresponding to the respective conditions.

8.1.3.2. **SCZ-Twin:** This protocol is prepared for replicating [Fig.S13](#), exemplified by analyzing the MTA results from 'abs' models. Similar logic must be extended for 'norm\_t1' ([Fig.S14](#)) and 'norm\_t2' models ([Fig.S15](#)).

- i. Start with six sets i.e., the MTA scores for,
  - iPS-Ctrl-b  $\rightleftharpoons$  iPS-ST. (one set for either direction).
  - iPS-Ctrl-b  $\rightleftharpoons$  iPS-HT. (one set for either direction).
  - iPS-Ctrl-b  $\rightleftharpoons$  Primary-Ctrl. (one set for either direction).
- ii. Identify reactions with top 20% MTA scores i.e., reactions that facilitate metabolic state transformations for "iPS-Ctrl-b  $\rightleftharpoons$  iPS-ST".
  - For instance, to pinpoint the top 20% of MTA reactions relevant to ST phenotype, run MTA between the iPS-Ctrl-b and iPS-ST models. This entails identifying the top 20% of reactions whose knockout transforms Ctrl  $\rightarrow$  ST, as well as the top 20% that transforms ST  $\rightarrow$  Ctrl. Subsequently, take the **union set of the top 20% reactions** from both runs.
- iii. Identify reactions with bottom 80% MTA scores i.e., reactions that do not facilitate metabolic state transformations for "iPS-Ctrl-a  $\rightleftharpoons$  iPS-HT/Primary-Ctrl".
  - Similar to the procedure in (ii), except in this case, focus on the **intersection of the bottom 80% reactions** from all four runs, namely Ctrl  $\rightarrow$  HT, HT  $\rightarrow$  Ctrl, Ctrl  $\rightarrow$  Primary and Primary  $\rightarrow$  Ctrl.

The above steps (ii, iii) generates two reaction sets for,

- ST (mentioned as "ST\_top" in [Fig.S13](#)).
  - Ctrl (mentioned as "Ctrl\_unchanged" in [Fig.S13](#)).
- iv. Visualize overlap between two sets using R's upset() function.
  - v. Apply filtering criteria from [Table.1](#):
    - Slice relevant subsets (reactions).
    - In [Fig.S13](#), ST relevant subsets are mentioned in red. The union set was considered if multiple subsets per phenotype were found.
  - vi. Obtain one reaction set for the phenotype (ST). Sets may overlap with BD/BD-R/BD-NR; refer to [Table.1](#) for overlap criteria.
  - vii. Perform [Metabolic subSystem Enrichment Analysis \(MSEA\)](#) on the filtered subset of reactions for the phenotypes (ST).

Perform step i-vii using this [script in github](#) which also generates [Fig.S13](#). These processes should be iterated for MTA outcomes obtained from 'norm\_t1' and 'norm\_t2' models as well. Modify the script's filename suffix from '\_abs' to '\_norm\_t1' and '\_norm\_t2' to generate results corresponding to the respective conditions.

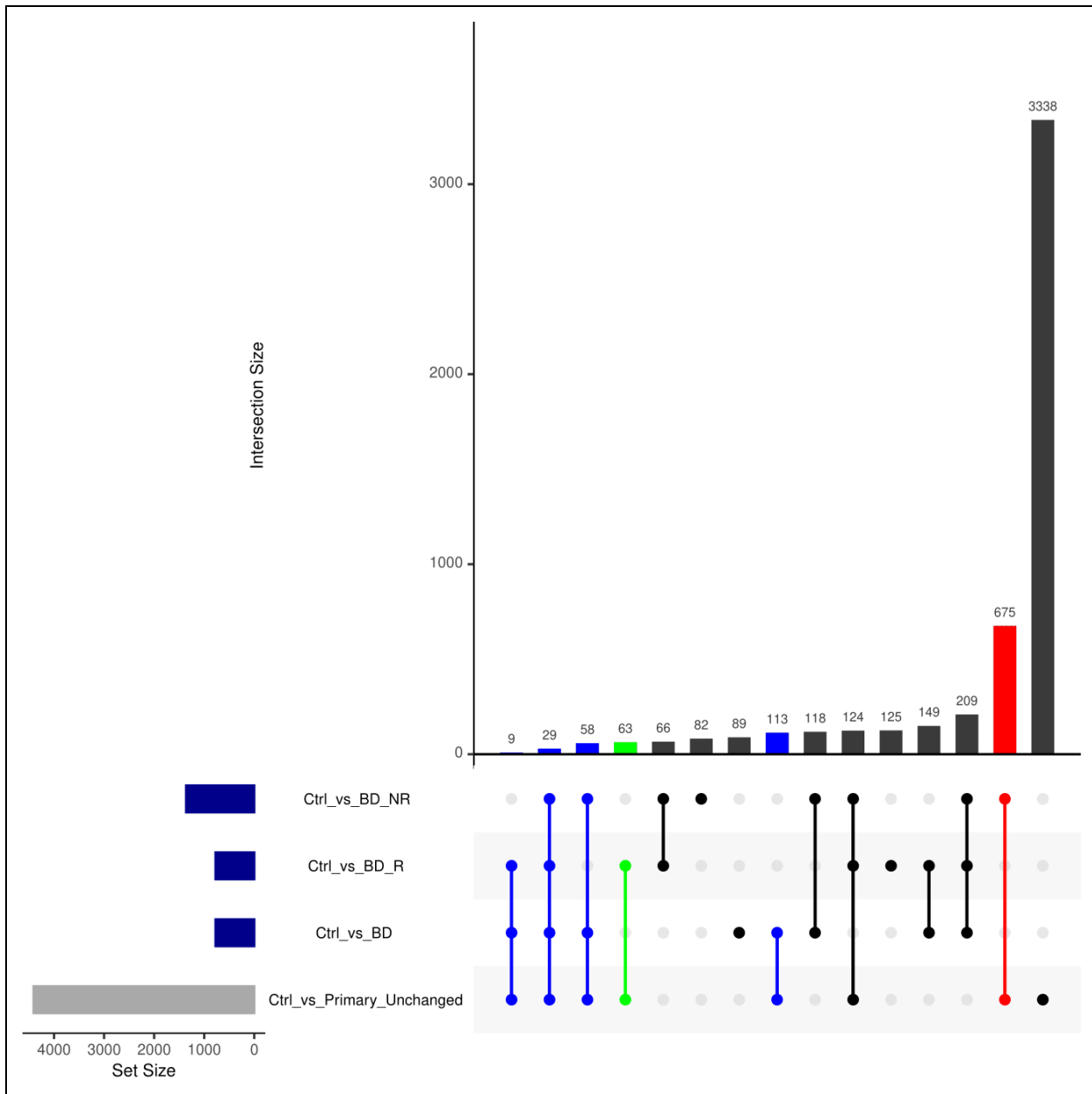


**Figure.S4: Identifying 'BD', 'BD-Responder' and 'BD-NonResponder' relevant reactions by FVA analysis of BD astrocyte (abs) metabolic models.**

UpSet plot depicting the intersections among four reaction sets derived from FVA analysis of BD astrocyte (abs) metabolic models. The reaction sets include 'Ctrl\_vs\_BD' (altered rates between iPS-Ctrl-a and iPS-BD), 'Ctrl\_vs\_BD\_R' (altered rates between iPS-Ctrl-a and iPS-BD-R), 'Ctrl\_vs\_BD\_NR' (altered rates between iPS-Ctrl-a and iPS-BD-NR), and 'Ctrl\_vs\_Primary\_Unc changed' (consistent rates between iPS-Ctrl-a and Primary-Ctrl). Colored intersections represent shortlisted and sliced reactions based on [Table.1](#) criteria. Blue, green, and red intersections denote BD, BD-Responder, and BD-NonResponder subset(s), respectively. For detailed information, refer to [Supplementary Section 8.1](#).

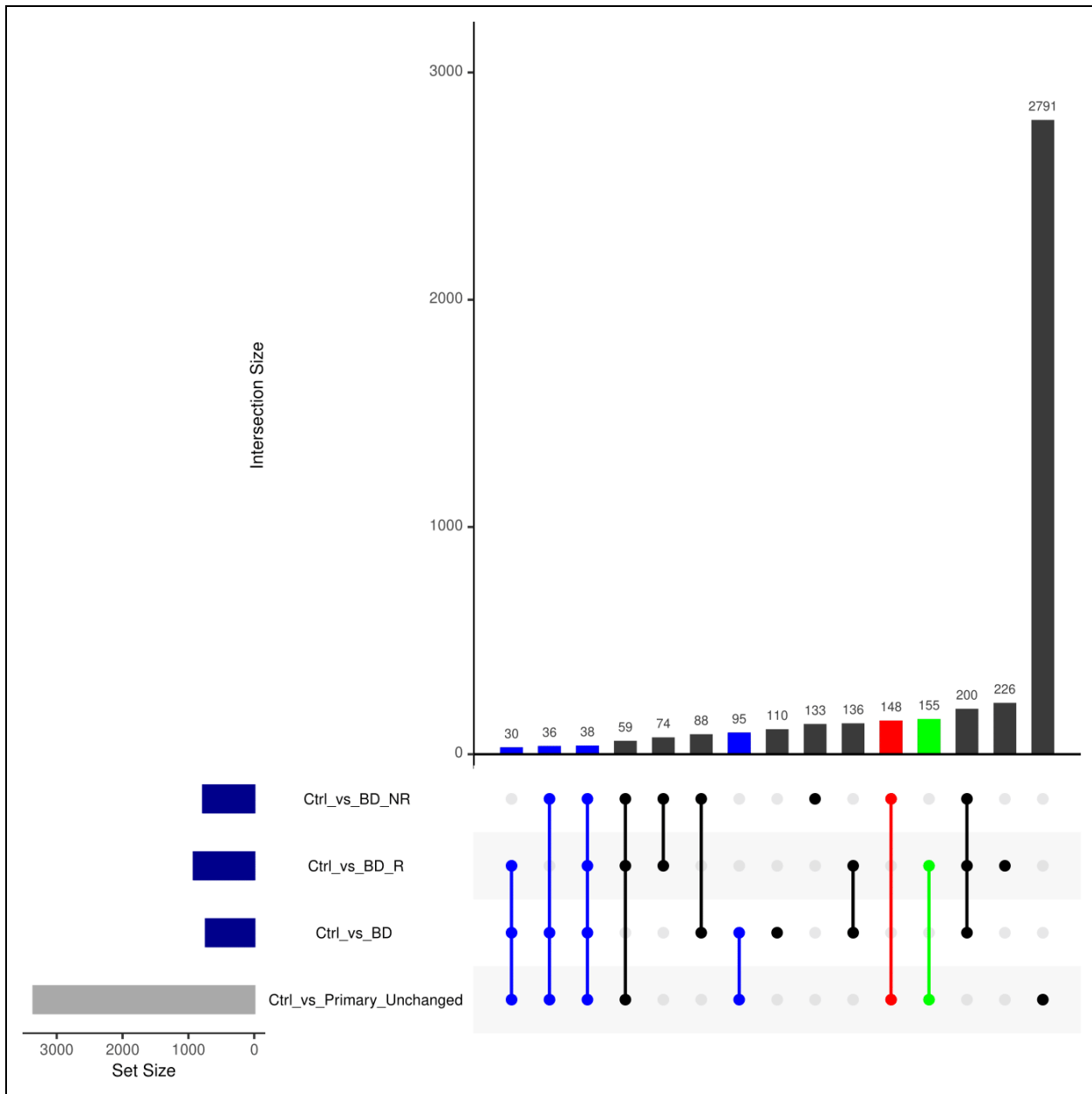


**Figure.S5: Identifying 'BD', 'BD-Responder' and 'BD-NonResponder' relevant reactions by FVA analysis of BD astrocyte (norm-t1) metabolic models.**

UpSet plot depicting the intersections among four reaction sets derived from FVA analysis of BD astrocyte (norm-t1) metabolic models. The reaction sets include 'Ctrl\_vs\_BD' (altered rates between iPS-Ctrl-a and iPS-BD), 'Ctrl\_vs\_BD\_R' (altered rates between iPS-Ctrl-a and iPS-BD-R), 'Ctrl\_vs\_BD\_NR' (altered rates between iPS-Ctrl-a and iPS-BD-NR), and 'Ctrl\_vs\_Primary\_Unc changed' (consistent rates between iPS-Ctrl-a and Primary-Ctrl). Colored intersections represent shortlisted and sliced reactions based on [Table.1](#) criteria. Blue, green, and red intersections denote BD, BD-Responder, and BD-NonResponder subset(s), respectively. For detailed information, refer to [Supplementary Section 8.1](#).

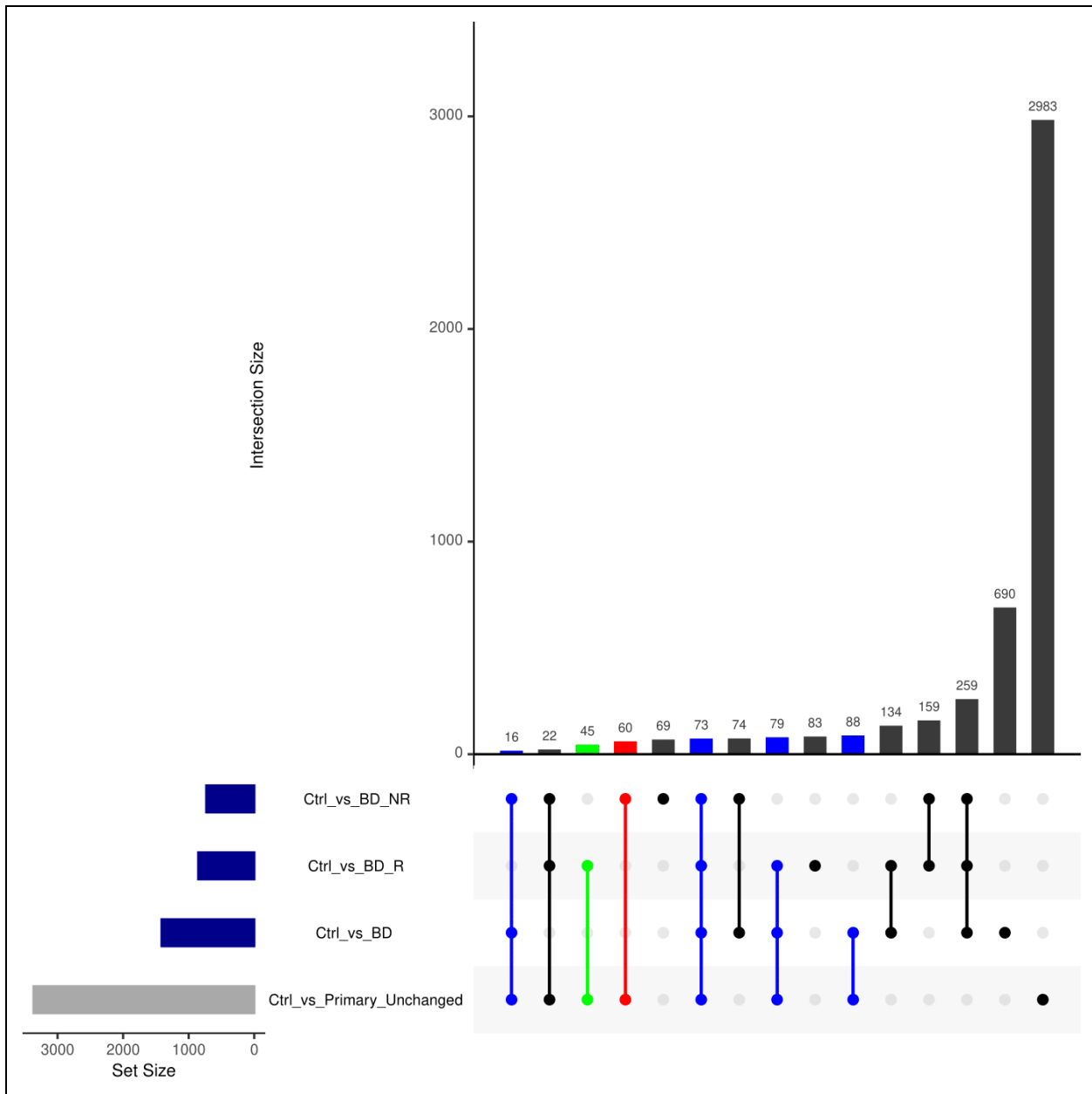


**Figure.S6: Identifying 'BD', 'BD-Responder' and 'BD-NonResponder' relevant reactions by FVA analysis of BD astrocyte (norm-t2) metabolic models.**

UpSet plot depicting the intersections among four reaction sets derived from FVA analysis of BD astrocyte (norm-t2) metabolic models. The reaction sets include 'Ctrl\_vs\_BD' (altered rates between iPS-Ctrl-a and iPS-BD), 'Ctrl\_vs\_BD\_R' (altered rates between iPS-Ctrl-a and iPS-BD-R), 'Ctrl\_vs\_BD\_NR' (altered rates between iPS-Ctrl-a and iPS-BD-NR), and 'Ctrl\_vs\_Primary\_Uncanged' (consistent rates between iPS-Ctrl-a and Primary-Ctrl). Colored intersections represent shortlisted and sliced reactions based on [Table.1](#) criteria. Blue, green, and red intersections denote BD, BD-Responder, and BD-NonResponder subset(s), respectively. For detailed information, refer to [Supplementary Section 8.1](#).

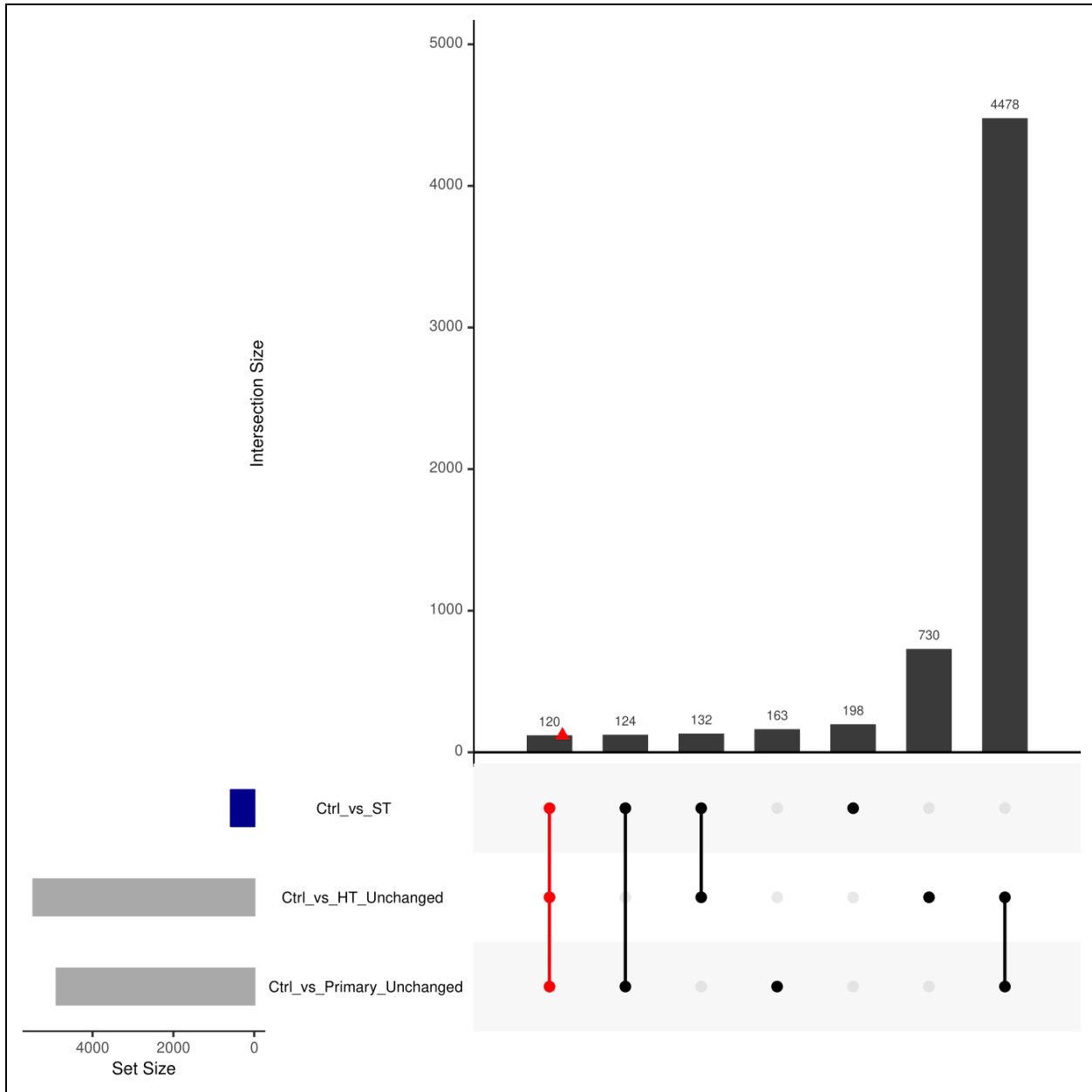


**Figure.S7: Identifying 'SCZ-Twin' relevant reactions by FVA analysis of SCZ astrocyte (abs) metabolic models.**

UpSet plot depicting the intersections among three reaction sets derived from FVA analysis of SCZ astrocyte (abs) metabolic models. The reaction sets include 'Ctrl\_vs\_ST' (altered rates between iPS-Ctrl-b and iPS-ST), 'Ctrl\_vs\_HT\_Uncchanged' (consistent rates between iPS-Ctrl-b and iPS-HT), and 'Ctrl\_vs\_Primary\_Uncchanged' (consistent rates between iPS-Ctrl-b and Primary-Ctrl). Colored intersections represent shortlisted and sliced reactions based on [Table 1](#) criteria. Red intersections denote SCZ-Twin subset(s). For detailed information, refer to [Supplementary Section 8.1](#).

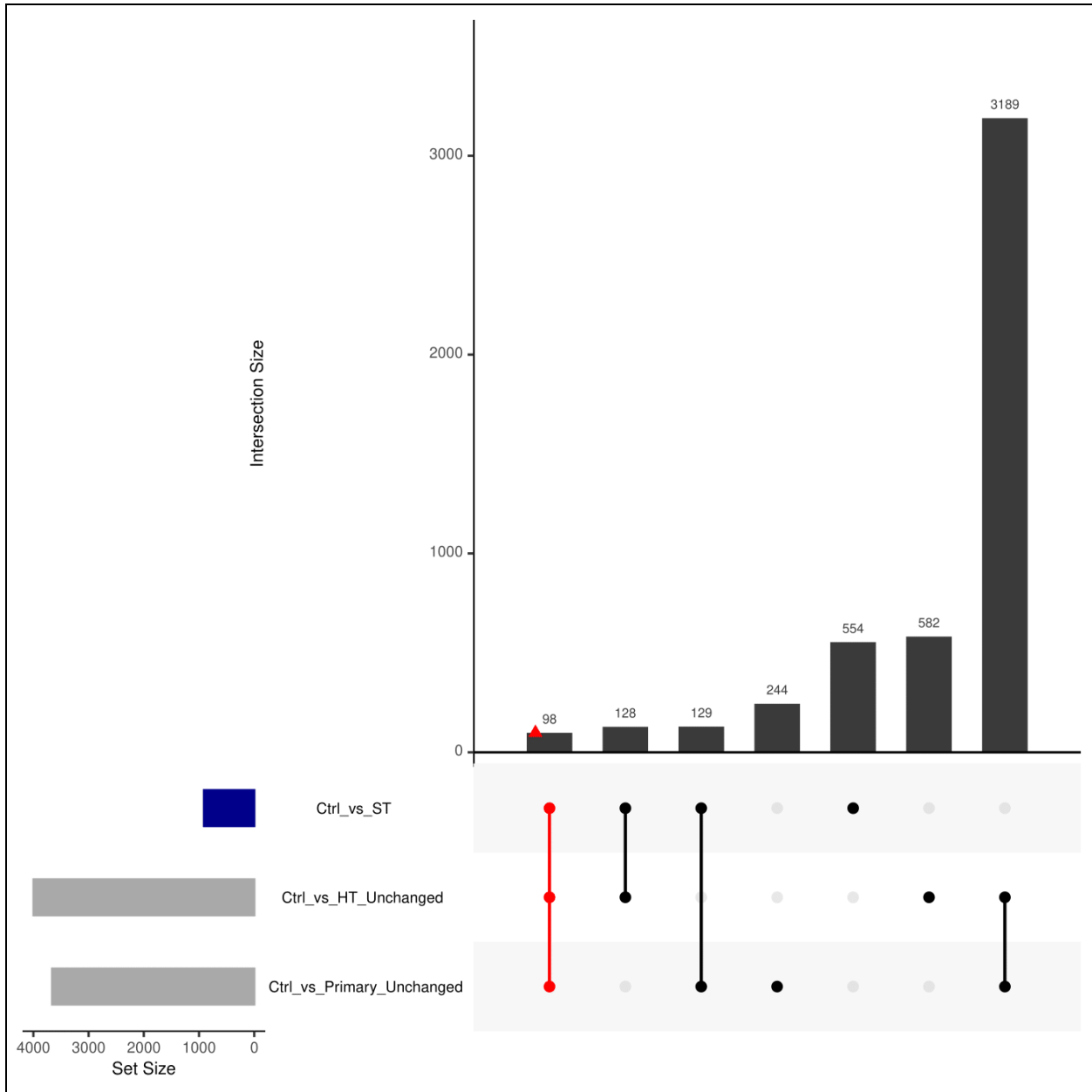


**Figure S8: Identifying 'SCZ-Twin' relevant reactions by FVA analysis of SCZ astrocyte (norm-t1) metabolic models.**

UpSet plot depicting the intersections among three reaction sets derived from FVA analysis of SCZ astrocyte (norm-t1) metabolic models. The reaction sets include 'Ctrl\_vs\_ST' (altered rates between iPS-Ctrl-b and iPS-ST), 'Ctrl\_vs\_HT\_Uncanged' (consistent rates between iPS-Ctrl-b and iPS-HT), and 'Ctrl\_vs\_Primary\_Uncanged' (consistent rates between iPS-Ctrl-b and Primary-Ctrl). Colored intersections represent shortlisted and sliced reactions based on [Table 1](#) criteria. Red intersections denote SCZ-Twin subset(s). For detailed information, refer to [Supplementary Section 8.1](#).

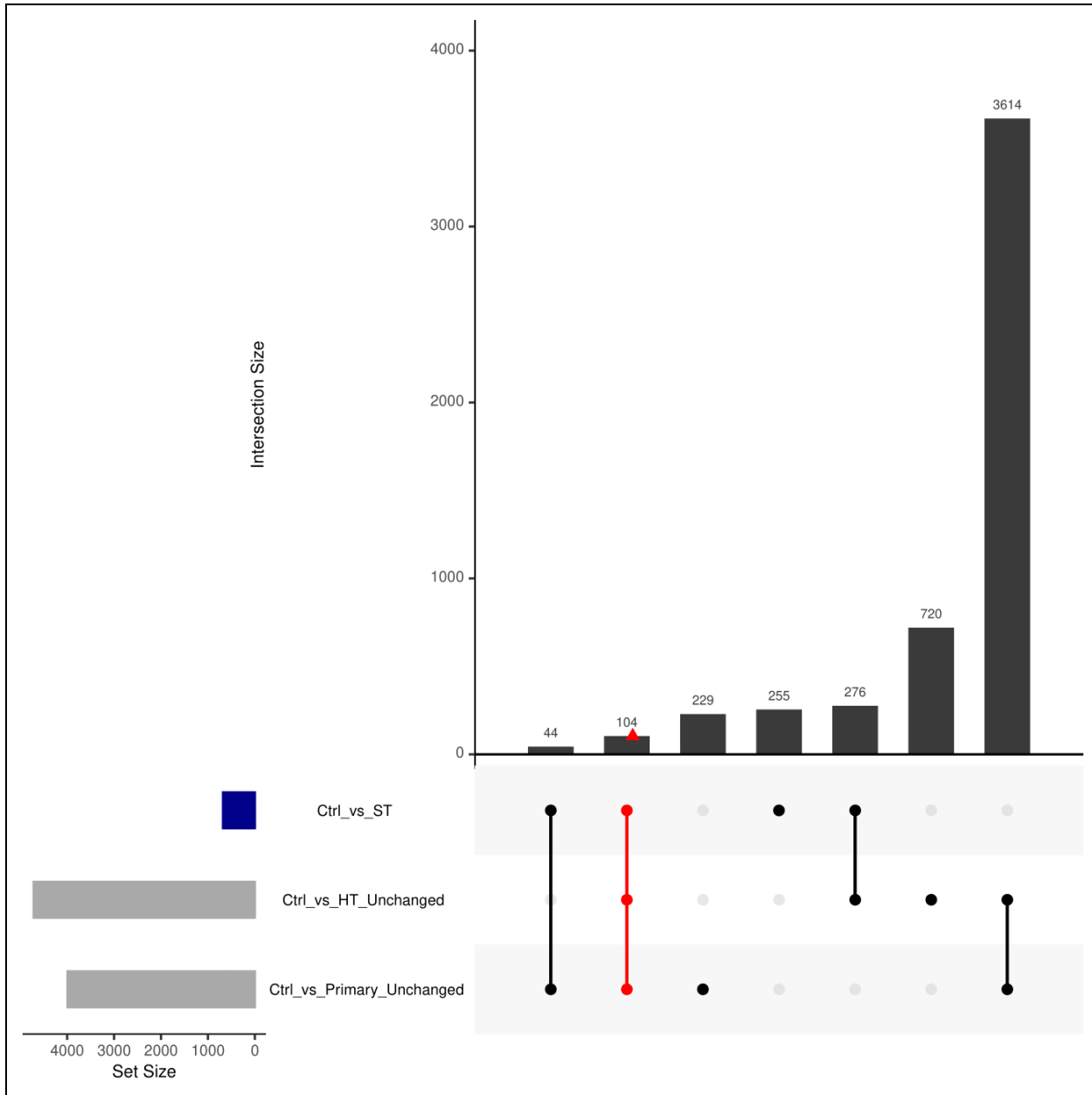


**Figure.S9: Identifying 'SCZ-Twin' relevant reactions by FVA analysis of SCZ astrocyte (norm-t2) metabolic models.**

UpSet plot depicting the intersections among three reaction sets derived from FVA analysis of SCZ astrocyte (norm-t2) metabolic models. The reaction sets include 'Ctrl\_vs\_ST' (altered rates between iPS-Ctrl-b and iPS-ST), 'Ctrl\_vs\_HT\_Uncanged' (consistent rates between iPS-Ctrl-b and iPS-HT), and 'Ctrl\_vs\_Primary\_Uncanged' (consistent rates between iPS-Ctrl-b and Primary-Ctrl). Colored intersections represent shortlisted and sliced reactions based on [Table 1](#) criteria. Red intersections denote SCZ-Twin subset(s). For detailed information, refer to [Supplementary Section 8.1](#).

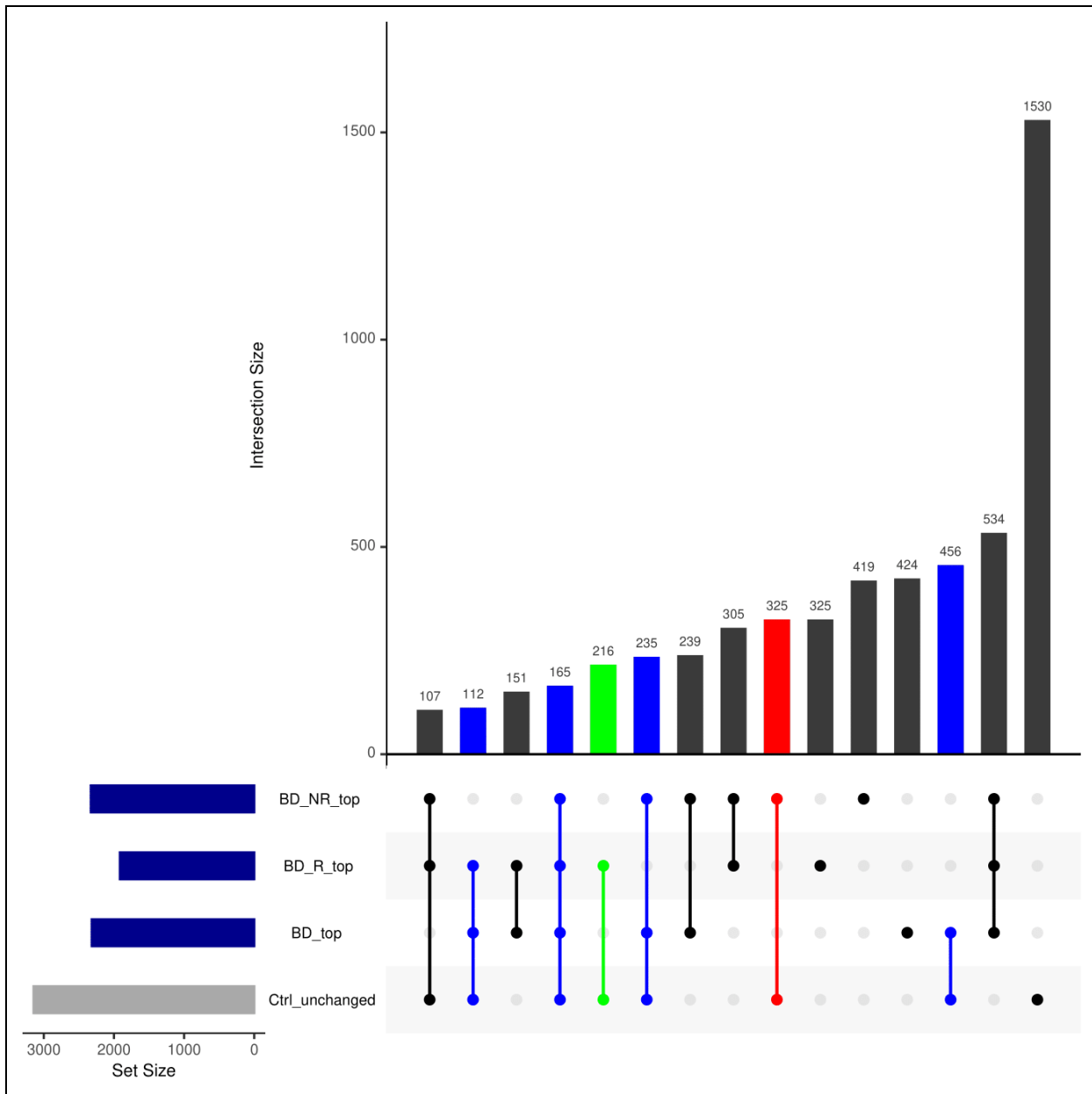


**Figure.S10: Identifying 'BD', 'BD-Responder' and 'BD-NonResponder' relevant reactions by MTA analysis of BD astrocyte (abs) metabolic models.**

UpSet plot depicting the intersections among four reaction sets derived from MTA analysis of BD astrocyte (abs) metabolic models. The reaction sets include 'BD\_top' (transforms iPS-Ctrl-a $\rightleftharpoons$ iPS-BD), 'BD\_R\_top' (transforms iPS-Ctrl-a $\rightleftharpoons$ iPS-BD-R), 'BD\_NR\_top' (transforms iPS-Ctrl-a $\rightleftharpoons$ iPS-BD-NR), and 'Ctrl\_unchanged' (does not transform iPS-Ctrl-a $\rightleftharpoons$ Primary-Ctrl). Colored intersections represent shortlisted and sliced reactions based on [Table.1](#) criteria. Blue, green, and red intersections denote BD, BD-Responder, and BD-NonResponder subset(s), respectively. For detailed information, refer to [Supplementary Section 8.1](#).

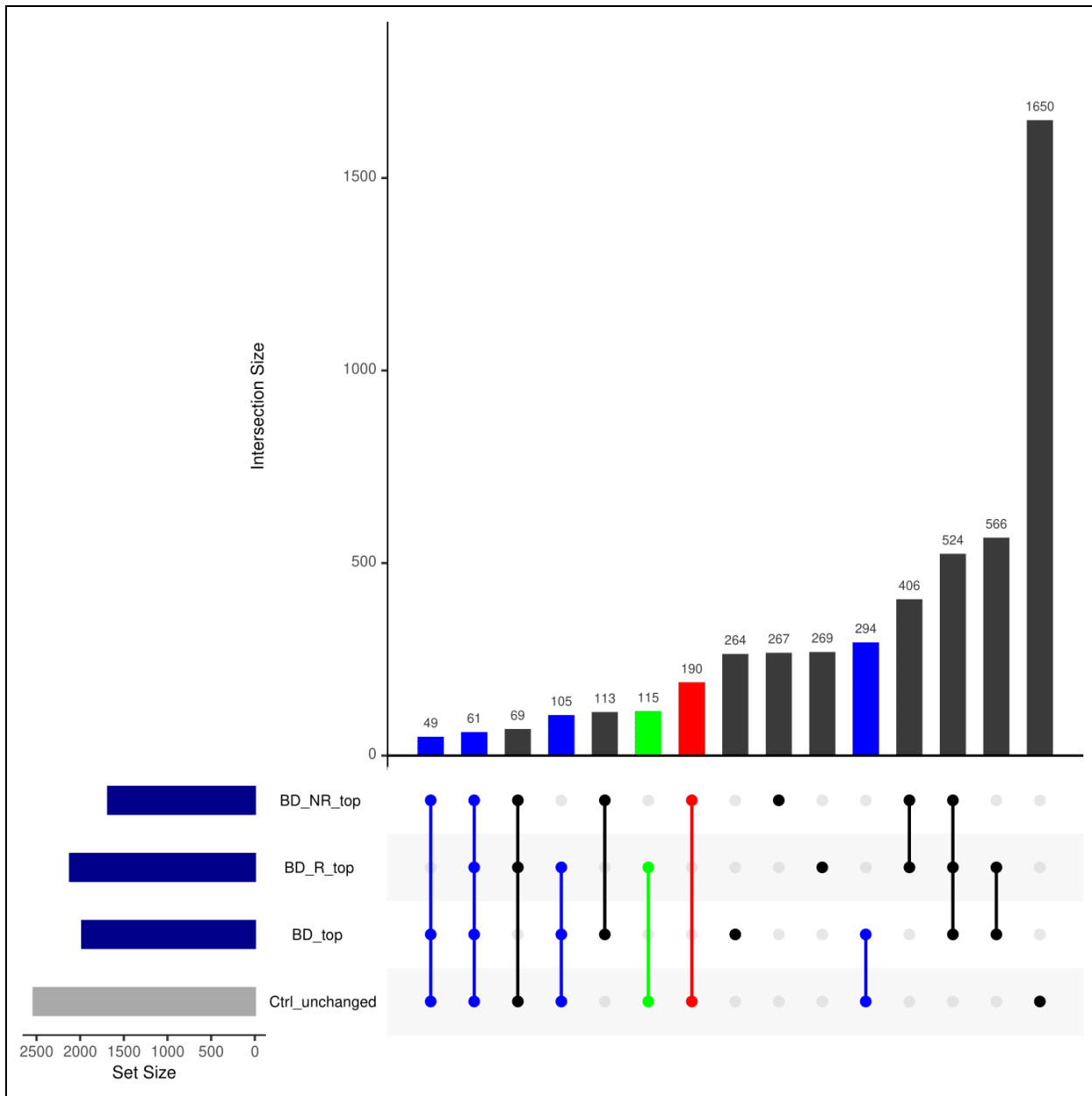


**Figure.S11: Identifying 'BD', 'BD-Responder' and 'BD-NonResponder' relevant reactions by MTA analysis of BD astrocyte (norm-t1) metabolic models.**

UpSet plot depicting the intersections among four reaction sets derived from MTA analysis of BD astrocyte (norm-t1) metabolic models. The reaction sets include 'BD\_top' (transforms iPS-Ctrl-a $\rightleftharpoons$ iPS-BD), 'BD\_R\_top' (transforms iPS-Ctrl-a $\rightleftharpoons$ iPS-BD-R), 'BD\_NR\_top' (transforms iPS-Ctrl-a $\rightleftharpoons$ iPS-BD-NR), and 'Ctrl\_unchanged' (does not transform iPS-Ctrl-a $\rightleftharpoons$ Primary-Ctrl). Colored intersections represent shortlisted and sliced reactions based on [Table.1](#) criteria. Blue, green, and red intersections denote BD, BD-Responder, and BD-NonResponder subset(s), respectively. For detailed information, refer to [Supplementary Section 8.1](#).

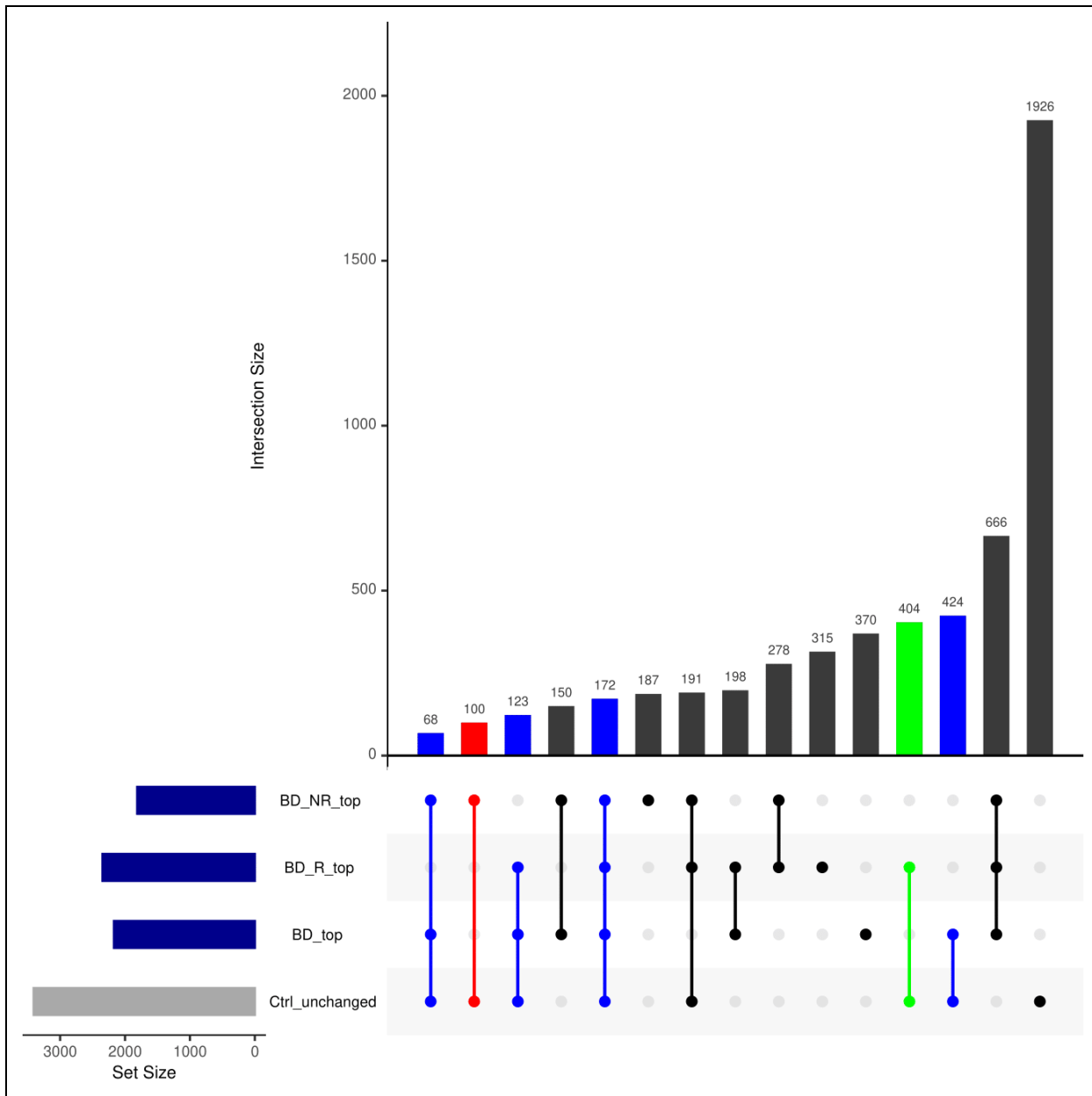


**Figure.S12: Identifying 'BD', 'BD-Responder' and 'BD-NonResponder' relevant reactions by MTA analysis of BD astrocyte (norm-t2) metabolic models.**

UpSet plot depicting the intersections among four reaction sets derived from MTA analysis of BD astrocyte (norm-t2) metabolic models. The reaction sets include 'BD\_top' (transforms iPS-Ctrl-a $\rightleftharpoons$ iPS-BD), 'BD\_R\_top' (transforms iPS-Ctrl-a $\rightleftharpoons$ iPS-BD-R), 'BD\_NR\_top' (transforms iPS-Ctrl-a $\rightleftharpoons$ iPS-BD-NR), and 'Ctrl\_unchanged' (does not transform iPS-Ctrl-a $\rightleftharpoons$ Primary-Ctrl). Colored intersections represent shortlisted and sliced reactions based on [Table.1](#) criteria. Blue, green, and red intersections denote BD, BD-Responder, and BD-NonResponder subset(s), respectively. For detailed information, refer to [Supplementary Section 8.1](#).

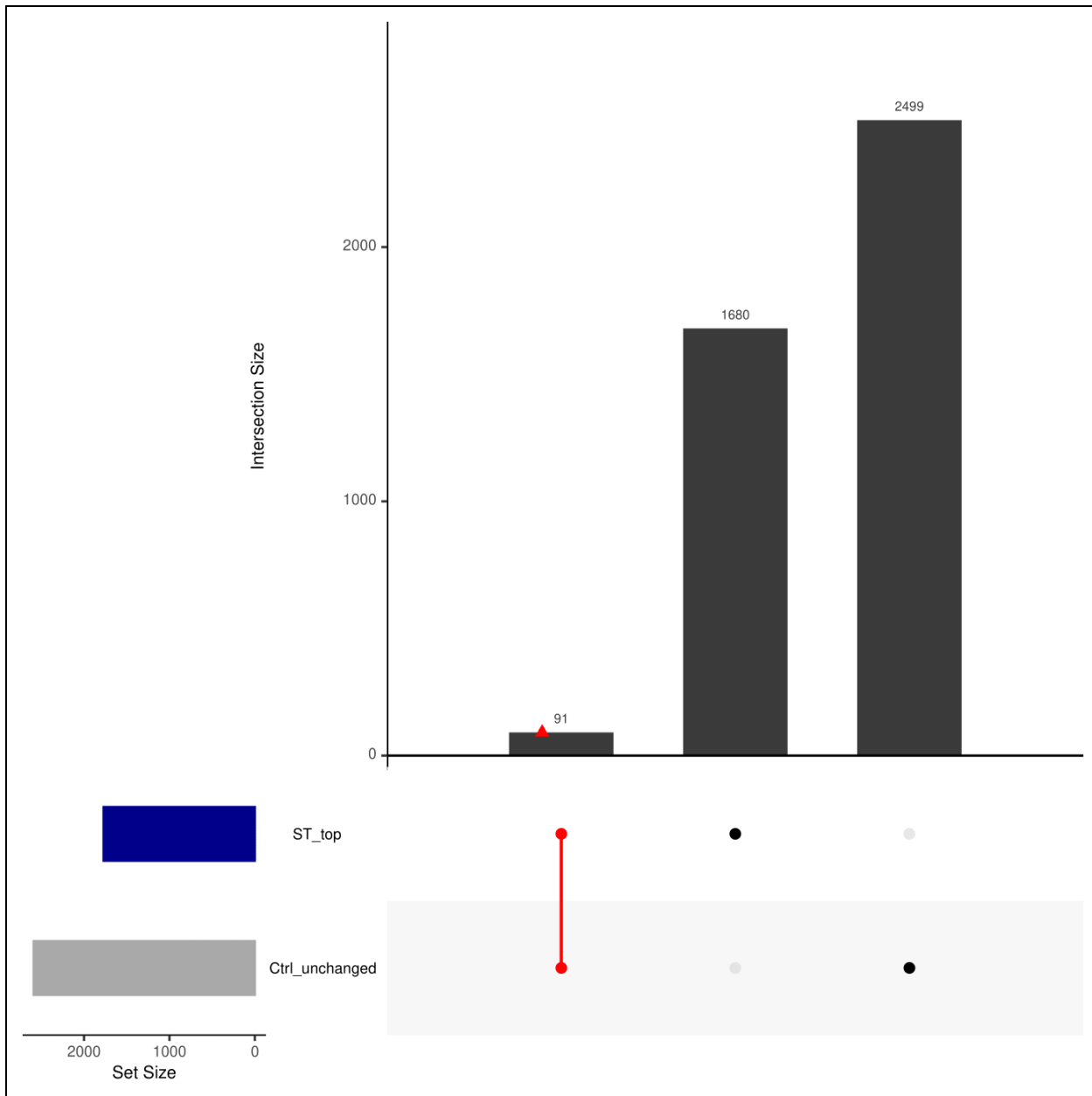


**Figure.S13: Identifying 'SCZ-Twin' relevant reactions by MTA analysis of SCZ astrocyte (abs) metabolic models.**

UpSet plot depicting the intersections among two reaction sets derived from MTA analysis of SCZ astrocyte (abs) metabolic models. The reaction sets include 'ST\_top' (transforms iPS-Ctrl-b $\rightleftharpoons$ iPS-ST), and 'Ctrl\_unchanged' (does not transform iPS-Ctrl-b $\rightleftharpoons$ iPS-HT/Primary-Ctrl). Colored intersections represent shortlisted and sliced reactions based on [Table 1](#) criteria. Red intersections denote SCZ-Twin subset(s). For detailed information, refer to [Supplementary Section 8.1](#).

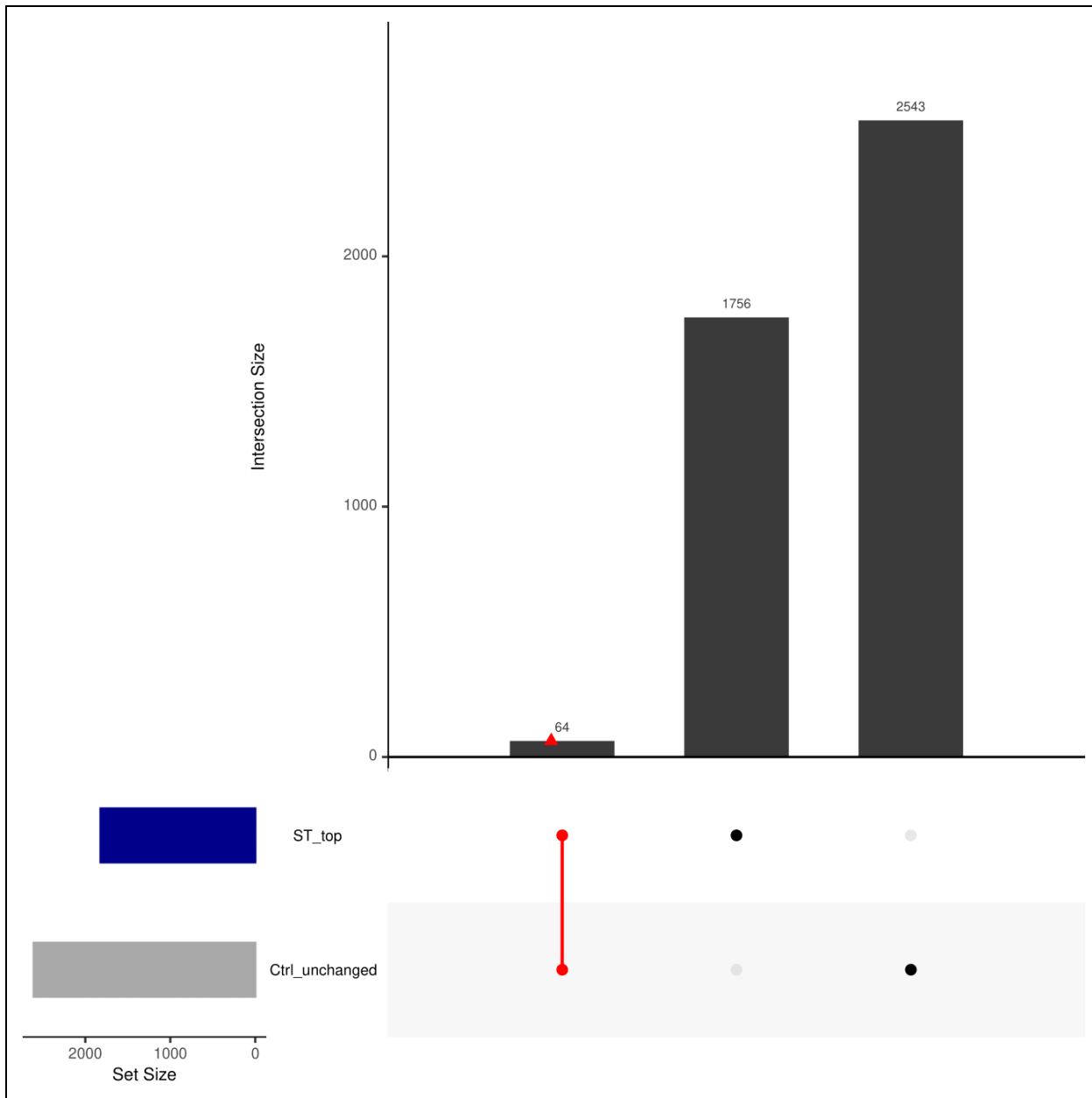


**Figure S14: Identifying 'SCZ-Twin' relevant reactions by MTA analysis of SCZ astrocyte (norm-t1) metabolic models.**

UpSet plot depicting the intersections among two reaction sets derived from MTA analysis of SCZ astrocyte (norm-t1) metabolic models. The reaction sets include 'ST\_top' (transforms iPS-Ctrl-b $\rightleftharpoons$ iPS-ST), and 'Ctrl\_unchanged' (does not transform iPS-Ctrl-b $\rightleftharpoons$ iPS-HT/Primary-Ctrl). Colored intersections represent shortlisted and sliced reactions based on [Table 1](#) criteria. Red intersections denote SCZ-Twin subset(s). For detailed information, refer to [Supplementary Section 8.1](#).

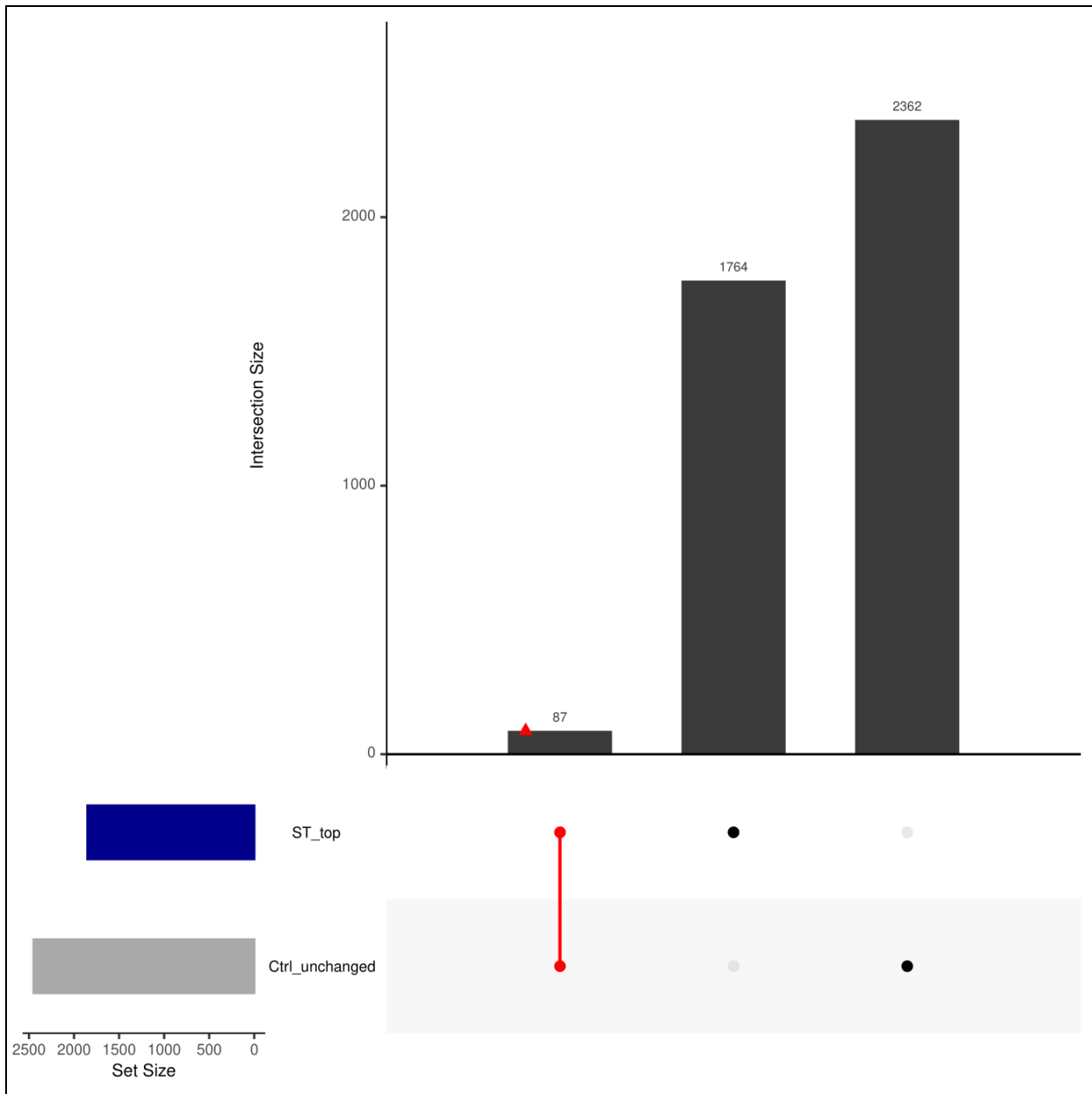


**Figure.S15: Identifying 'SCZ-Twin' relevant reactions by MTA analysis of SCZ astrocyte (norm-t2) metabolic models.**

UpSet plot depicting the intersections among two reaction sets derived from MTA analysis of SCZ astrocyte (norm-t2) metabolic models. The reaction sets include 'ST\_top' (transforms iPS-Ctrl-b $\rightleftharpoons$ iPS-ST), and 'Ctrl\_unchanged' (does not transform iPS-Ctrl-b $\rightleftharpoons$ iPS-HT/Primary-Ctrl). Colored intersections represent shortlisted and sliced reactions based on [Table 1](#) criteria. Red intersections denote SCZ-Twin subset(s). For detailed information, refer to [Supplementary Section 8.1](#).

## 9. References.

1. Global, regional, and national burden of 12 mental disorders in 204 countries and territories, 1990–2019: a systematic analysis for the Global Burden of Disease Study 2019. *Lancet Psychiatry* **9**, 137–150 (2022).
2. Walker, E. R., McGee, R. E. & Druss, B. G. Mortality in mental disorders and global disease burden implications: a systematic review and meta-analysis. *JAMA Psychiatry* **72**, 334–341 (2015).
3. Polderman, T. J. C. *et al.* Meta-analysis of the heritability of human traits based on fifty years of twin studies. *Nat. Genet.* **47**, 702–709 (2015).
4. Sullivan, P. F. & Kendler, K. S. The state of the science in psychiatric genomics. *Psychol. Med.* **51**, 2145–2147 (2021).
5. Angst, J. Historical aspects of the dichotomy between manic–depressive disorders and schizophrenia. *Schizophr. Res.* **57**, 5–13 (2002).
6. Cross-Disorder Group of the Psychiatric Genomics Consortium. Genetic relationship between five psychiatric disorders estimated from genome-wide SNPs. *Nat. Genet.* **45**, 984–994 (2013).
7. Identification of risk loci with shared effects on five major psychiatric disorders: a genome-wide analysis. *The Lancet* **381**, 1371–1379 (2013).
8. Ruderfer, D. M. *et al.* Genomic Dissection of Bipolar Disorder and Schizophrenia, Including 28 Subphenotypes. *Cell* **173**, 1705–1715.e16 (2018).
9. de Zwart, S. M. C. *et al.* The Association Between Familial Risk and Brain Abnormalities Is Disease Specific: An ENIGMA-Relatives Study of Schizophrenia and Bipolar Disorder. *Biol. Psychiatry* **86**, 545–556 (2019).

10. van Erp, T. G. M. *et al.* Cortical Brain Abnormalities in 4474 Individuals With Schizophrenia and 5098 Control Subjects via the Enhancing Neuro Imaging Genetics Through Meta Analysis (ENIGMA) Consortium. *Biol. Psychiatry* **84**, 644–654 (2018).
11. Aryal, S. *et al.* Deep proteomics identifies shared molecular pathway alterations in synapses of patients with schizophrenia and bipolar disorder and mouse model. *Cell Rep.* **42**, 112497 (2023).
12. Gandal, M. J. *et al.* Shared molecular neuropathology across major psychiatric disorders parallels polygenic overlap. *Science* **359**, 693–697 (2018).
13. Correll, C. U., Detraux, J., De Lepeleire, J. & De Hert, M. Effects of antipsychotics, antidepressants and mood stabilizers on risk for physical diseases in people with schizophrenia, depression and bipolar disorder. *World Psychiatry Off. J. World Psychiatr. Assoc. WPA* **14**, 119–136 (2015).
14. Linden, M. & Schermuly-Haupt, M.-L. Definition, assessment and rate of psychotherapy side effects. *World Psychiatry Off. J. World Psychiatr. Assoc. WPA* **13**, 306–309 (2014).
15. Sullivan, P. F. & Geschwind, D. H. Defining the Genetic, Genomic, Cellular, and Diagnostic Architectures of Psychiatric Disorders. *Cell* **177**, 162–183 (2019).
16. Visscher, P. M., Yengo, L., Cox, N. J. & Wray, N. R. Discovery and implications of polygenicity of common diseases. *Science* **373**, 1468–1473 (2021).
17. Mullins, N. *et al.* Genome-wide association study of more than 40,000 bipolar disorder cases provides new insights into the underlying biology. *Nat. Genet.* **53**, 817–829 (2021).
18. Bryois, J. *et al.* Genetic identification of cell types underlying brain complex traits yields insights into the etiology of Parkinson's disease. *Nat. Genet.* **52**, 482–493 (2020).

19. Skene, N. G. *et al.* Genetic identification of brain cell types underlying schizophrenia. *Nat. Genet.* **50**, 825–833 (2018).
20. Goudriaan, A. *et al.* Specific Glial Functions Contribute to Schizophrenia Susceptibility. *Schizophr. Bull.* **40**, 925–935 (2014).
21. Toker, L., Mancarci, B. O., Tripathy, S. & Pavlidis, P. Transcriptomic Evidence for Alterations in Astrocytes and Parvalbumin Interneurons in Subjects With Bipolar Disorder and Schizophrenia. *Biol. Psychiatry* **84**, 787–796 (2018).
22. Pietiläinen, O. *et al.* Astrocytic cell adhesion genes linked to schizophrenia correlate with synaptic programs in neurons. *Cell Rep.* **42**, 111988 (2023).
23. Verkhratsky, A. & Nedergaard, M. Physiology of Astroglia. *Physiol. Rev.* **98**, 239–389 (2018).
24. Allen, N. J. & Lyons, D. A. Glia as Architects of Central Nervous System Formation and Function. *Science* **362**, 181–185 (2018).
25. Chung, W.-S., Allen, N. J. & Eroglu, C. Astrocytes Control Synapse Formation, Function, and Elimination. *Cold Spring Harb. Perspect. Biol.* **7**, a020370 (2015).
26. Hösli, L. *et al.* Direct vascular contact is a hallmark of cerebral astrocytes. *Cell Rep.* **39**, 110599 (2022).
27. Bayraktar, O. A., Fuentealba, L. C., Alvarez-Buylla, A. & Rowitch, D. H. Astrocyte development and heterogeneity. *Cold Spring Harb. Perspect. Biol.* **7**, a020362 (2014).
28. Batiuk, M. Y. *et al.* Identification of region-specific astrocyte subtypes at single cell resolution. *Nat. Commun.* **11**, 1220 (2020).
29. Bayraktar, O. A. *et al.* Astrocyte layers in the mammalian cerebral cortex revealed by a single-cell *in situ* transcriptomic map. *Nat. Neurosci.* **23**, 500–509 (2020).

30. Raichle, M. E. & Gusnard, D. A. Appraising the brain's energy budget. *Proc. Natl. Acad. Sci. U. S. A.* **99**, 10237–10239 (2002).
31. Dienel, G. A. & Hertz, L. Glucose and lactate metabolism during brain activation. *J. Neurosci. Res.* **66**, 824–838 (2001).
32. Dimmer, K. S., Friedrich, B., Lang, F., Deitmer, J. W. & Bröer, S. The low-affinity monocarboxylate transporter MCT4 is adapted to the export of lactate in highly glycolytic cells. *Biochem. J.* **350 Pt 1**, 219–227 (2000).
33. Hu, Y. & Wilson, G. S. A temporary local energy pool coupled to neuronal activity: fluctuations of extracellular lactate levels in rat brain monitored with rapid-response enzyme-based sensor. *J. Neurochem.* **69**, 1484–1490 (1997).
34. Korf, J. Is brain lactate metabolized immediately after neuronal activity through the oxidative pathway? *J. Cereb. Blood Flow Metab. Off. J. Int. Soc. Cereb. Blood Flow Metab.* **26**, 1584–1586 (2006).
35. Schurr, A. Lactate: the ultimate cerebral oxidative energy substrate? *J. Cereb. Blood Flow Metab. Off. J. Int. Soc. Cereb. Blood Flow Metab.* **26**, 142–152 (2006).
36. Rose, C. R. *et al.* Astroglial Glutamate Signaling and Uptake in the Hippocampus. *Front. Mol. Neurosci.* **10**, 451 (2018).
37. Bellot-Saez, A., Kékesi, O., Morley, J. W. & Buskila, Y. Astrocytic modulation of neuronal excitability through K<sup>+</sup> spatial buffering. *Neurosci. Biobehav. Rev.* **77**, 87–97 (2017).
38. Buskila, Y., Farkash, S., Hershfinkel, M. & Amitai, Y. Rapid and reactive nitric oxide production by astrocytes in mouse neocortical slices. *Glia* **52**, 169–176 (2005).
39. Chen, Y. *et al.* Astrocytes protect neurons from nitric oxide toxicity by a glutathione-dependent mechanism: Astrocytes block NO-mediated neurotoxicity. *J.*

- Neurochem.* **77**, 1601–1610 (2001).
40. Almeida, A., Almeida, J., Bolaños, J. P. & Moncada, S. Different responses of astrocytes and neurons to nitric oxide: The role of glycolytically generated ATP in astrocyte protection. *Proc. Natl. Acad. Sci.* **98**, 15294–15299 (2001).
41. Desagher, S., Glowinski, J. & Premont, J. Astrocytes protect neurons from hydrogen peroxide toxicity. *J. Neurosci.* **16**, 2553–2562 (1996).
42. Chun, H. *et al.* Severe reactive astrocytes precipitate pathological hallmarks of Alzheimer's disease via H<sub>2</sub>O<sub>2</sub>– production. *Nat. Neurosci.* **23**, 1555–1566 (2020).
43. Drews, L. *et al.* Ammonia inhibits energy metabolism in astrocytes in a rapid and glutamate dehydrogenase 2-dependent manner. *Dis. Model. Mech.* **13**, dmm047134 (2020).
44. Ebert, D., Haller, R. G. & Walton, M. E. Energy Contribution of Octanoate to Intact Rat Brain Metabolism Measured by <sup>13</sup>C Nuclear Magnetic Resonance Spectroscopy. *J. Neurosci.* **23**, 5928–5935 (2003).
45. Bélanger, M., Allaman, I. & Magistretti, P. J. Brain Energy Metabolism: Focus on Astrocyte-Neuron Metabolic Cooperation. *Cell Metab.* **14**, 724–738 (2011).
46. Bushong, E. A., Martone, M. E., Jones, Y. Z. & Ellisman, M. H. Protoplasmic Astrocytes in CA1 Stratum Radiatum Occupy Separate Anatomical Domains. *J. Neurosci.* **22**, 183–192 (2002).
47. Drögemüller, K. *et al.* Astrocyte gp130 expression is critical for the control of Toxoplasma encephalitis. *J. Immunol. Baltim. Md 1950* **181**, 2683–2693 (2008).
48. Soung, A. & Klein, R. S. Viral Encephalitis and Neurologic Diseases: Focus on Astrocytes. *Trends Mol. Med.* **24**, 950–962 (2018).

49. Geyer, S., Jacobs, M. & Hsu, N.-J. Immunity Against Bacterial Infection of the Central Nervous System: An Astrocyte Perspective. *Front. Mol. Neurosci.* **12**, 57 (2019).
50. Bush, T. G. *et al.* Leukocyte infiltration, neuronal degeneration, and neurite outgrowth after ablation of scar-forming, reactive astrocytes in adult transgenic mice. *Neuron* **23**, 297–308 (1999).
51. Faulkner, J. R. *et al.* Reactive astrocytes protect tissue and preserve function after spinal cord injury. *J. Neurosci. Off. J. Soc. Neurosci.* **24**, 2143–2155 (2004).
52. Wanner, I. B. *et al.* Glial scar borders are formed by newly proliferated, elongated astrocytes that interact to corral inflammatory and fibrotic cells via STAT3-dependent mechanisms after spinal cord injury. *J. Neurosci. Off. J. Soc. Neurosci.* **33**, 12870–12886 (2013).
53. Diaz-Castro, B., Gangwani, M. R., Yu, X., Coppola, G. & Khakh, B. S. Astrocyte molecular signatures in Huntington's disease. *Sci. Transl. Med.* **11**, eaaw8546 (2019).
54. Al-Dalahmah, O. *et al.* Single-nucleus RNA-seq identifies Huntington disease astrocyte states. *Acta Neuropathol. Commun.* **8**, 19 (2020).
55. Sekar, S. *et al.* Alzheimer's disease is associated with altered expression of genes involved in immune response and mitochondrial processes in astrocytes. *Neurobiol. Aging* **36**, 583–591 (2015).
56. Wu, T. *et al.* Complement C3 Is Activated in Human AD Brain and Is Required for Neurodegeneration in Mouse Models of Amyloidosis and Tauopathy. *Cell Rep.* **28**, 2111–2123.e6 (2019).
57. Booth, H. D. E., Hirst, W. D. & Wade-Martins, R. The Role of Astrocyte Dysfunction in Parkinson's Disease Pathogenesis. *Trends Neurosci.* **40**, 358–370 (2017).

58. Henrik Heiland, D. *et al.* Tumor-associated reactive astrocytes aid the evolution of immunosuppressive environment in glioblastoma. *Nat. Commun.* **10**, 2541 (2019).
59. Vadodaria, K. C. *et al.* Altered Neuronal Support and Inflammatory Response in Bipolar Disorder Patient-Derived Astrocytes. *Stem Cell Rep.* **16**, 825–835 (2021).
60. Koskuvi, M. *et al.* Contribution of astrocytes to familial risk and clinical manifestation of schizophrenia. *Glia* **70**, 650–660 (2022).
61. Dohrenwend, B. P. *et al.* Socioeconomic status and psychiatric disorders: the causation-selection issue. *Science* **255**, 946–952 (1992).
62. Knapp, M. & Wong, G. Economics and mental health: the current scenario. *World Psychiatry* **19**, 3–14 (2020).
63. CORRIGAN, P. W. & WATSON, A. C. Understanding the impact of stigma on people with mental illness. *World Psychiatry* **1**, 16–20 (2002).
64. Kessler, R. C. The epidemiology of dual diagnosis. *Biol. Psychiatry* **56**, 730–737 (2004).
65. DE HERT, M. *et al.* Physical illness in patients with severe mental disorders. I. Prevalence, impact of medications and disparities in health care. *World Psychiatry* **10**, 52–77 (2011).
66. Erlangsen, A. *et al.* Cause-specific life-years lost in people with mental disorders: a nationwide, register-based cohort study. *Lancet Psychiatry* **4**, 937–945 (2017).
67. Correll, C. U. *et al.* Prevalence, incidence and mortality from cardiovascular disease in patients with pooled and specific severe mental illness: a large-scale meta-analysis of 3,211,768 patients and 113,383,368 controls. *World Psychiatry* **16**, 163–180 (2017).
68. Plana-Ripoll, O. *et al.* A comprehensive analysis of mortality-related health metrics associated with mental disorders: a nationwide, register-based cohort study. *Lancet*

- Lond. Engl.* **394**, 1827–1835 (2019).
69. Chesney, E., Goodwin, G. M. & Fazel, S. Risks of all-cause and suicide mortality in mental disorders: a meta-review. *World Psychiatry* **13**, 153–160 (2014).
70. KESSLER, R. C. *et al.* Lifetime prevalence and age-of-onset distributions of mental disorders in the World Health Organization's World Mental Health Survey Initiative. *World Psychiatry* **6**, 168–176 (2007).
71. Perälä, J. *et al.* Lifetime prevalence of psychotic and bipolar I disorders in a general population. *Arch. Gen. Psychiatry* **64**, 19–28 (2007).
72. Freeman, M. The World Mental Health Report: transforming mental health for all. *World Psychiatry* **21**, 391–392 (2022).
73. Cipriani, A. *et al.* Comparative efficacy and acceptability of 21 antidepressant drugs for the acute treatment of adults with major depressive disorder: a systematic review and network meta-analysis. *Lancet Lond. Engl.* **391**, 1357–1366 (2018).
74. Chen, P. *et al.* Mood stabilizers and risk of all-cause, natural, and suicide mortality in bipolar disorder: A nationwide cohort study. *Acta Psychiatr. Scand.* **147**, 234–247 (2023).
75. Hofmann, S. G., Asnaani, A., Vonk, I. J. J., Sawyer, A. T. & Fang, A. The Efficacy of Cognitive Behavioral Therapy: A Review of Meta-analyses. *Cogn. Ther. Res.* **36**, 427–440 (2012).
76. Espinoza, R. T. & Kellner, C. H. Electroconvulsive Therapy. *N. Engl. J. Med.* **386**, 667–672 (2022).
77. Leichsenring, F., Steinert, C., Rabung, S. & Ioannidis, J. P. A. The efficacy of psychotherapies and pharmacotherapies for mental disorders in adults: an umbrella review and meta-analytic evaluation of recent meta-analyses. *World Psychiatry* **21**,

- 133–145 (2022).
78. Harrison, J. E., Weber, S., Jakob, R. & Chute, C. G. ICD-11: an international classification of diseases for the twenty-first century. *BMC Med. Inform. Decis. Mak.* **21**, 206 (2021).
79. Kendler, K. S. A history of the DSM-5 scientific review committee. *Psychol. Med.* **43**, 1793–1800 (2013).
80. Kahneman, D., Sibony, O. & Sunstein, C. R. *Noise: a flaw in human judgment*. (Little, Brown Spark, 2021).
81. Clark, L. A., Cuthbert, B., Lewis-Fernández, R., Narrow, W. E. & Reed, G. M. Three Approaches to Understanding and Classifying Mental Disorder: ICD-11, DSM-5, and the National Institute of Mental Health's Research Domain Criteria (RDoC). *Psychol. Sci. Public Interest J. Am. Psychol. Soc.* **18**, 72–145 (2017).
82. Kendell, R. & Jablensky, A. Distinguishing between the validity and utility of psychiatric diagnoses. *Am. J. Psychiatry* **160**, 4–12 (2003).
83. Plana-Ripoll, O. *et al.* Exploring Comorbidity Within Mental Disorders Among a Danish National Population. *JAMA Psychiatry* **76**, 259–270 (2019).
84. Barr, P. B., Bigdeli, T. B. & Meyers, J. L. Prevalence, Comorbidity, and Sociodemographic Correlates of Psychiatric Disorders Reported in the All of Us Research Program. *JAMA Psychiatry* **79**, 622–628 (2022).
85. Galatzer-Levy, I. R. & Bryant, R. A. 636,120 Ways to Have Posttraumatic Stress Disorder. *Perspect. Psychol. Sci. J. Assoc. Psychol. Sci.* **8**, 651–662 (2013).
86. Sullivan, P. F. *et al.* Psychiatric Genomics: An Update and an Agenda. *Am. J. Psychiatry* **175**, 15–27 (2018).
87. Kallmann, F. J. THE GENETIC THEORY OF SCHIZOPHRENIA: An Analysis of 691

- Schizophrenic Twin Index Families. *Am. J. Psychiatry* **103**, 309–322 (1946).
88. Kendler, K. S. The Prehistory of Psychiatric Genetics: 1780–1910. *Am. J. Psychiatry* **178**, 490–508 (2021).
89. Halpin, M. Psychiatric genetics: from hereditary madness to big biology: by Michael Arribas-Ayllon, Andrew Bartlett, and Jamie Lewis, London, Routledge, 2019, 234 pp, \$124.00 (Hardback), ISBN-978-1-13-899998-5. *New Genet. Soc.* **39**, 502–504 (2020).
90. Evans, K., McGrath, J. & Milns, R. Searching for schizophrenia in ancient Greek and Roman literature: a systematic review: **Searching for schizophrenia**. *Acta Psychiatr. Scand.* **107**, 323–330 (2003).
91. Shih, R. A., Belmonte, P. L. & Zandi, P. P. A review of the evidence from family, twin and adoption studies for a genetic contribution to adult psychiatric disorders. *Int. Rev. Psychiatry* **16**, 260–283 (2004).
92. Rasic, D., Hajek, T., Alda, M. & Uher, R. Risk of Mental Illness in Offspring of Parents With Schizophrenia, Bipolar Disorder, and Major Depressive Disorder: A Meta-Analysis of Family High-Risk Studies. *Schizophr. Bull.* **40**, 28–38 (2014).
93. Carroll, L. S. & Owen, M. J. Genetic overlap between autism, schizophrenia and bipolar disorder. *Genome Med.* **1**, 102 (2009).
94. Hyman, S., Parikh, R., Collins, P. Y. & Patel, V. Adult Mental Disorders. in *Mental, Neurological, and Substance Use Disorders: Disease Control Priorities, Third Edition (Volume 4)* (eds. Patel, V., Chisholm, D., Dua, T., Laxminarayan, R. & Medina-Mora, M. E.) (The International Bank for Reconstruction and Development / The World Bank, 2016).
95. Heim, C. & Nemeroff, C. B. The role of childhood trauma in the neurobiology of mood and anxiety disorders: preclinical and clinical studies. *Biol. Psychiatry* **49**, 1023–1039

- (2001).
96. Kendler, K. S., Karkowski, L. M. & Prescott, C. A. Causal relationship between stressful life events and the onset of major depression. *Am. J. Psychiatry* **156**, 837–841 (1999).
97. Fiorentini, A. *et al.* Substance-Induced Psychoses: An Updated Literature Review. *Front. Psychiatry* **12**, 694863 (2021).
98. The Lancet Psychiatry, null. Of mice and mental health. *Lancet Psychiatry* **6**, 877 (2019).
99. Tricklebank, M. D., Robbins, T. W., Simmons, C. & Wong, E. H. F. Time to re-engage psychiatric drug discovery by strengthening confidence in preclinical psychopharmacology. *Psychopharmacology (Berl.)* **238**, 1417–1436 (2021).
100. Krystal, J. H., Abdallah, C. G., Sanacora, G., Charney, D. S. & Duman, R. S. Ketamine: A Paradigm Shift for Depression Research and Treatment. *Neuron* **101**, 774–778 (2019).
101. Daws, R. E. *et al.* Increased global integration in the brain after psilocybin therapy for depression. *Nat. Med.* **28**, 844–851 (2022).
102. V, A. *et al.* Analysis of shared heritability in common disorders of the brain. *Science* **360**, (2018).
103. Duncan, L. E., Ostacher, M. & Ballon, J. How genome-wide association studies (GWAS) made traditional candidate gene studies obsolete. *Neuropsychopharmacol. Off. Publ. Am. Coll. Neuropsychopharmacol.* **44**, 1518–1523 (2019).
104. Border, R. *et al.* No Support for Historical Candidate Gene or Candidate Gene-by-Interaction Hypotheses for Major Depression Across Multiple Large Samples. *Am. J. Psychiatry* **176**, 376–387 (2019).
105. International Human Genome Sequencing Consortium. Finishing the euchromatic sequence of the human genome. *Nature* **431**, 931–945 (2004).

106. 1000 Genomes Project Consortium *et al.* A map of human genome variation from population-scale sequencing. *Nature* **467**, 1061–1073 (2010).
107. International HapMap Consortium. The International HapMap Project. *Nature* **426**, 789–796 (2003).
108. Claussnitzer, M. *et al.* A brief history of human disease genetics. *Nature* **577**, 179–189 (2020).
109. Ak, W., Rsg, S., Cl, T. & Og, T. Decoding disease: from genomes to networks to phenotypes. *Nat. Rev. Genet.* **22**, (2021).
110. Uffelmann, E. & Posthuma, D. Emerging Methods and Resources for Biological Interrogation of Neuropsychiatric Polygenic Signal. *Biol. Psychiatry* **89**, 41–53 (2021).
111. Flint, J. & Ideker, T. The great hairball gambit. *PLoS Genet.* **15**, e1008519 (2019).
112. Grande, I., Berk, M., Birmaher, B. & Vieta, E. Bipolar disorder. *The Lancet* **387**, 1561–1572 (2016).
113. Murray, C. J. L. & Lopez, A. D. Measuring global health: motivation and evolution of the Global Burden of Disease Study. *The Lancet* **390**, 1460–1464 (2017).
114. Miller, J. N. & Black, D. W. Bipolar Disorder and Suicide: a Review. *Curr. Psychiatry Rep.* **22**, 6 (2020).
115. Trede, K. *et al.* Manic-Depressive Illness: Evolution in Kraepelin's Textbook, 1883–1926. *Harv. Rev. Psychiatry* **13**, 155–178 (2005).
116. Lanczik, M. & Fritze, J. Leonhard-Klassifikation endogener Psychosen - erste biologische Befunde und differentialtherapeutische Erwägungen. *Fortschritte Neurol. Psychiatr.* **60**, 296–304 (1992).

117. Tsuang, M. T., Taylor, L. & Faraone, S. V. An overview of the genetics of psychotic mood disorders. *J. Psychiatr. Res.* **38**, 3–15 (2004).
118. Smoller, J. W. & Finn, C. T. Family, twin, and adoption studies of bipolar disorder. *Am. J. Med. Genet. C Semin. Med. Genet.* **123C**, 48–58 (2003).
119. Mendlewicz, J. & Rainer, J. D. Adoption study supporting genetic transmission in manic-depressive illness. *Nature* **268**, 327–329 (1977).
120. Kendler, K. S., Ohlsson, H., Sundquist, J. & Sundquist, K. An Extended Swedish National Adoption Study of Bipolar Disorder Illness and Cross-Generational Familial Association With Schizophrenia and Major Depression. *JAMA Psychiatry* **77**, 814 (2020).
121. Schürhoff, F. *et al.* Early and late onset bipolar disorders: two different forms of manic-depressive illness? *J. Affect. Disord.* **58**, 215–221 (2000).
122. Alda, M., Grof, P., Grof, E., Zvolsky, P. & Walsh, M. Mode of inheritance in families of patients with lithium-responsive affective disorders. *Acta Psychiatr. Scand.* **90**, 304–310 (1994).
123. Potash, J. B. *et al.* The familial aggregation of psychotic symptoms in bipolar disorder pedigrees. *Am. J. Psychiatry* **158**, 1258–1264 (2001).
124. Jones, I. & Craddock, N. Do puerperal psychotic episodes identify a more familial subtype of bipolar disorder? Results of a family history study. *Psychiatr. Genet.* **12**, 177–180 (2002).
125. MacKinnon, D. F., McMahon, F. J., Simpson, S. G., McInnis, M. G. & DePaulo, J. R. Panic disorder with familial bipolar disorder. *Biol. Psychiatry* **42**, 90–95 (1997).
126. Angst, J., Frey, R., Lohmeyer, B. & Zerbin-Rüdin, E. Bipolar manic-depressive psychoses: results of a genetic investigation. *Hum. Genet.* **55**, 237–254 (1980).

127. Angst, J. & Grobler, C. Unipolar mania: a necessary diagnostic concept. *Eur. Arch. Psychiatry Clin. Neurosci.* **265**, 273–280 (2015).
128. Charney, A. W. *et al.* Evidence for genetic heterogeneity between clinical subtypes of bipolar disorder. *Transl. Psychiatry* **7**, e993 (2017).
129. Psychiatric GWAS Consortium Bipolar Disorder Working Group. Large-scale genome-wide association analysis of bipolar disorder identifies a new susceptibility locus near ODZ4. *Nat. Genet.* **43**, 977–983 (2011).
130. Baum, A. E. *et al.* A genome-wide association study implicates diacylglycerol kinase eta (DGKH) and several other genes in the etiology of bipolar disorder. *Mol. Psychiatry* **13**, 197–207 (2008).
131. Chen, D. T. *et al.* Genome-wide association study meta-analysis of European and Asian-ancestry samples identifies three novel loci associated with bipolar disorder. *Mol. Psychiatry* **18**, 195–205 (2013).
132. Mühleisen, T. W. *et al.* Genome-wide association study reveals two new risk loci for bipolar disorder. *Nat. Commun.* **5**, 3339 (2014).
133. Palmer, D. S. *et al.* Exome sequencing in bipolar disorder identifies AKAP11 as a risk gene shared with schizophrenia. *Nat. Genet.* **54**, 541–547 (2022).
134. Cade, J. F. J. Lithium salts in the treatment of psychotic excitement. *Med. J. Aust.* **2**, 349–352 (1949).
135. Tondo, L. *et al.* Clinical use of lithium salts: guide for users and prescribers. *Int. J. Bipolar Disord.* **7**, (2019).
136. Burdick, K. E. *et al.* The association between lithium use and neurocognitive performance in patients with bipolar disorder. *Neuropsychopharmacology* **45**,

- 1743–1749 (2020).
137. Hou, L. *et al.* Genetic variants associated with response to lithium treatment in bipolar disorder: a genome-wide association study. *The Lancet* **387**, 1085–1093 (2016).
138. Papiol, S., Schulze, T. G. & Alda, M. Genetics of Lithium Response in Bipolar Disorder. *Pharmacopsychiatry* **51**, 206–211 (2018).
139. Dudev, T., Mazmanian, K., Weng, W. H., Grauffel, C. & Lim, C. Free and Bound Therapeutic Lithium in Brain Signaling. *Acc. Chem. Res.* **52**, 2960–2970 (2019).
140. Hallcher, L. M. & Sherman, W. R. The effects of lithium ion and other agents on the activity of myo-inositol-1-phosphatase from bovine brain. *J. Biol. Chem.* **255**, 10896–10901 (1980).
141. Klein, P. S. & Melton, D. A. A molecular mechanism for the effect of lithium on development. *Proc. Natl. Acad. Sci. U. S. A.* **93**, 8455–8459 (1996).
142. Phiel, C. J. & Klein, P. S. Molecular targets of lithium action. *Annu. Rev. Pharmacol. Toxicol.* **41**, 789–813 (2001).
143. Berridge, M. J., Downes, C. P. & Hanley, M. R. Neural and developmental actions of lithium: A unifying hypothesis. *Cell* **59**, 411–419 (1989).
144. Sade, Y. *et al.* IP<sub>3</sub> accumulation and/or inositol depletion: two downstream lithium's effects that may mediate its behavioral and cellular changes. *Transl. Psychiatry* **6**, e968 (2016).
145. Gould, T. D., Zarate, C. A. & Manji, H. K. Glycogen synthase kinase-3: a target for novel bipolar disorder treatments. *J. Clin. Psychiatry* **65**, 10–21 (2004).
146. Busa, W. B. & Gimlich, R. L. Lithium-induced teratogenesis in frog embryos prevented by a polyphosphoinositide cycle intermediate or a diacylglycerol analog. *Dev. Biol.* **132**,

- 315–324 (1989).
147. Azab, A. N., He, Q., Ju, S., Li, G. & Greenberg, M. L. Glycogen synthase kinase-3 is required for optimal de novo synthesis of inositol. *Mol. Microbiol.* **63**, 1248–1258 (2007).
148. Ye, C. & Greenberg, M. L. Inositol synthesis regulates the activation of GSK-3 $\alpha$  in neuronal cells. *J. Neurochem.* **133**, 273–283 (2015).
149. Lichtenstein, P. *et al.* Common genetic determinants of schizophrenia and bipolar disorder in Swedish families: a population-based study. *The Lancet* **373**, 234–239 (2009).
150. Maier, W. Continuity and Discontinuity of Affective Disorders and Schizophrenia: Results of a Controlled Family Study. *Arch. Gen. Psychiatry* **50**, 871 (1993).
151. The Schizophrenia Psychiatric Genome-Wide Association Study (GWAS) Consortium. Genome-wide association study identifies five new schizophrenia loci. *Nat. Genet.* **43**, 969–976 (2011).
152. The International Schizophrenia Consortium. Common polygenic variation contributes to risk of schizophrenia and bipolar disorder. *Nature* **460**, 748–752 (2009).
153. Curtis, D. *et al.* Case-case genome-wide association analysis shows markers differentially associated with schizophrenia and bipolar disorder and implicates calcium channel genes. *Psychiatr. Genet.* **21**, 1–4 (2011).
154. Ruderfer, D. M. *et al.* Polygenic dissection of diagnosis and clinical dimensions of bipolar disorder and schizophrenia. *Mol. Psychiatry* **19**, 1017–1024 (2014).
155. Gulsuner, S. & McClellan, J. M. Copy Number Variation in Schizophrenia. *Neuropsychopharmacology* **40**, 252–254 (2015).

156. Kirov, G. *et al.* De novo CNV analysis implicates specific abnormalities of postsynaptic signalling complexes in the pathogenesis of schizophrenia. *Mol. Psychiatry* **17**, 142–153 (2012).
157. Psychosis Endophenotypes International Consortium *et al.* Contribution of copy number variants to schizophrenia from a genome-wide study of 41,321 subjects. *Nat. Genet.* **49**, 27–35 (2017).
158. The International Schizophrenia Consortium. Rare chromosomal deletions and duplications increase risk of schizophrenia. *Nature* **455**, 237–241 (2008).
159. Szatkiewicz, J. P. *et al.* Copy number variation in schizophrenia in Sweden. *Mol. Psychiatry* **19**, 762–773 (2014).
160. Maury, E. A. *et al.* Schizophrenia-associated somatic copy number variants from 12,834 cases reveal contribution to risk and recurrent, isoform-specific NRXN1 disruptions. <http://medrxiv.org/lookup/doi/10.1101/2021.12.24.21268385> (2022)  
doi:10.1101/2021.12.24.21268385.
161. Brownstein, C. A. *et al.* Similar Rates of Deleterious Copy Number Variants in Early-Onset Psychosis and Autism Spectrum Disorder. *Am. J. Psychiatry* **179**, 853–861 (2022).
162. Green, E. K. *et al.* Copy number variation in bipolar disorder. *Mol. Psychiatry* **21**, 89–93 (2016).
163. Charney, A. W. *et al.* Contribution of Rare Copy Number Variants to Bipolar Disorder Risk Is Limited to Schizoaffective Cases. *Biol. Psychiatry* **86**, 110–119 (2019).
164. Fromer, M. *et al.* De novo mutations in schizophrenia implicate synaptic networks. *Nature* **506**, 179–184 (2014).

165. Kataoka, M. *et al.* Exome sequencing for bipolar disorder points to roles of de novo loss-of-function and protein-altering mutations. *Mol. Psychiatry* **21**, 885–893 (2016).
166. Arnone, D. *et al.* Magnetic resonance imaging studies in bipolar disorder and schizophrenia: meta-analysis. *Br. J. Psychiatry* **195**, 194–201 (2009).
167. Ellison-Wright, I. & Bullmore, E. Anatomy of bipolar disorder and schizophrenia: A meta-analysis. *Schizophr. Res.* **117**, 1–12 (2010).
168. Hajjma, S. V. *et al.* Brain Volumes in Schizophrenia: A Meta-Analysis in Over 18 000 Subjects. *Schizophr. Bull.* **39**, 1129–1138 (2013).
169. the Costa Rica/Colombia Consortium for Genetic Investigation of Bipolar Endophenotypes *et al.* Subcortical volumetric abnormalities in bipolar disorder. *Mol. Psychiatry* **21**, 1710–1716 (2016).
170. McDonald, C. *et al.* Association of Genetic Risks for Schizophrenia and Bipolar Disorder With Specific and Generic Brain Structural Endophenotypes. *Arch. Gen. Psychiatry* **61**, 974 (2004).
171. for the ENIGMA Schizophrenia Working Group *et al.* Subcortical brain volume abnormalities in 2028 individuals with schizophrenia and 2540 healthy controls via the ENIGMA consortium. *Mol. Psychiatry* **21**, 547–553 (2016).
172. COCERO *et al.* Abnormal asymmetries in subcortical brain volume in schizophrenia. *Mol. Psychiatry* **21**, 1460–1466 (2016).
173. van Baal, G. C. M. Overlapping and Segregating Structural Brain Abnormalities in Twins With Schizophrenia or Bipolar Disorder. *Arch. Gen. Psychiatry* **69**, 349 (2012).
174. Sugranyes, G. *et al.* Gray Matter Volume Decrease Distinguishes Schizophrenia From Bipolar Offspring During Childhood and Adolescence. *J. Am. Acad. Child Adolesc. Psychiatry* **55**, 333–341 (2016).

- Psychiatry* **54**, 677–684.e2 (2015).
175. Collin, G., Scholtens, L. H., Kahn, R. S., Hillegers, M. H. J. & van den Heuvel, M. P. Affected Anatomical Rich Club and Structural–Functional Coupling in Young Offspring of Schizophrenia and Bipolar Disorder Patients. *Biol. Psychiatry* **82**, 746–755 (2017).
176. McDonald, C. *et al.* Regional Brain Morphometry in Patients With Schizophrenia or Bipolar Disorder and Their Unaffected Relatives. *Am. J. Psychiatry* **163**, 478–487 (2006).
177. Brown, G. G. *et al.* Voxel-based morphometry of patients with schizophrenia or bipolar I disorder: A matched control study. *Psychiatry Res. Neuroimaging* **194**, 149–156 (2011).
178. Schizophrenia Working Group of the Psychiatric Genomics Consortium. Biological insights from 108 schizophrenia-associated genetic loci. *Nature* **511**, 421–427 (2014).
179. Trubetskoy, V. *et al.* Mapping genomic loci implicates genes and synaptic biology in schizophrenia. *Nature* **604**, 502–508 (2022).
180. Singh, T. *et al.* Rare coding variants in ten genes confer substantial risk for schizophrenia. *Nature* **604**, 509–516 (2022).
181. Gulsuner, S. *et al.* Genetics of schizophrenia in the South African Xhosa. *Science* **367**, 569–573 (2020).
182. The BrainSeq Consortium *et al.* Developmental and genetic regulation of the human cortex transcriptome illuminate schizophrenia pathogenesis. *Nat. Neurosci.* **21**, 1117–1125 (2018).
183. Zandi, P. P. *et al.* Amygdala and anterior cingulate transcriptomes from individuals with bipolar disorder reveal downregulated neuroimmune and synaptic pathways. *Nat. Neurosci.* **25**, 381–389 (2022).

184. Bayés, À. *et al.* Characterization of the proteome, diseases and evolution of the human postsynaptic density. *Nat. Neurosci.* **14**, 19–21 (2011).
185. Sheng, M. & Hoogenraad, C. C. The Postsynaptic Architecture of Excitatory Synapses: A More Quantitative View. *Annu. Rev. Biochem.* **76**, 823–847 (2007).
186. Dejanovic, B. *et al.* Changes in the Synaptic Proteome in Tauopathy and Rescue of Tau-Induced Synapse Loss by C1q Antibodies. *Neuron* **100**, 1322–1336.e7 (2018).
187. Sullivan, P. IS BRAIN CELL TYPE THE KEY READOUT OF GWAS? *Eur. Neuropsychopharmacol.* **63**, e35 (2022).
188. ReproGen Consortium *et al.* Partitioning heritability by functional annotation using genome-wide association summary statistics. *Nat. Genet.* **47**, 1228–1235 (2015).
189. de Leeuw, C. A., Mooij, J. M., Heskes, T. & Posthuma, D. MAGMA: Generalized Gene-Set Analysis of GWAS Data. *PLOS Comput. Biol.* **11**, e1004219 (2015).
190. Habib, N. *et al.* Massively parallel single-nucleus RNA-seq with DroNc-seq. *Nat. Methods* **14**, 955–958 (2017).
191. Mauri, M. C. *et al.* Clinical pharmacology of atypical antipsychotics: an update. *EXCLI J.* **13**, 1163–1191 (2014).
192. Kim, Y. *et al.* Comparative genomic evidence for the involvement of schizophrenia risk genes in antipsychotic effects. *Mol. Psychiatry* **23**, 708–712 (2018).
193. Abrantes, A. *et al.* Gene expression changes following chronic antipsychotic exposure in single cells from mouse striatum. *Mol. Psychiatry* **27**, 2803–2812 (2022).
194. Clarke, L. E. & Barres, B. A. Emerging roles of astrocytes in neural circuit development. *Nat. Rev. Neurosci.* **14**, 311–321 (2013).
195. Palmer, A. L. & Ousman, S. S. Astrocytes and Aging. *Front. Aging Neurosci.* **10**, 337

- (2018).
196. Alberini, C. M., Cruz, E., Descalzi, G., Bessières, B. & Gao, V. Astrocyte glycogen and lactate: new insights into learning and memory mechanisms. *Glia* **66**, 1244–1262 (2018).
197. Shigetomi, E. & Koizumi, S. The role of astrocytes in behaviors related to emotion and motivation. *Neurosci. Res.* **187**, 21–39 (2023).
198. Montalant, A., Carlsen, E. M. M. & Perrier, J. Role of astrocytes in rhythmic motor activity. *Physiol. Rep.* **9**, (2021).
199. Hasan, M. *et al.* Chemogenetic activation of astrocytes promotes remyelination and restores cognitive deficits in visceral hypersensitive rats. *iScience* **26**, 105840 (2023).
200. Burda, J. E., Bernstein, A. M. & Sofroniew, M. V. Astrocyte roles in traumatic brain injury. *Exp. Neurol.* **275 Pt 3**, 305–315 (2016).
201. Burda, J. E. & Sofroniew, M. V. Reactive gliosis and the multicellular response to CNS damage and disease. *Neuron* **81**, 229–248 (2014).
202. Parpura, V. *et al.* Glial cells in (patho)physiology. *J. Neurochem.* **121**, 4–27 (2012).
203. Pekny, M. & Pekna, M. Astrocyte reactivity and reactive astrogliosis: costs and benefits. *Physiol. Rev.* **94**, 1077–1098 (2014).
204. Pekny, M. *et al.* Astrocytes: a central element in neurological diseases. *Acta Neuropathol. (Berl.)* **131**, 323–345 (2016).
205. Sofroniew, M. V. Astrocyte barriers to neurotoxic inflammation. *Nat. Rev. Neurosci.* **16**, 249–263 (2015).
206. Sofroniew, M. V. Astrogliosis. *Cold Spring Harb. Perspect. Biol.* **7**, a020420 (2014).
207. Verkhratsky, A., Parpura, V., Pekna, M., Pekny, M. & Sofroniew, M. Glia in the

- pathogenesis of neurodegenerative diseases. *Biochem. Soc. Trans.* **42**, 1291–1301 (2014).
208. Verkhratsky, A. *et al.* Neurological diseases as primary gliopathies: a reassessment of neurocentrism. *ASN Neuro* **4**, e00082 (2012).
209. Cabezas, R. *et al.* Astrocytic modulation of blood brain barrier: perspectives on Parkinson's disease. *Front. Cell. Neurosci.* **8**, 211 (2014).
210. Linnerbauer, M., Wheeler, M. A. & Quintana, F. J. Astrocyte crosstalk in CNS inflammation. *Neuron* **108**, 608–622 (2020).
211. Beard, E., Lengacher, S., Dias, S., Magistretti, P. J. & Finsterwald, C. Astrocytes as Key Regulators of Brain Energy Metabolism: New Therapeutic Perspectives. *Front. Physiol.* **12**, 825816 (2022).
212. Bonvento, G. & Bolaños, J. P. Astrocyte-neuron metabolic cooperation shapes brain activity. *Cell Metab.* **33**, 1546–1564 (2021).
213. McGann, J. C. & Mandel, G. Neuronal activity induces glutathione metabolism gene expression in astrocytes. *Glia* **66**, 2024–2039 (2018).
214. Mahmoud, S., Gharagozloo, M., Simard, C. & Gris, D. Astrocytes Maintain Glutamate Homeostasis in the CNS by Controlling the Balance between Glutamate Uptake and Release. *Cells* **8**, 184 (2019).
215. Jessen, N. A., Munk, A. S. F., Lundgaard, I. & Nedergaard, M. The Glymphatic System – A Beginner's Guide. *Neurochem. Res.* **40**, 2583–2599 (2015).
216. Chung, W.-S. *et al.* Astrocytes mediate synapse elimination through MEGF10 and MERTK pathways. *Nature* **504**, 394–400 (2013).
217. Lee, J.-H. *et al.* Astrocytes phagocytose adult hippocampal synapses for circuit

- homeostasis. *Nature* **590**, 612–617 (2021).
218. Walker, C. D., Risher, W. C. & Risher, M.-L. Regulation of Synaptic Development by Astrocyte Signaling Factors and Their Emerging Roles in Substance Abuse. *Cells* **9**, 297 (2020).
219. Oberheim, N. A. *et al.* Uniquely hominid features of adult human astrocytes. *J. Neurosci. Off. J. Soc. Neurosci.* **29**, 3276–3287 (2009).
220. Kriegstein, A. & Alvarez-Buylla, A. The Glial Nature of Embryonic and Adult Neural Stem Cells. *Annu. Rev. Neurosci.* **32**, 149–184 (2009).
221. Akdemir, E. S., Huang, A. Y.-S. & Deneen, B. Astrocytogenesis: where, when, and how. *F1000Research* **9**, F1000 Faculty Rev-233 (2020).
222. Oberheim, N. A., Goldman, S. A. & Nedergaard, M. Heterogeneity of Astrocytic Form and Function. *Methods Mol. Biol. Clifton NJ* **814**, 23–45 (2012).
223. Khakh, B. S. & Sofroniew, M. V. Diversity of astrocyte functions and phenotypes in neural circuits. *Nat. Neurosci.* **18**, 942–952 (2015).
224. Chaboub, L. S. *et al.* Temporal Profiling of Astrocyte Precursors Reveals Parallel Roles for Asef during Development and after Injury. *J. Neurosci.* **36**, 11904–11917 (2016).
225. Freeman, M. R. Specification and Morphogenesis of Astrocytes. *Science* **330**, 774 (2010).
226. Preston, A. N., Cervasio, D. A. & Laughlin, S. T. Visualizing the brain's astrocytes. *Methods Enzymol.* **622**, 129–151 (2019).
227. Jurga, A. M., Paleczna, M., Kadluczka, J. & Kuter, K. Z. Beyond the GFAP-Astrocyte Protein Markers in the Brain. *Biomolecules* **11**, 1361 (2021).
228. Krupenko, S. A. FDH: an Aldehyde Dehydrogenase Fusion Enzyme in Folate

- Metabolism. *Chem. Biol. Interact.* **178**, 84–93 (2009).
229. Escartin, C. *et al.* Reactive astrocyte nomenclature, definitions, and future directions. *Nat. Neurosci.* **24**, 312–325 (2021).
230. Zamanian, J. L. *et al.* Genomic Analysis of Reactive Astrogliosis. *J. Neurosci.* **32**, 6391–6410 (2012).
231. Teh, D. B. L. *et al.* Transcriptome Analysis Reveals Neuroprotective aspects of Human Reactive Astrocytes induced by Interleukin 1 $\beta$ . *Sci. Rep.* **7**, 13988 (2017).
232. Chai, H. *et al.* Neural Circuit-Specialized Astrocytes: Transcriptomic, Proteomic, Morphological, and Functional Evidence. *Neuron* **95**, 531–549.e9 (2017).
233. Matusova, Z., Hol, E. M., Pekny, M., Kubista, M. & Valihrach, L. Reactive astrogliosis in the era of single-cell transcriptomics. *Front. Cell. Neurosci.* **17**, (2023).
234. Sofroniew, M. V. Astrocyte Reactivity: Subtypes, States, and Functions in CNS Innate Immunity. *Trends Immunol.* **41**, 758–770 (2020).
235. Hasel, P. & Liddelow, S. A. Astrocytes. *Curr. Biol. CB* **31**, R326–R327 (2021).
236. Acaz-Fonseca, E., Avila-Rodriguez, M., Garcia-Segura, L. M. & Barreto, G. E. Regulation of astroglia by gonadal steroid hormones under physiological and pathological conditions. *Prog. Neurobiol.* **144**, 5–26 (2016).
237. Marpegan, L. *et al.* Circadian regulation of ATP release in astrocytes. *J. Neurosci. Off. J. Soc. Neurosci.* **31**, 8342–8350 (2011).
238. Jackson, F. R. Glial cell modulation of circadian rhythms. *Glia* **59**, 1341–1350 (2011).
239. Falcone, C. Evolution of astrocytes: From invertebrates to vertebrates. *Front. Cell Dev. Biol.* **10**, 931311 (2022).
240. Hamby, M. E. *et al.* Inflammatory Mediators Alter the Astrocyte Transcriptome and

- Calcium Signaling Elicited by Multiple G-Protein-Coupled Receptors. *J. Neurosci.* **32**, 14489–14510 (2012).
241. Sun, D. & Jakobs, T. C. Structural Remodeling of Astrocytes in the Injured CNS. *Neurosci. Rev. J. Bringing Neurobiol. Neurol. Psychiatry* **18**, 567–588 (2012).
242. Silva, B. *et al.* Glia fuel neurons with locally synthesized ketone bodies to sustain memory under starvation. *Nat. Metab.* **4**, 213–224 (2022).
243. Bezzi, P. & Volterra, A. Astrocytes: Powering Memory. *Cell* **144**, 644–645 (2011).
244. Tadi, M., Allaman, I., Lengacher, S., Grenningloh, G. & Magistretti, P. J. Learning-Induced Gene Expression in the Hippocampus Reveals a Role of Neuron-Astrocyte Metabolic Coupling in Long Term Memory. *PLOS ONE* **10**, e0141568 (2015).
245. Xiong, X.-Y., Tang, Y. & Yang, Q.-W. Metabolic changes favor the activity and heterogeneity of reactive astrocytes. *Trends Endocrinol. Metab.* **33**, 390–400 (2022).
246. Chen, Y. *et al.* The role of astrocytes in oxidative stress of central nervous system: A mixed blessing. *Cell Prolif.* **53**, e12781 (2020).
247. Park, M. W. *et al.* NOX4 promotes ferroptosis of astrocytes by oxidative stress-induced lipid peroxidation via the impairment of mitochondrial metabolism in Alzheimer's diseases. *Redox Biol.* **41**, 101947 (2021).
248. Ioannou, M. S. *et al.* Neuron-Astrocyte Metabolic Coupling Protects against Activity-Induced Fatty Acid Toxicity. *Cell* **177**, 1522-1535.e14 (2019).
249. Halassa, M. M. & Haydon, P. G. Integrated brain circuits: astrocytic networks modulate neuronal activity and behavior. *Annu. Rev. Physiol.* **72**, 335–355 (2010).
250. Magistretti, P. J. & Pellerin, L. Cellular bases of brain energy metabolism and their relevance to functional brain imaging: evidence for a prominent role of astrocytes.

- Cereb. Cortex N. Y. N* **6**, 50–61 (1996).
251. Raichle, M. E. & Mintun, M. A. Brain work and brain imaging. *Annu. Rev. Neurosci.* **29**, 449–476 (2006).
252. Figley, C. R. & Stroman, P. W. The role(s) of astrocytes and astrocyte activity in neurometabolism, neurovascular coupling, and the production of functional neuroimaging signals. *Eur. J. Neurosci.* **33**, 577–588 (2011).
253. Roumes, H. *et al.* Lactate transporters in the rat barrel cortex sustain whisker-dependent BOLD fMRI signal and behavioral performance. *Proc. Natl. Acad. Sci. U. S. A.* **118**, e2112466118 (2021).
254. Pellerin, L. & Magistretti, P. J. Glutamate uptake into astrocytes stimulates aerobic glycolysis: a mechanism coupling neuronal activity to glucose utilization. *Proc. Natl. Acad. Sci. U. S. A.* **91**, 10625–10629 (1994).
255. Barros, L. F. Metabolic signaling by lactate in the brain. *Trends Neurosci.* **36**, 396–404 (2013).
256. Mason, S. Lactate Shuttles in Neuroenergetics—Homeostasis, Allostasis and Beyond. *Front. Neurosci.* **11**, (2017).
257. Magistretti, P. J., Sorg, O., Yu, N., Martin, J. L. & Pellerin, L. Neurotransmitters regulate energy metabolism in astrocytes: implications for the metabolic trafficking between neural cells. *Dev. Neurosci.* **15**, 306–312 (1993).
258. Coggan, J. S. *et al.* Norepinephrine stimulates glycogenolysis in astrocytes to fuel neurons with lactate. *PLoS Comput. Biol.* **14**, e1006392 (2018).
259. Fink, K., Velebit, J., Vardjan, N., Zorec, R. & Kreft, M. Noradrenaline-induced l-lactate production requires d-glucose entry and transit through the glycogen shunt in

- single-cultured rat astrocytes. *J. Neurosci. Res.* **99**, 1084–1098 (2021).
260. Chih, C.-P. & Roberts, E. L. Energy substrates for neurons during neural activity: a critical review of the astrocyte-neuron lactate shuttle hypothesis. *J. Cereb. Blood Flow Metab. Off. J. Int. Soc. Cereb. Blood Flow Metab.* **23**, 1263–1281 (2003).
261. Li, X. *et al.* Lactate metabolism in human health and disease. *Signal Transduct. Target. Ther.* **7**, 1–22 (2022).
262. Lee, T.-Y. Lactate: a multifunctional signaling molecule. *Yeungnam Univ. J. Med.* **38**, 183–193 (2021).
263. Yao, S. *et al.* Astrocytic lactate dehydrogenase A regulates neuronal excitability and depressive-like behaviors through lactate homeostasis in mice. *Nat. Commun.* **14**, 729 (2023).
264. Muraleedharan, R. *et al.* AMPK-Regulated Astrocytic Lactate Shuttle Plays a Non-Cell-Autonomous Role in Neuronal Survival. *Cell Rep.* **32**, 108092 (2020).
265. Cauli, B., Dusart, I. & Li, D. Lactate as a determinant of neuronal excitability, neuroenergetics and beyond. *Neurobiol. Dis.* **184**, 106207 (2023).
266. Allen, N. J. & Eroglu, C. Cell Biology of Astrocyte-Synapse Interactions. *Neuron* **96**, 697–708 (2017).
267. Yang, J. *et al.* Lactate promotes plasticity gene expression by potentiating NMDA signaling in neurons. *Proc. Natl. Acad. Sci.* **111**, 12228–12233 (2014).
268. Margineanu, M. B., Mahmood, H., Fiumelli, H. & Magistretti, P. J. L-Lactate Regulates the Expression of Synaptic Plasticity and Neuroprotection Genes in Cortical Neurons: A Transcriptome Analysis. *Front. Mol. Neurosci.* **11**, 375 (2018).
269. Zhang, W. *et al.* Lactate Is a Natural Suppressor of RLR Signaling by Targeting MAVS.

- Cell* **178**, 176-189.e15 (2019).
270. Zhang, D. *et al.* Metabolic regulation of gene expression by histone lactylation. *Nature* **574**, 575–580 (2019).
271. Brown, T. P. *et al.* The lactate receptor GPR81 promotes breast cancer growth via a paracrine mechanism involving antigen-presenting cells in the tumor microenvironment. *Oncogene* **39**, 3292–3304 (2020).
272. Kantarci, H., Gou, Y. & Riley, B. B. The Warburg Effect and lactate signaling augment Fgf-MAPK to promote sensory-neural development in the otic vesicle. *eLife* **9**, e56301 (2020).
273. Daw, C. C. *et al.* Lactate Elicits ER-Mitochondrial Mg<sup>2+</sup> Dynamics to Integrate Cellular Metabolism. *Cell* **183**, 474-489.e17 (2020).
274. Liu, W. *et al.* Lactate modulates iron metabolism by binding soluble adenylyl cyclase. *Cell Metab.* (2023) doi:10.1016/j.cmet.2023.06.017.
275. Magistretti, P. J. How lactate links cannabis to social behaviour. *Nature* **583**, 526–527 (2020).
276. Liu, W. *et al.* Lactate regulates cell cycle by remodelling the anaphase promoting complex. *Nature* **616**, 790–797 (2023).
277. Sanmarco, L. M. *et al.* Lactate limits CNS autoimmunity by stabilizing HIF-1 $\alpha$  in dendritic cells. *Nature* **1–9** (2023) doi:10.1038/s41586-023-06409-6.
278. Cai, X. *et al.* Lactate activates the mitochondrial electron transport chain independent of its metabolism. <http://biorxiv.org/lookup/doi/10.1101/2023.08.02.551712> (2023) doi:10.1101/2023.08.02.551712.
279. Bi, Q. *et al.* Relationship between the disrupted topological efficiency of the

- structural brain connectome and glucose hypometabolism in normal aging. *NeuroImage* **226**, 117591 (2021).
280. Gong, G. *et al.* Age- and gender-related differences in the cortical anatomical network. *J. Neurosci. Off. J. Soc. Neurosci.* **29**, 15684–15693 (2009).
281. Goyal, M. S. *et al.* Loss of Brain Aerobic Glycolysis in Normal Human Aging. *Cell Metab.* **26**, 353-360.e3 (2017).
282. Zulfiqar, S., Garg, P. & Nieweg, K. Contribution of astrocytes to metabolic dysfunction in the Alzheimer's disease brain. *Biol. Chem.* **400**, 1113–1127 (2019).
283. Costantini, L. C., Barr, L. J., Vogel, J. L. & Henderson, S. T. Hypometabolism as a therapeutic target in Alzheimer's disease. *BMC Neurosci.* **9 Suppl 2**, S16 (2008).
284. Arendt, T., Brückner, M. K., Morawski, M., Jäger, C. & Gertz, H.-J. Early neurone loss in Alzheimer's disease: cortical or subcortical? *Acta Neuropathol. Commun.* **3**, 10 (2015).
285. Bergau, N., Maul, S., Rujescu, D., Simm, A. & Navarrete Santos, A. Reduction of Glycolysis Intermediate Concentrations in the Cerebrospinal Fluid of Alzheimer's Disease Patients. *Front. Neurosci.* **13**, 871 (2019).
286. Aubert, A., Pellerin, L., Magistretti, P. J. & Costalat, R. A coherent neurobiological framework for functional neuroimaging provided by a model integrating compartmentalized energy metabolism. *Proc. Natl. Acad. Sci. U. S. A.* **104**, 4188–4193 (2007).
287. Escartin, C., Valette, J., Lebon, V. & Bonvento, G. Neuron-astrocyte interactions in the regulation of brain energy metabolism: a focus on NMR spectroscopy. *J. Neurochem.* **99**, 393–401 (2006).
288. Hertz, L., Peng, L. & Dienel, G. A. Energy metabolism in astrocytes: high rate of

- oxidative metabolism and spatiotemporal dependence on glycolysis/glycogenolysis. *J. Cereb. Blood Flow Metab. Off. J. Int. Soc. Cereb. Blood Flow Metab.* **27**, 219–249 (2007).
289. Sokoloff, L. Energetics of functional activation in neural tissues. *Neurochem. Res.* **24**, 321–329 (1999).
290. Verkhratsky, A. & Toescu, E. C. Neuronal-glial networks as substrate for CNS integration. *J. Cell. Mol. Med.* **10**, 826–836 (2006).
291. Hall, C. N., Klein-Flügge, M. C., Howarth, C. & Attwell, D. Oxidative Phosphorylation, Not Glycolysis, Powers Presynaptic and Postsynaptic Mechanisms Underlying Brain Information Processing. *J. Neurosci.* **32**, 8940–8951 (2012).
292. Bolaños, J. P., Almeida, A. & Moncada, S. Glycolysis: a bioenergetic or a survival pathway? *Trends Biochem. Sci.* **35**, 145–149 (2010).
293. Mangia, S. et al. Metabolic and hemodynamic events after changes in neuronal activity: current hypotheses, theoretical predictions and in vivo NMR experimental findings. *J. Cereb. Blood Flow Metab. Off. J. Int. Soc. Cereb. Blood Flow Metab.* **29**, 441–463 (2009).
294. Rouach, N., Koulakoff, A., Abudara, V., Willecke, K. & Giaume, C. Astroglial metabolic networks sustain hippocampal synaptic transmission. *Science* **322**, 1551–1555 (2008).
295. Tsacopoulos, M. & Magistretti, P. J. Metabolic coupling between glia and neurons. *J. Neurosci. Off. J. Soc. Neurosci.* **16**, 877–885 (1996).
296. Brown, A. M. et al. Astrocyte glycogen metabolism is required for neural activity during aglycemia or intense stimulation in mouse white matter. *J. Neurosci. Res.* **79**, 74–80 (2005).
297. Gruetter, R. Glycogen: the forgotten cerebral energy store. *J. Neurosci. Res.* **74**,

- 179–183 (2003).
298. Abi-Saab, W. M. *et al.* Striking differences in glucose and lactate levels between brain extracellular fluid and plasma in conscious human subjects: effects of hyperglycemia and hypoglycemia. *J. Cereb. Blood Flow Metab. Off. J. Int. Soc. Cereb. Blood Flow Metab.* **22**, 271–279 (2002).
299. Magnoni, S. *et al.* Lack of improvement in cerebral metabolism after hyperoxia in severe head injury: a microdialysis study. *J. Neurosurg.* **98**, 952–958 (2003).
300. Galeffi, F., Foster, K. A., Sadgrove, M. P., Beaver, C. J. & Turner, D. A. Lactate uptake contributes to the NAD(P)H biphasic response and tissue oxygen response during synaptic stimulation in area CA1 of rat hippocampal slices. *J. Neurochem.* **103**, 2449–2461 (2007).
301. Öz, G. *et al.* Neuroglial metabolism in the awake rat brain: CO<sub>2</sub> fixation increases with brain activity. *J. Neurosci.* **24**, 11273–11279 (2004).
302. Herde, M. K. *et al.* Local Efficacy of Glutamate Uptake Decreases with Synapse Size. *Cell Rep.* **32**, 108182 (2020).
303. Martyn, J. A. J., Fagerlund, M. J. & Eriksson, L. I. Basic principles of neuromuscular transmission. *Anaesthesia* **64**, 1–9 (2009).
304. Gibbons, H. M. & Dragunow, M. Adult human brain cell culture for neuroscience research. *Int. J. Biochem. Cell Biol.* **42**, 844–856 (2010).
305. Kadish, I. *et al.* Hippocampal and Cognitive Aging across the Lifespan: A Bioenergetic Shift Precedes and Increased Cholesterol Trafficking Parallels Memory Impairment. *J. Neurosci.* **29**, 1805–1816 (2009).
306. Kapogiannis, D. & Avgerinos, K. I. Brain glucose and ketone utilization in brain aging

- and neurodegenerative diseases. in *International Review of Neurobiology* vol. 154 79–110 (Elsevier, 2020).
307. Chocron, E. S. *et al.* The Trifunctional Protein Mediates Thyroid Hormone Receptor-Dependent Stimulation of Mitochondria Metabolism. *Mol. Endocrinol.* **26**, 1117–1128 (2012).
308. Sayre, N. L. *et al.* Stimulation of astrocyte fatty acid oxidation by thyroid hormone is protective against ischemic stroke-induced damage. *J. Cereb. Blood Flow Metab.* **37**, 514–527 (2017).
309. Olzmann, J. A. & Carvalho, P. Dynamics and functions of lipid droplets. *Nat. Rev. Mol. Cell Biol.* **20**, 137–155 (2019).
310. Mejhert, N. *et al.* The Lipid Droplet Knowledge Portal: A resource for systematic analyses of lipid droplet biology. *Dev. Cell* **57**, 387–397.e4 (2022).
311. Eraso-Pichot, A. *et al.* GSEA of mouse and human mitochondriomes reveals fatty acid oxidation in astrocytes. *Glia* **66**, 1724–1735 (2018).
312. Polyzos, A. A. *et al.* Metabolic Reprogramming in Astrocytes Distinguishes Region-Specific Neuronal Susceptibility in Huntington Mice. *Cell Metab.* **29**, 1258–1273.e11 (2019).
313. Giaume, C., Koulakoff, A., Roux, L., Holcman, D. & Rouach, N. Astroglial networks: a step further in neuroglial and gliovascular interactions. *Nat. Rev. Neurosci.* **11**, 87–99 (2010).
314. Porkka-Heiskanen, T. *et al.* Adenosine: A Mediator of the Sleep-Inducing Effects of Prolonged Wakefulness. *Science* **276**, 1265–1268 (1997).
315. Halassa, M. M. *et al.* Astrocytic Modulation of Sleep Homeostasis and Cognitive

- Consequences of Sleep Loss. *Neuron* **61**, 213–219 (2009).
316. Clasadonte, J., Scemes, E., Wang, Z., Boison, D. & Haydon, P. G. Connexin 43-Mediated Astroglial Metabolic Networks Contribute to the Regulation of the Sleep-Wake Cycle. *Neuron* **95**, 1365-1380.e5 (2017).
317. Fan, T. W. M. *et al.* Stable isotope-resolved metabolomic analysis of lithium effects on glial-neuronal metabolism and interactions. *Metabolomics* **6**, 165–179 (2010).
318. Friede, R. L. The Enzymatic Response of Astrocytes To Various Ions in Vitro. *J. Cell Biol.* **20**, 5–15 (1964).
319. Santos, R. *et al.* Differentiation of Inflammation-Responsive Astrocytes from Glial Progenitors Generated from Human Induced Pluripotent Stem Cells. *Stem Cell Rep.* **8**, 1757–1769 (2017).
320. Rivera, A. D. & Butt, A. M. Astrocytes are direct cellular targets of lithium treatment: novel roles for lysyl oxidase and peroxisome-proliferator activated receptor- $\gamma$  as astroglial targets of lithium. *Transl. Psychiatry* **9**, 211 (2019).
321. Harris, J. L., Choi, I. Y. & Brooks, W. M. Probing astrocyte metabolism in vivo: Proton magnetic resonance spectroscopy in the injured and aging brain. *Front. Aging Neurosci.* **7**, 1–8 (2015).
322. Daniel, E. D., Cheng, L., Maycox, P. R. & Mudge, A. W. The common inositol-reversible effect of mood stabilizers on neurons does not involve GSK3 inhibition, myo-inositol-1-phosphate synthase or the sodium-dependent myo-inositol transporters. *Mol. Cell. Neurosci.* **32**, 27–36 (2006).
323. Heirendt, L. *et al.* Creation and analysis of biochemical constraint-based models using the COBRA Toolbox v.3.0. *Nat. Protoc.* **14**, 639–702 (2019).

324. Leucht, S., Helfer, B., Dold, M., Kissling, W. & McGrath, J. J. Lithium for schizophrenia. *Cochrane Database Syst. Rev.* **2015**, (2015).
325. Brunk, E. *et al.* Recon3D enables a three-dimensional view of gene variation in human metabolism. *Nat. Biotechnol.* **36**, 272–281 (2018).
326. Auslander, N. *et al.* An integrated computational and experimental study uncovers FUT9 as a metabolic driver of colorectal cancer. *Mol. Syst. Biol.* **13**, 956 (2017).
327. Baloni, P. *et al.* Metabolic Network Analysis Reveals Altered Bile Acid Synthesis and Metabolism in Alzheimer's Disease. *Cell Rep. Med.* **1**, 100138 (2020).
328. Dougherty, B. V. *et al.* Identifying functional metabolic shifts in heart failure with the integration of omics data and a heart-specific, genome-scale model. *Cell Rep.* **34**, 108836 (2021).
329. Styr, B. *et al.* Mitochondrial Regulation of the Hippocampal Firing Rate Set Point and Seizure Susceptibility. *Neuron* **102**, 1009-1024.e8 (2019).
330. Zhang, Y. *et al.* Purification and Characterization of Progenitor and Mature Human Astrocytes Reveals Transcriptional and Functional Differences with Mouse. *Neuron* **89**, 37–53 (2016).
331. Uhlén, M. *et al.* Tissue-based map of the human proteome. *Science* **347**, (2015).
332. Kim, D., Paggi, J. M., Park, C., Bennett, C. & Salzberg, S. L. Graph-based genome alignment and genotyping with HISAT2 and HISAT-genotype. *Nat. Biotechnol.* **37**, 907–915 (2019).
333. Li, H. *et al.* The Sequence Alignment/Map format and SAMtools. *Bioinformatics* **25**, 2078–2079 (2009).
334. Trapnell, C. *et al.* Transcript assembly and quantification by RNA-Seq reveals

- unannotated transcripts and isoform switching during cell differentiation. *Nat. Biotechnol.* **28**, 511–5 (2010).
335. Zur, H., Ruppin, E. & Shlomi, T. iMAT: an integrative metabolic analysis tool. *Bioinformatics* **26**, 3140–3142 (2010).
336. Becker, S. A. & Palsson, B. O. Context-Specific Metabolic Networks Are Consistent with Experiments. *PLoS Comput. Biol.* **4**, e1000082 (2008).
337. Jerby, L., Shlomi, T. & Ruppin, E. Computational reconstruction of tissue-specific metabolic models: Application to human liver metabolism. *Mol. Syst. Biol.* **6**, 1–9 (2010).
338. Vlassis, N., Pacheco, M. P. & Sauter, T. Fast Reconstruction of Compact Context-Specific Metabolic Network Models. *PLoS Comput. Biol.* **10**, e1003424 (2014).
339. Cheng, K. *et al.* Genome-scale metabolic modeling reveals SARS-CoV-2-induced metabolic changes and antiviral targets. *Mol. Syst. Biol.* **17**, (2021).
340. Yizhak, K., Gabay, O., Cohen, H. & Ruppin, E. Model-based identification of drug targets that revert disrupted metabolism and its application to ageing. *Nat. Commun.* **4**, 2632 (2013).
341. Kuo, C.-C., Chiang, A. W. T., Baghdassarian, H. M. & Lewis, N. E. Dysregulation of the secretory pathway connects Alzheimer's disease genetics to aggregate formation. *Cell Syst.* **12**, 873-884.e4 (2021).
342. Cantor, J. R. *et al.* Physiologic Medium Rewires Cellular Metabolism and Reveals Uric Acid as an Endogenous Inhibitor of UMP Synthase. *Cell* **169**, 258-272.e17 (2017).
343. Zhao, C. *et al.* Mutant C9orf72 human iPSC-derived astrocytes cause non-cell autonomous motor neuron pathophysiology. *Glia* **68**, 1046–1064 (2020).
344. Thiele, I. *et al.* Personalized whole-body models integrate metabolism, physiology,

- and the gut microbiome. *Mol. Syst. Biol.* **16**, (2020).
345. Orth, J. D., Thiele, I. & Palsson, B. Ø. What is flux balance analysis?., *Nat Biotechnol* **28**, 245–248 (2011).
346. Sahoo, S. & Thiele, I. Predicting the impact of diet and enzymopathies on human small intestinal epithelial cells. *Hum. Mol. Genet.* **22**, 2705–2722 (2013).
347. Benjamini, Y. & Hochberg, Y. Controlling the False Discovery Rate: A Practical and Powerful Approach to Multiple Testing. *J. R. Stat. Soc. Ser. B Methodol.* **57**, 289–300 (1995).
348. Opdam, S. *et al.* A Systematic Evaluation of Methods for Tailoring Genome-Scale Metabolic Models. *Cell Syst.* **4**, 318-329.e6 (2017).
349. Dai, G., Yu, H., Kruse, M., Traynor-Kaplan, A. & Hille, B. Osmoregulatory inositol transporter SMIT1 modulates electrical activity by adjusting PI(4,5)P<sub>2</sub> levels. *Proc. Natl. Acad. Sci.* **113**, (2016).
350. Saiardi, A. & Mudge, A. W. Lithium and fluoxetine regulate the rate of phosphoinositide synthesis in neurons: a new view of their mechanisms of action in bipolar disorder. *Transl. Psychiatry* **8**, (2018).
351. Raghu, P., Joseph, A., Krishnan, H., Singh, P. & Saha, S. Phosphoinositides: Regulators of Nervous System Function in Health and Disease. *Front. Mol. Neurosci.* **12**, (2019).
352. Flam, E. & Arany, Z. Metabolite signaling in the heart. *Nat. Cardiovasc. Res.* **2**, 504–516 (2023).
353. Mocking, R. J. T., Assies, J., Ruhé, H. G. & Schene, A. H. Focus on fatty acids in the neurometabolic pathophysiology of psychiatric disorders. *J. Inherit. Metab. Dis.* **41**, 597–611 (2018).

354. Mi, Y. *et al.* Loss of fatty acid degradation by astrocytic mitochondria triggers neuroinflammation and neurodegeneration. *Nat. Metab.* **5**, 445–465 (2023).
355. Edelman, G. M. & Gally, J. A. Degeneracy and complexity in biological systems. *Proc. Natl. Acad. Sci.* **98**, 13763–13768 (2001).
356. Igarashi, M. *et al.* Brain lipid concentrations in bipolar disorder. *J. Psychiatr. Res.* **44**, 177–182 (2010).
357. Zadoorian, A., Du, X. & Yang, H. Lipid droplet biogenesis and functions in health and disease. *Nat. Rev. Endocrinol.* **19**, 443–459 (2023).
358. Smolič, T. *et al.* Astrocytes in stress accumulate lipid droplets. *Glia* **69**, 1540–1562 (2021).
359. Windham, I. A. *et al.* *APOE traffics to astrocyte lipid droplets and modulates triglyceride saturation and droplet size.*  
<http://biorxiv.org/lookup/doi/10.1101/2023.04.28.538740> (2023)  
doi:10.1101/2023.04.28.538740.
360. Nguyen Trung, M. *et al.* Stable Isotopomers of myo-Inositol Uncover a Complex MINPP1-Dependent Inositol Phosphate Network. *ACS Cent. Sci.* **8**, 1683–1694 (2022).
361. Raman, K. & Chandra, N. Flux balance analysis of biological systems: applications and challenges. *Brief. Bioinform.* **10**, 435–449 (2009).
362. Palsson, B. *Systems biology: constraint-based reconstruction and analysis.* (Cambridge University Press, 2015).